Zinc Phosphating on 6061-T6 Aluminum Alloy

by

Lei Shi

B.Sc., Xiamen University, 1994

A THESIS SUBMITTED IN PARTIAL FULFILLMENT OF
THE REQUIREMENTS FOR THE DEGREE OF
MASTER OF SCIENCE

in

THE FACULTY OF GRADUATE STUDIES
Department of Chemistry

We accept this thesis as conforming
to the required standard

THE UNIVERSITY OF BRITISH COLUMBIA

September 2000

Department of ___Chemistry___

The University of British Columbia
Vancouver, Canada

Date ___September 6 /2000___

DE-6 (2/88)

Abstract

There is an urgent need to develop new non-chromating coating methods for the corrosion protection of aluminum alloys, and this thesis reports studies to establish optimal working conditions for forming zinc phosphate coatings on 6061-T6 aluminum alloy. Scanning electron microscopy (SEM), X-ray photoelectron spectroscopy (XPS) and corrosion tests were used to characterize the treated 6061-Al surface, and to assess the effects of different parameters in the coating bath, as well as different pre-treatments and post-treatments.

The initial study investigated different working conditions for the zinc phosphating, and this built on other studies from this laboratory. An initially considered coating bath had 16.0 ml H_3PO_4 (85%), 5.36 g ZnO and 0.5 g NaF per liter, and optimal conditions for coating involved dipping the 6061-Al samples into this bath at 60 $^{\circ}$C for 6 min. But the addition of more fluoride was shown to be effective for increasing the zinc phosphate coverage on the aluminum alloy; the optimal range of F$^-$ being from 400 ppm to 600 ppm for these conditions.

Based on the working condition study, the effects of pre-treatments, post-treatments, and associated procedures involved with the zinc phosphating of 6061-Al alloy on the quality of the final coating were investigated. Comparisons were made between acid etching and mechanical polishing in the pre-treatment stages, and the mechanical polishing involved was done by either machine polishing or hand polishing. New post-treatment procedures were investigated using methyltriethoxysilane. It results in a considerable increase in the zinc phosphate coverage and coating thickness on the aluminum surface. This gave a greatly improved corrosion resistance by the coating

compared with samples that did not have the silane post-treatment. A related silane treatment can also be used at an intermediate stage in the zinc phosphating immersion.

In order to improve the final coating, Cu^{2+} and Ni^{2+} ions were studied as accelerators. $Cu(NO_3)_2$ (0.002 wt%) and $Ni(NO_3)_2$ (0.0004 wt%) were separately introduced to the basic phosphating baths containing H_3PO_4, ZnO and NaF, and each was shown to not only increase the phosphating speed, but also to improve the corrosion resistance and adhesion, insofar as the coating contained smaller crystalline grains and increased coverage of zinc phosphate on the surface. Of these two accelerators, Ni^{2+} appeared especially effective at increasing the corrosion protection ability of the final coating. Although NO_3^- has some capabilities as an accelerator it was shown that its effect was negligible in this context at the concentrations used.

Table of Contents

List of Tables

List of Figures

Acknowledgements

I sincerely thank my supervisor, Professor K.A.R. Mitchell, for his guidance and encouragement during the course of this work and for his careful reading and comments on this thesis.

I am especially grateful to Dr. X.L. Sun for helping me on my project and for reading my thesis draft and making valuable comments. I also owe special gratitude to Dr. P.C. Wong , Dr. M.Y. Zhou and Dr. Y.L. Leung for their active involvement and helpful discussions in this work. I am also very grateful to my group members, Dr. K. Wong, Mr. W.H. Kok, Ms. R.Y. Li, Ms. M. Kono, Ms. D. Susac, Ms. J. Fang, Dr. M. Saidy, Ms. J. Jin and Mr. M. Lee, for their help in the laboratory. I also acknowledge the staff from the mechanical workshop for preparing the aluminum panels for this research, and the Defence Research Establishment Pacific for their financial support. I appreciate the help from Professor T. Tiedje's laboratory for all the SEM measurements.

Finally, I would like to thank my parents, my sisters and my husband, Letian Wang, for their continuous support and encouragement throughout all these years. To them, I dedicate this thesis.

Chapter 1 Phosphating for Aluminum

1.1 Introduction

Aluminum and its alloys are employed widely in modern industry, and among metals aluminum is second only to iron in annual consumption. Aluminum is certainly the most important non-ferrous metal and the rapid expansion of production facilities continues, spurred on by the prospect of increasing world demand [1].

Metallic aluminum often has excellent corrosion resistance, which is due to its affinity for oxygen that results in the production of a very thin but tenacious oxide film. It covers the surface as soon as a freshly cut piece of the metal is exposed to the atmosphere. Hence, pure aluminum needs less protection than most metals. On the other hand, the commercial metal and its alloys, though resistant, are distinctly more sensitive to corrosion, and the development of high strength light alloys, containing quantities of other metals such as copper, zinc or nickel, has heightened the need for protective surface treatments. The nature of these metallic additions appreciably influences the alloy's susceptibility to corrosion; high mechanical strength and corrosion resistance have so far proved largely incompatible. Therefore, the development of satisfactory protective finishes for these metals has very great importance [2].

Chemical conversion treatments in chromate or in chromate-phosphate solutions have frequently been used as protective finishes for aluminum alloys. However, there are now concerns about the carcinogenic nature of chromates, both in industrial use and in its waste removal. Current environmental legislation is moving toward a total ban on chromate-based treatments. Thus, there is a strong incentive to explore and evaluate

alternative treatments for aluminum surface modification [3]. Zinc phosphate has been seen as one possible replacement coating material, and this follows its extensive application for steels and other metals [4,5]. World-wide a lot of study had been applied to this general topic, but the particular recipes produced depend on the particular metal and other alloying elements, and they are generally subject to heavy patent protection.

Over the last several years, researchers in our group developed a recipe for zinc phosphating on 7075-T6 aluminum alloy [6]. Based on that experience, studies in this thesis focus on applying the previous recipe to the 6061-T6 aluminum alloy, and on improving its composition and mode of application. The thin-film zinc phosphate coatings were characterized by X-ray photoelectron spectroscopy (XPS) for surface composition and scanning electron microscopy (SEM) for coating morphology [7-12].

1.2 Characteristics of Aluminum

1.2.1 Aluminum and Its Alloys

Aluminum is a strongly electropositive metal and possesses a strong affinity for oxygen. It was discovered in 1809 by Sir Humphrey Davy and was first isolated in 1825 by H. C. Oersted. In 1885, the brothers Cowle produced the first aluminum alloys containing iron and copper, soon after which the invention of the dynamo made a cheaper supply of electricity available and resulted, in 1886, in Heroult's and Hall's independent French and American patents for the electrolytic production of aluminum from alumina and molten cryolite (Na_3AlF_6) [1].

The important properties of aluminum are low density of approximately 2.7 g/cm^3, high mechanical strength and relatively high corrosion resistance. Other valuable

properties include its high thermal and electrical conductance, its reflectivity, its high ductility and resultant low working cost, its magnetic neutrality, high scrap-value, and the non-poisonous and colorless nature of its corrosion products which facilitates its use in the chemical and food-processing industries [2].

The chief alloying constituents added to aluminum are copper, magnesium, silicon, manganese, nickel and zinc which are used to increase the strength of this metal. There are two classes of alloys. The first are the 'cast alloys' which are cast directly into their desired forms by one of three methods of sand casting, gravity die casting or pressure die casting; the second class, the 'wrought alloys', are cast in ingots or billets and are later processed into extrusions, sheets, wires etc. The main classes of these alloys are the 2000 series (Al-Cu alloys), which are high-strength materials used mainly in the aircraft industry, the 3000 series (Al-Mn alloys) used mainly in the canning industry, the 5000 series (Al-Mg alloys) which are used unprotected for structural and architectural applications, the 6000 series (Al-Mg-Si alloys) which are the most common extrusion alloys, and are used particularly in the building industry, and the 7000 series (Al-Zn-Mg alloys) which are again high strength alloys for aircraft and military vehicle applications [1,2].

1.2.2 Aluminum Oxide Film

As soon as a freshly formed aluminum metal surface is exposed to the atmosphere, it becomes covered with a thin oxide film, and this film can re-form quickly when damaged. Since there is an increase in volume during the conversion of metal to its oxide, the latter is under compressive stress and will not only cover the metal

3

continuously, but can cope with a certain amount of substrate deformation without rupturing. As a consequence, the film provides a barrier between the aluminum surface and the prevailing environment. However, the filmed substrate is in general far from perfect, the oxide film contains defects which, under appropriate circumstances, may act as nucleation sites for film breakdown, thereby exposing the aluminum to the environment [2].

1.2.3 Corrosion of Aluminum and Its Alloys

An aluminum surface, with its insulating oxide film, cannot be considered homogenous. Even with samples of 99.99% purity, the surfaces are microscopically heterogeneous. Amounts of impurities, such as Fe, Si and Cu, are not just distributed uniformly through the solid-solution matrix, but they can segregate to grain or cellular boundaries [13]. Further, surface damage caused by mechanical deformation or mechanical scratching is frequently present at the surface. Such features contribute to the presence of flaws. Flaws, associated with microscopic heterogeneity, such as grain boundaries, sub-grain boundaries and second phase particles, are termed residual flaws. Mechanical flaws are associated with scratches and other surface irregularities [14]. The presence of discrete flawed areas within the film at aluminum surfaces may contribute to the development of anodic and cathodic regions. Under appropriate conditions, the anodic regions are attacked resulting in metal dissolution, while the cathodic regions show reduction in the overall redox process.

The dissolution of aluminum corresponds the anodic reaction

$$Al \rightarrow Al^{3+} + 3e^- , \qquad\qquad (1.0)$$

but the ions become immediately solvated through contact with the electrolyte:

$$Al^{3+} + 6H_2O \rightarrow [Al(H_2O)_6]^{3+} . \tag{1.1}$$
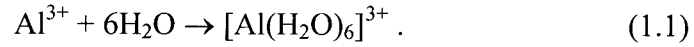
This solvated hex-aqua complex may then hydrolyze:

$$[Al(H_2O)_6]^{3+} \rightarrow Al(OH)_3 + 3H_2O + 3H^+ \tag{1.2}$$
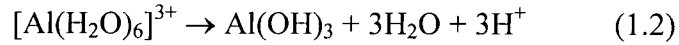
Concerning cathodic reactions, there are two possibilities in aqueous electrolyte:

Oxygen reduction: $\quad\quad O_2 + 2H_2O + 4e^- \rightarrow 4OH^-$ $\quad\quad\quad$ (1.3)

Hydrogen evolution: $\quad\quad 2H^+ + 2e^- \rightarrow H_2$ $\quad\quad\quad\quad\quad$ (1.4)
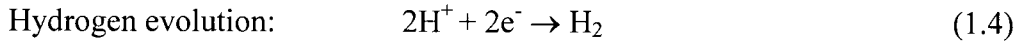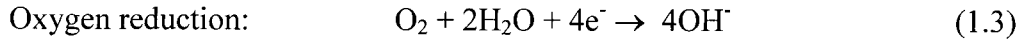
The relatively insulating nature of the oxide helps protect against electrochemical attack although such corrosive reactions can occur at flaws and defects on the surface.

1.2.4 Corrosion Protection

Aluminum and its alloys support an air-formed oxide film that provides a barrier between the aluminum surface and the prevailing environment [15]. However, to ensure enhanced corrosion resistance in the more aggressive environments, some form of protection is needed. The possibilities include cathodic protection systems, inhibitors, and applied coatings or finishes.

Cathodic systems

In a corrosive situation, the regions on a metal surface that suffer oxidative attack are termed anodes, while those regions that gain electrons (and do not suffer metallic degradation) are called cathodes. Cathodic protection may be achieved in three ways: by cladding with a more anodic material, by using a sacrificial anode, or by applying to the component a potential which is sufficiently positive to inhibit the oxidation [2].

Inhibitors

An inhibitor is a chemical compound that effectively reduces the corrosion rate of a metal when added in small concentrations to an otherwise mildly aggressive medium or environment. It may occur by conditioning the metal surface, or the environment, or both, depending on the individual system. Inhibitors are classified as anodic, cathodic, or mixed inhibitors. They interfere with one or more of the corrosion reactions, and thereby reduce the corrosion process as a whole [16].

Protective finishes

Protective finishes are employed primarily for protection against corrosion, although they are often decorative as well. The finishes available for aluminum alloys include the following:

Chemical conversion coatings – thin oxide, phosphate or chromate films used for light service conditions and as a basis for application of paint and other organic coatings.

Anodic oxidation coatings – electrochemically produced oxide coatings with a wide range of thickness, corrosion protection, color, hardness, and optical and electrical properties; generally used where maximum protection is required.

Organic finishing – paint, lacquer and resin finishes in a very wide range of types, giving great flexibility in finish, color, corrosion resistance and functional properties.

Electroplated finishes – with suitable surface preparation a full range of decorative and functional electroplated coatings can be applied to aluminum [2].

1.3 Phosphate Conversion Coating

The phosphating process can be described as a treatment of a metal surface which gives a reasonably hard surface coating of insoluble phosphate that is contiguous and highly adherent to the underlying metal and is much easier to paint than the metal [17]. The coating is formed by a topochemical reaction that causes the near surface region of the base to become an integral part of the corrosion resistant film. Phosphate coatings can be applied on various metals such as iron, zinc, aluminum, cadium and manganese. Due to its economy, speed of operation and ability to afford excellent corrosion resistance, wear resistance, adhesion and lubricating properties, phosphating has a significant role in finishing processes associated with the automobile and appliance industries. Physical properties like hardness, tensile strength and workability of the original metal are retained after phosphating. The dimensional change caused by phosphate coatings on the metal surface is of the order of 10^{-3} mm.

The origin of the phosphating process goes back to the Romans of the third century A.D [18]. In more modern times, such processes were first applied on steel in 1859 and patented by T. W. Costlett in 1906 [19], who used a solution containing phosphoric acid, ferrous sulfate and iron filings to give a protective phosphate coating on iron and steel articles. Some addition of zinc sulfate was later shown to give improved

results. These processes were soon followed by those of the Parker Company in 1918, who added primary manganous phosphate to the bath and developed the process known as Parkerizing, to which was later added the speedier process called Bonderizing which utilizes a Cu^{2+} catalyst and yields an excellent paint-base. Since then numerous developments have taken place, including the use of nitrate as an accelerator and the use of disodium phosphate containing titanium for surface conditioning before phosphating. During the last 20 years, work has concentrated mainly on improvements in quality, particularly to keep pace with the evolving needs of organic finishing systems [20-23].

Initially phosphating studies focused on steel, but applications to aluminum are more recent. When aluminum is treated with dilute phosphoric acid, a thin passive film is obtained which is similar to the chromate film obtained from a chromating bath containing chromic acid, sodium dichromate and sodium fluoride. A film of aluminum phosphate generally gives improved paint adhesion, however, the corrosion resistance is less good than that shown by chromate coatings. Moreover, this gives another reason why improvements are needed for the phosphating of aluminum [24].

1.3.1 Phosphating Chemistry

Phosphating baths usually contain three main components: (i) free phosphoric acid; (ii) $Me(H_2PO_4)_2$, where Me represents the heavier metal used in the coating; and (iii) at least one accelerator. A certain amount of free phosphoric acid must always be present in the phosphating bath in order to repress hydrolysis and keep the bath stable. The accelerator is present both to speed up the process and improve the coating quality.

The phosphating process is based on the following equilibria involving phosphoric

acid:

$$H_3PO_4 \ = \ H^+ + H_2PO_4^- \qquad\qquad (1.5)$$

$$H_2PO_4^- \ = \ H^+ + HPO_4^{2-} \qquad\qquad (1.6)$$

$$HPO_4^{2-} \ = \ H^+ + PO_4^{3-} \qquad\qquad (1.7)$$

When the metal M to be coated is immersed into the phosphating bath, the coating occurs by a basically electrochemical process with different microcells formed on its surface. The electrode reactions are:

At micro-anodes: $\quad M - 2e = M^{2+} \qquad\qquad (1.8)$

At micro-cathodes: $\quad 2H^+ + 2e = H_2 \qquad\qquad (1.9)$
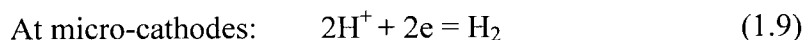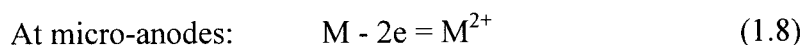
Because of the H^+ consumption, the solution near the micro-cathode surface will have a higher pH, so shifting equilibria in Equations (1.5) - (1.7) to the right. Then the insoluble heavy metal secondary and/or tertiary phosphates can precipitate at the micro-cathodes according to such processes as:

$$Me(H_2PO_4)_2 = MeHPO_4 + H_3PO_4 \qquad\qquad (1.10)$$

$$3MeHPO_4 = Me_3(PO_4)_2 + H_3PO_4 \qquad\qquad (1.11)$$

$$M + Me(HPO_4)_2 = MMe(PO_4)_2 + H_2 \qquad\qquad (1.12)$$
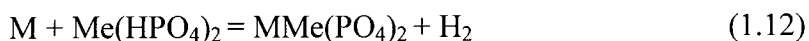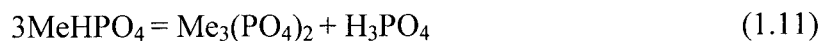
This outlines the simplest mechanism for phosphate coating, but further complications

are present in general because of the involvement of various additives and pre-treatment steps [4-5].

1.3.2 Use of Accelerators

In practice, the phosphating reaction tends to be slow owing to polarisation caused by hydrogen evolution at the cathode, but the process can become more practical by employing some form of acceleration. The different approaches to accelerating the formation of phosphate coatings can be broadly divided into three classes: chemical acceleration, mechanical acceleration and electrochemical acceleration. They are all widely practised in industry for other metals, but chemical acceleration appears as the most promising approach for aluminium.

Oxidising substances (e.g. chlorates and peroxides) and metal ions such as Cu^{2+} or Ni^{2+}, represent important classes of chemical accelerators [5]. They accelerate the deposition process through different mechanisms. Oxidising agents depolarise the cathodic sites, whereas the transition metal ions promote metal dissolution by providing additional cathodic areas. Since acceleration through depolarisation is the preferred route, oxidising agents have found more widespread use than metals. Moreover, these agents prevent the build up of the substrate metal in the bath that can be detrimental to good coating formation [25]. The most commonly employed oxidising accelerators are nitrites, chlorates, nitrates, peroxides and organic nitro compounds either alone or in combination. Common combinations are nitrite-nitrate, nitrite-chlorate-nitrate and chlorate-nitrobenzene sulphonic acid [4].

Some reducing agents, such as alkali metal sulphites, hypophosphites, phosphites,

formaldehyde, benzaldehyde, hydrozylamine, have also been tried as accelerators but they have been less successful from the industrial point of view [26].

1.3.3 Steps in Phosphating Process

A typical phosphating sequence comprises of seven operations, namely, surface cleaning, rinsing, surface conditioning, phosphating, rinsing, chromic acid sealing and drying [25]. However, depending upon the surface conditions of the metal, some of these operations may be omitted or additional operations may be incorporated into the system, but the following outlines some relevant points.

(1) Surface cleaning

A necessary first step to form a proper coating is to start with a substrate which is clean and free from contaminants such as oil, grease, corrosion products etc. Many coating failures can be attributed to a poor initial surface preparation. A good cleaning agent is one that removes all contaminants from the metal surface and prevents their redeposition or the formation of other detrimental reaction products [27]. A variety of methods such as sand blasting, solvent degreasing, vapour degreasing, alkaline cleaning and pickling have been used to achieve this end.

Sand blasting is an effective method of mechanical cleaning. However, it is expensive in industry practice; its use can only be justified as a field procedure where chemical treatments cannot be used and it is necessary to remove loosened mill scale as well as paint [28].

Organic solvents are widely used to remove organic contaminants from metal substrates, but they are toxic and flammable, and often need to be used in large quantities.

A more economical method is to use the vapour degreasing technique, which works by continuous cleaning with small quantities of solvent [29].

Alkaline cleaning can also be effective to remove greases, oils and waxes, and this is done in conjunction with surface active (wetting) agents and emulsified hydrocarbon solvents. Alkaline cleaners are particularly efficient when used hot (e.g. at ~ 80°C). While alkaline cleaning is free from the fire and toxicity hazards associated with organic solvent cleaning (unless emulsified solvents have been incorporated), care must be taken in relation to the corrosive effects of alkaline materials on skin and clothing. Caustic soda, in particular, can cause serious burns to the skin and eyes, and is extremely irritating to the nasal and bronchial membranes if inhaled [27].

Cleaning or pickling with acids such as HCl, H_2SO_4, and H_3PO_4 can be very effective for the removal of rust and mill scale. Dilute solutions (5 - 10% by weight) of H_2SO_4 and HCl are used in the presence of inhibitors to remove inorganic contaminants by converting them into their metal salts. Pickling in H_2SO_4 is usually performed at around 60°C. H_3PO_4 is an excellent time-tested cleaning agent, which not only removes organic and inorganic solids present on the metal but also causes chemical etching of the surface by reacting with it to produce a mechanically and chemically receptive surface for subsequent coating formation [30].

(2) Rinsing

The rinsing step plays a vital role in the sequence since it prevents leftover chemicals used in the initial cleaning being present to contaminate the subsequent phosphating process [28].

(3) Surface conditioning

This step refers to immersion of the metal into an activator solution for 1-2 min before phosphating to remove inappropriate structures from the surface cleaning and add more nucleation sites for the coating formation [31].

(4) Phosphating

Suitably cleaned and conditioned surfaces are next subjected to the phosphating step that causes the formation of an insoluble, corrosion resistant phosphate layer on the substrate surface. A wide variety of phosphating compositions are available for the different metals. However, the choice of components and operating conditions for the phosphating bath must be made based on the nature of the material to be treated and its end use. Based on the nature of the heavy metal ion constituting the major component of the phosphating bath, these solutions are classified by their compositions as zinc, manganese and iron phosphating baths [32].

Phosphate deposition can be achieved through the use of both spraying and immersion processes, and the choice of the appropriate method depends upon the size and shape of the substrate to be coated and the end use for which the coating is made. Spraying is preferred where shorter processing times are required. This method, however, requires more factory floor space and special equipment for application. Immersion processes tend to be slower, but they produce uniform coatings and they may require less factory floor space if the process tanks are arranged in a compact manner. On the other hand, the immersion processes are more susceptible to contamination during continuous operation than are spray processes. Smaller parts can be effectively and economically phosphated by immersion, whereas spraying is unavoidable for larger structures. Nowadays, a combination of spraying and immersion has been used

successfully in the automobile industry [33].

Phosphating temperatures have ranged from 30 to 99°C, and the processing time can vary from a few seconds to several minutes. Suitable choices of these parameters are determined by the nature of the metal to be coated, the bath composition and the thickness and weight of the coating required [25].

(5) Rinsing after phosphating

A surface, which has been phosphated, should immediately be thoroughly rinsed with deionized water to remove any acid residue, soluble salts and non-adherent particles present which could otherwise promote blistering of paint films used for finishing. Generally overflow rinsing and spray rinsing is preferred [34].

(6) Chromic acid sealing

The phosphate coatings are usually porous in nature, and this can have a detrimental influence on the corrosion resistance unless the phosphate coating is sealed. A hot (70-80°C) dilute chromic acid rinse is generally used for this purpose. This treatment reduces the porosity by about 50%. It improves the corrosion resistance by deposition of insoluble chromate to seal pores in the coating. The dilute chromic acid is advantageous because the residue is slightly acidic, and most paints can tolerate an acidic residue better than one that is alkaline [35].

Though chromic acid sealing improves corrosion resistance, the need for regular disposal of the Cr(VI) effluents is a matter of concern because of the health hazards mentioned above. Several alternatives have been proposed following the introduction of new regulations imposed by the pollution control authorities, and these alternatives include phosphoric acid derivatives, dicarboxylic acids, Mo solution rinses, and tannins.

To date the corrosion protection provided by these alternatives is not as good as that provided by the chromic acid treatment and this indicates an important area for future research.

(7) Drying

After the chromic acid rinsing, the treated parts must be dried before finishing; the conventional methods used for this are simple evaporation and forced drying either by blowing air or by heating [33]. Where evaporation conditions are good, warm air-circulating fans and compressed air blow offs are the most economical methods. After drying the phosphated panels are ready for the finishing treatment, such as the application of paint or other decorative materials.

1.3.4 Current Developments

Over the last 30 years or so, studies of phosphate coating have focused on: (1) use of low temperature phosphating bath to reduce energy consumption [20]; (2) use of low zinc technology (traditional zinc phosphating baths have contents in the range 2000-4000 ppm zinc and 5000-10,000 ppm P_2O_5; low zinc phosphating baths have 400-1700 ppm zinc and 12,000-16,000 ppm P_2O_5) [5]; (3) use of special additives having more than one role in the phosphating bath [23]; (4) use of other phosphate coatings such as tin, nickel and lead phosphate [36]; (5) use of two or more different metals in the same phosphate coating (e.g. $Zn_3Ca_3Fe(PO_4)_5$) [37]; (6) development of compositions for simultaneous phosphating of different metals [38]. As interest grows in using aluminum alloys for car body manufacture, more research related to phosphating on aluminum has been conducted. Although a number of patents [39-42] pertaining to the phosphating of

aluminum alloys are available, and such processes are being used in the automotive industry, only a few mechanistic investigations [43] have been reported to date. Therefore, it is necessary to study the mechanism of the phosphating on aluminum as well as to develop improved coating recipes.

1.4 Corrosion Protection of 7075-T6 Alloy

In our group, two main lines of study have been adopted in investigations related to the background for developing new procedures for the corrosion protection of 7075-T6-aluminum alloy: (1) investigations of new recipes for zinc phosphate (ZPO) chemical conversion coatings, and (2) investigations of adhesive bonding associated with the use of silane coupling agents. In all these works the details of the surface pre-treatments and conditioning appear as very important.

A phosphating recipe based on a mixture of phosphoric acid, zinc oxide and fluoride additives was developed for 7075-T6-aluminum alloy. The formed phosphate coatings are structured with an amorphous base with crystal grains on top, and their compositions were designated as $Zn_xAl_yPO_4$ and Zn_xPO_4 respectively by XPS and SIMS [10]. To increase the phosphating speed and meet the requirements of industry, the dipping recipe was extended to a spraying recipe by adding accelerators $KClO_3$ and $NaNO_2$. Further studies with the spraying method showed that the details of substrate polishing could affect both the composition and the morphology of the subsequent coatings. For example, samples polished by Al_2O_3 sandpaper gave much better ZPO coatings than those polished by SiC sandpaper, and this emphasizes the importance of the pre-treatments in the coating process [11].

In earlier work in our laboratory for silane coupling agents, evidence was presented from using the potential-bias angular-dependent technique in XPS, and from static SIMS, that direct bonding between the Si and the oxide layer on the metal substrate may occur for the γ-GPS or γ-MGPS coated aluminum surfaces [44,45], but further testings of this are still needed.

1.5 Aims of Research and Outline of Thesis

Based on previous research in this laboratory applied to the 7075-T6 aluminum alloy, this thesis extends to investigate zinc phosphate coatings produced on the 6061-T6 aluminum alloy by the dipping procedure.

The primary goal of the work is to determine whether the previously developed recipe can be applied to the 6061-T6 alloy or whether extensions on it are needed. XPS and SEM are used to characterize the composition and morphology of the phosphated coatings produced in this work. The second objective is to study the influence of different pre-treatments on the final phosphated coatings. Hand polishing, mechanical polishing and acid etching were compared in this context again using XPS and SEM to compare the subsequent coatings. The use of silane as a post-treatment to replace chromic acid sealing for the phosphated layer was also introduced. The third objective of this study is to examine the effects of different accelerators on the coatings produced. Several traditional accelerators used for phosphating steel were tested, but detailed studies using XPS, SEM and corrosion tests were made of the use of the accelerators NO_3^-, Cu^{2+} and Ni^{2+}.

An outline of the subsequent chapters of this thesis is as follows: Chapter 2 introduces the principle and instrumentation of the key characterization techniques used, namely x-ray photoelectron spectroscopy and scanning electron microscopy. In Chapter 3, a review is given of new observations for ZPO coatings formed on 6061-T6 aluminum alloy on varying basic bath conditions including phosphating time, temperature and F^- concentration. Chapter 4 explores the influences on the final coatings of different surface pre-treatments, in particular hand polishing and machine polishing, and silane exposure as a post-treatment. Chapter 5 discusses the effects of adding accelerators ($Cu^{2+,}$ Ni^{2+} and NO_3^-) on the phosphating process, and Chapter 6 gives an overview and discusses possibilities for future work.

Chapter 2 Instrumental Analysis

2.1 Introduction

To obtain a suitable phosphating formulation for a metallic alloy it is essential to have a good understanding of the composition and chemistry of the alloy surface before and after the phosphating. X-ray photoelectron spectroscopy (XPS) is an excellent surface analytical technique for supplying such information. It has been applied to the investigation of surface properties of solid materials including catalysts, polymers and electronic materials [46]. In recent years, it has become a powerful aid in coating studies. XPS can provide both qualitative and quantitative information on the chemical composition of phosphate coatings over its sampling depth, and the spectra are relatively straightforward to interpret. Indications on the distribution of elements with depth can be obtained by non-destructive angle dependent measurements, but information beyond the regular sampling depth can be studied by XPS in conjunction with depth profiling [47].

XPS provides chemical information but poor spatial resolution. Since coatings for corrosion protection tend to be heterogeneous with variations in coating phase, grain morphology and size [48-49], scanning electron microscopy (SEM) provides another important technique for characterization by surface imaging, and this is particularly useful when a field emission gun is available to provide high spatial resolution. In this work, a combination of SEM and XPS was used to study changes in morphological and chemical properties of the phosphate coatings for different conditions of the coating process.

2.2 Electron Spectroscopy for Chemical Analysis

XPS, which has earlier been called electron spectroscopy for chemical analysis (ESCA), has a history that goes back to the time of Heinrich Hertz [50], who in 1887 produced photoelectrons between gap electrodes. Then Einstein provided an interpretation of this phenomenon in 1905 [51]. Experiments with higher energy sources were carried out by Mosely, Robinson and Rawlinson before the first World War and continued by Robinson afterwards [52]. During the 1950's, Siegbahn and his co-workers [53] demonstrated the applicability of photoelectron spectra to chemical structure analysis. They found that shifts in electron binding energies could be related to changes in chemical environment for the atom that produced the photoelectron. Thus, the foundations of XPS were established. With the development of commercial spectrometers during the mid-1960's, XPS became one of the most powerful and widely used techniques with applications to surfaces and interfaces on solid materials.

The basic principle of the XPS technique is depicted in Fig. 2.1 (a) [47]. An incident X-ray photon causes an electron to be ejected from a core level and the photoelectron escapes with a kinetic energy (E_k). To a first approximation, E_k is

$$E_k = h\nu - E_b \qquad (2.1)$$

where $h\nu$ is the energy of the photon and E_b is the binding energy of the core electron in the sample. As different atoms have different sets of electronic binding energies, elemental identification is possible through the measurement of photoelectron kinetic energies.

After photoemission, the resulting ion is in an excited state but it can relax to a

Photoemission

(a)

X-ray fluorescence   Auger emission

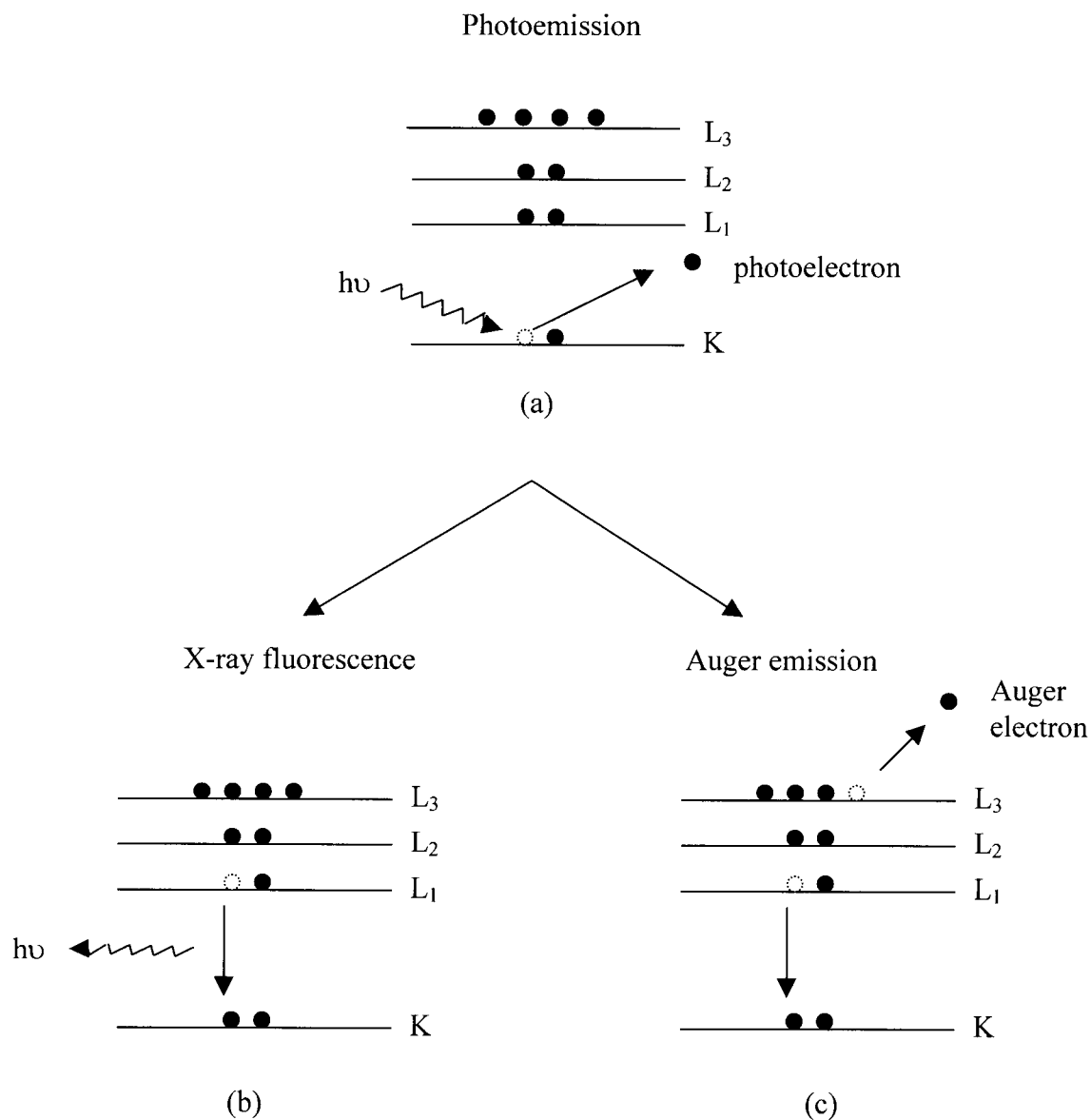(b)   (c)

Figure 2.1 Schematics for the photoelectric effect showing emission of a photoelectron and the formation of an atomic core hole in (a). The relaxation of the ion produced in (a) may occur by either X-ray fluorescence in (b) or by Auger emission in (c). Note that the ion is doubly charged after the Auger emission.

lower-energy state either by photon or electron emission. In the former case an electron from an outer orbital may fill the vacant orbital and the energy emitted as a photon (Fig. 2.1b), or an electron from an outer orbital may drop down into the atomic core hole and a second electron is ejected (Fig. 2.1c) [54]. These two relaxation processes are labeled as "X-ray fluorescence" and "Auger emission" in Fig. 2.1. The relative probabilities of these two processes vary with atomic number and atomic state, but the Auger process is generally dominant when the initial binding energy is 2 keV or less [55]. Fig. 2.1c shows the formation of a KL_1L_3 Auger electron, for which the kinetic energy can be expressed approximately as:

$$E_{KL_1L_3} = E_k - E_{L_1} - E_{L_3} \qquad (2.2)$$

where E_k, E_{L_1}, E_{L_3} are the binding energies for the levels involved. Observed kinetic energies therefore depend directly on the atomic energy levels, and that gives the basis for such measurements providing information about the chemical composition of the sample.

2.3 X-ray Photoelectron Spectroscopy

2.3.1 Qualitative Analysis

The basic application of XPS is elemental identification, which can be done by recording and analyzing a survey or wide scan XPS spectrum. Figure 2.2 shows a survey scan spectrum from a phosphate coating on an aluminum alloy. A series of peaks are observed on a background, which increases at the high binding energy side at each peak. By comparing binding energies of the peaks with reference data in Handbooks [56,60], individual peaks can be identified. There may be several peaks in a spectrum belonging
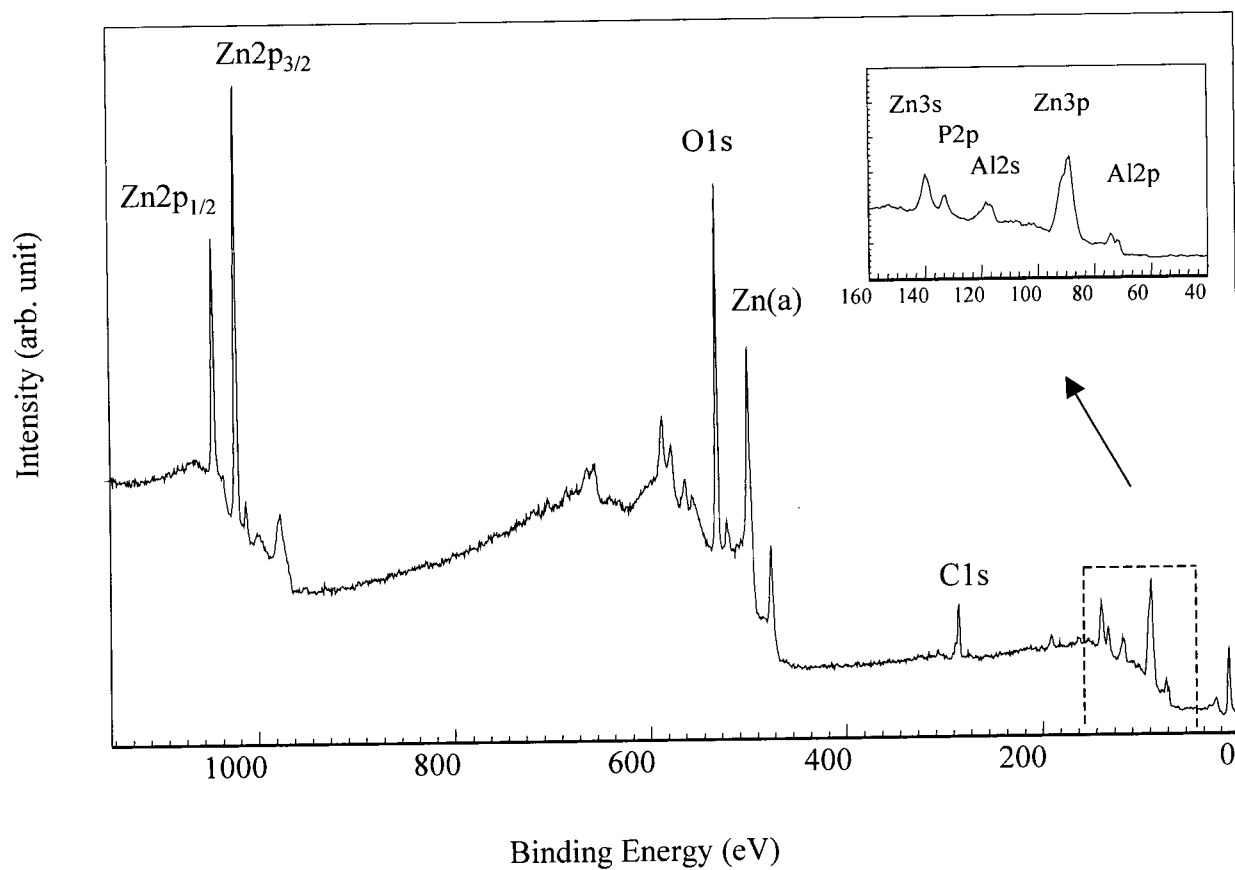
Figure 2.2   XPS survey spectrum of a phosphate coated aluminum alloy excited with Al

Kα radiation.

to one element. For instance, both Al 2s and Al 2p peaks can be seen in Fig. 2.2. They occur at the same time due to electron emission from the different subshells. For Zn, the increased spin-obit interaction yields the Zn $2p_{1/2}$ and Zn $2p_{3/2}$ doublet, where the subscripts identify the possible j values.

A high-resolution XPS spectrum reveals information about chemical bonding or chemical state of a particular element. This is because placing an atom in a different chemical environment (e.g. different oxidation state, or lattice site), gives small changes in the binding energies of the core-level electrons. This variation gives rise to a chemical shift, and Figure 2.3 shows an example for an Al 2p spectrum from an aluminum alloy with a phosphated layer. Due to different chemical environments, two Al 2p peaks are observed. One is for metallic aluminum at binding energy 71.6 eV, and the other is for aluminum oxide at 74.7 eV. The change in binding energy from 71.6 eV to 74.7 eV identifies the "chemical shift", and the trend follows expectation. Aluminum atoms that are bonded to oxygen have a net positive charge compared to the metallic aluminum atoms, and accordingly more energy is required to remove the electron in the first case.

2.3.2 Quantitative Analysis

(1) Sampling Depth and Surface Sensitivity

The sampling depth in practice is determined by the inelastic mean free path (λ), and this is defined as the average distance traveled by an electron in the solid before it suffers inelastic scattering [57]. Figure 2.4 shows some measured values of λ as a function of energy for different materials. For a given material and energy, the sampling depth is conventionally taken as 3λ; that is the depth from which 95% of the signal is contributed
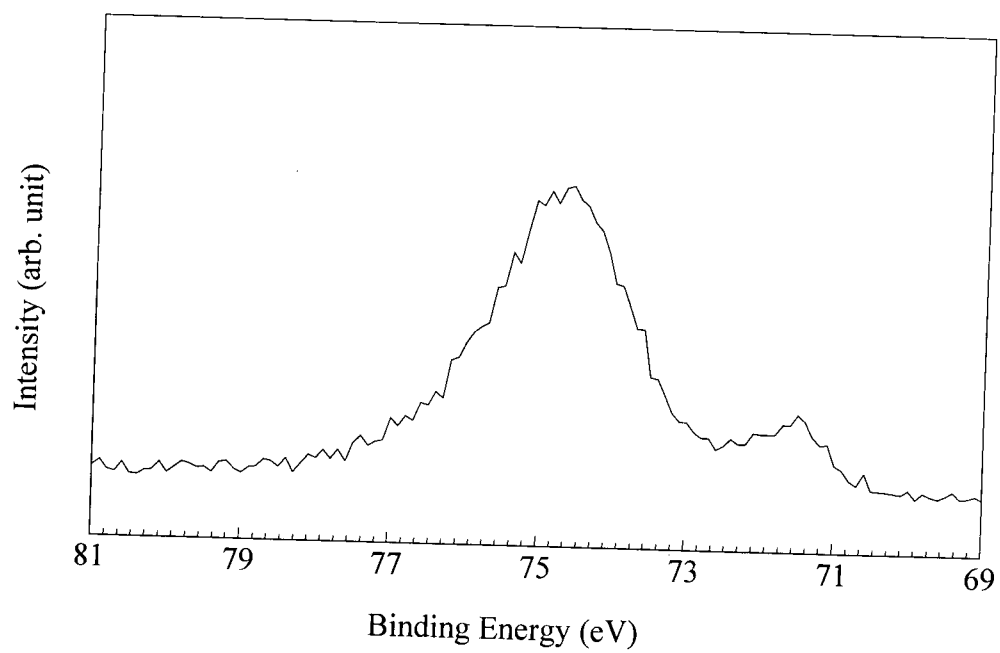
Figure 2.3   High-resolution Al 2p photoelectron spectrum from a sample showing
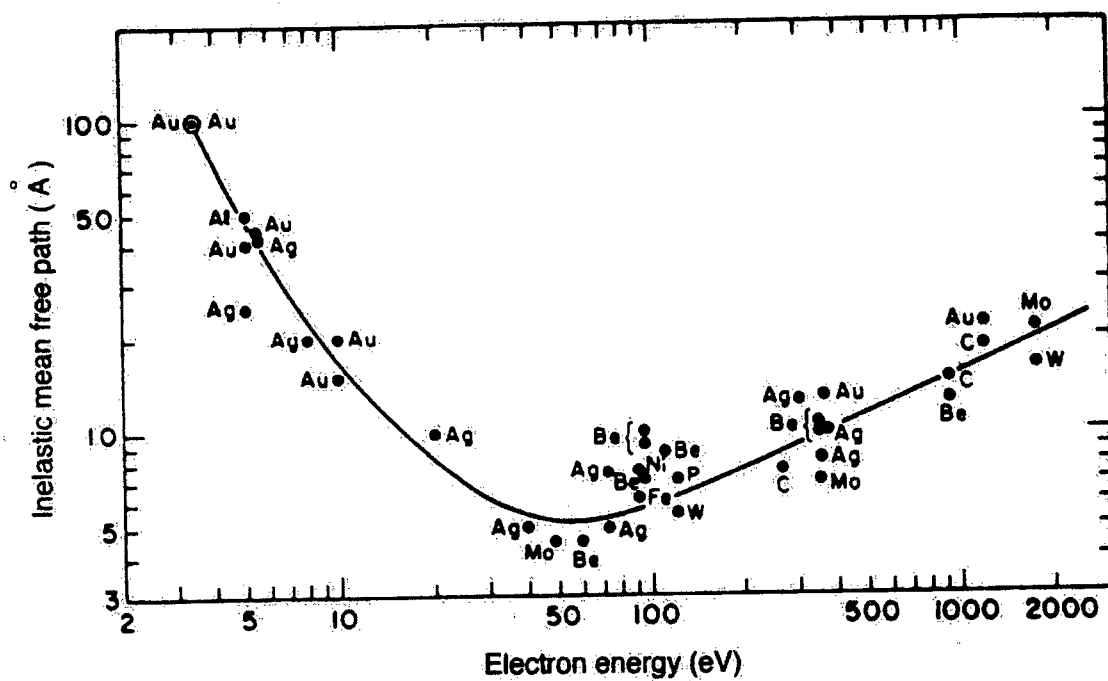
metallic and oxide components.

Figure 2.4 Inelastic mean free path of electrons as a function of kinetic energy inside a solid [58].

for a normal exit direction [59]. Since the measured kinetic energies of photoelectrons or Auger electrons are usually in the 100 to 1000 eV range, values of λ of around 6 to 20 Å are typical in this energy range and this gives XPS and AES their surface sensitivities.

For a monoenergetic beam of electrons of energy Ep striking a solid surface, Fig. 2.5 shows a typical plot of the number of scattered electrons, N(E), as a function of kinetic energy, E. The peak of backscattered electrons at the incident energy (i.e. E = Ep) results from elastic collisions, while all electrons which emerge at lower kinetic energies have undergone some inelastic scattering. The large peak at low energies is sometimes referred to as the "(true) secondary peak" and it is the elements which are studied in the scanning electron microscope

(2) Atomic concentration determination

The intensity of a photoelectron peak is generally defined as the area of the peak left after making a background correction for the inelastically scattered electrons. The number of elastically scattered photoelectrons collected by the analyser per unit time is determined by the X-ray flux (f), the photoelectron cross section (σ), the number of relevant atoms per unit volume (n), the area of the sample from which the photoelectrons are collected (A), the instrumental transmission function (T) and the inelastic mean free path (λ). The intensity contribution from an incremental thickness dx in the sample at depth x below the surface (Fig.2.6) is:

$$dI = f \, \sigma \, n \, A \, T \exp(-x/\lambda) \, dx \qquad (2.4)$$

Then simple integration from x = 0 to x = ∞ for a semi-finite homogeneous sample gives:

$$I = f \, \sigma \, n \, A \, T \, \lambda \qquad (2.5)$$

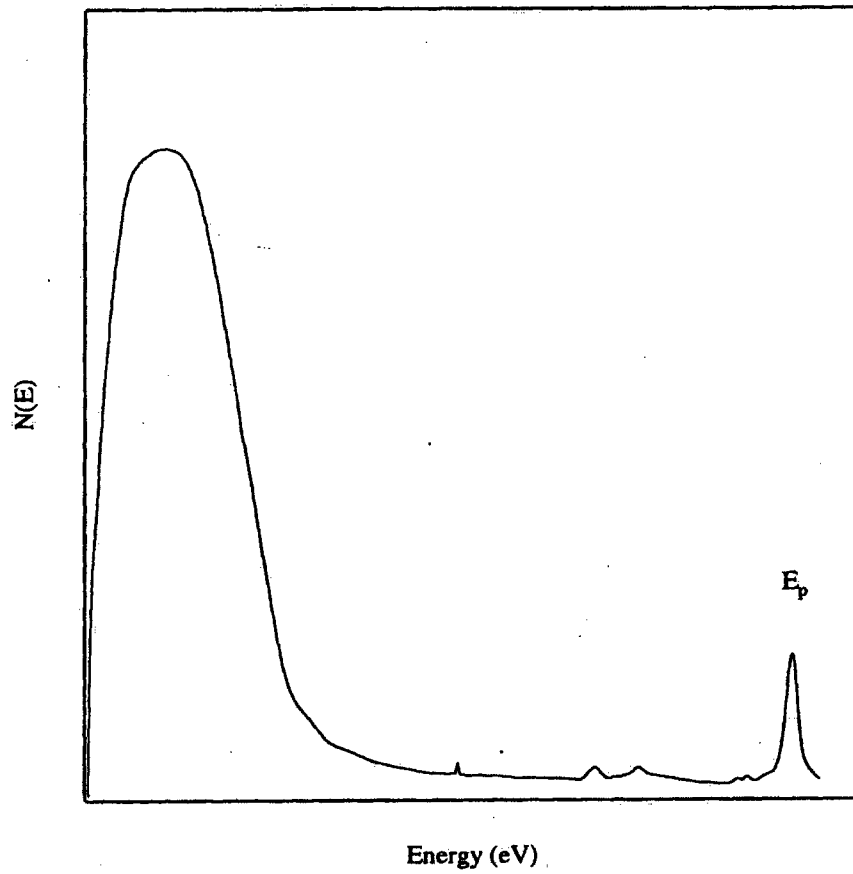To compare relative compositions of two elements in a sample, the instrumental factors f,

Figure 2.5 Schematic energy distribution N(E) of scattered electrons as a function of their exiting energy for primary energy E_p.
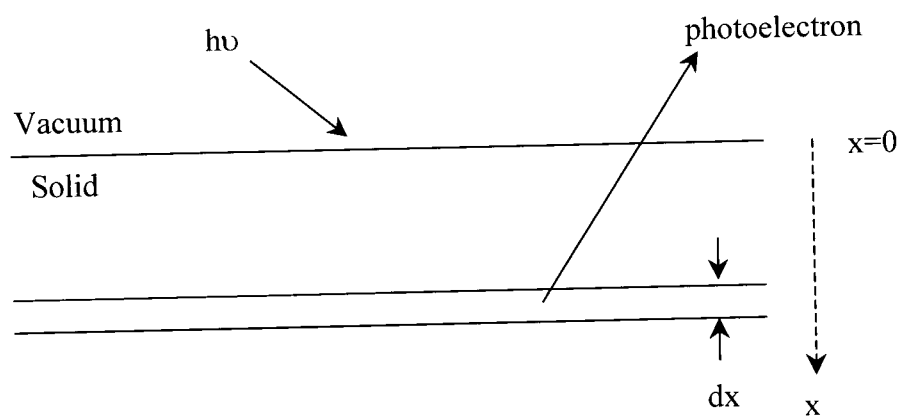
Figure 2.6 Some notation for a semi-infinite homogeneous sample.

A, T and σ (for each particular photoelectron peak) are usually grouped into a sensitivity factor S. These factors for different peaks, derived relatively to the F 1s peak, are available for the MAX200 spectrometer where the transmission function from the manufacturer corrects for the particular instrumental conditions used for each measurement [62]. Then the composition ratio for two elements in a sample can be expressed as:

$$n_1/n_2 = [(I_1/S_1)/(I_2/S_2)] \ (\lambda_2/\lambda_1) \qquad\qquad (2.7)$$

In principle, the atomic ratio (n_1/n_2) is determined by using tabulated values of λ_1 and λ_2 for the appropriate photoelectrons in the material of interest [60], although for semi-quantitative work (as in this thesis), the ratio λ_2/λ_1 is often taken as effectively constant so that the I_1/I_2 ratio (from the measured peak intensities) helps estimate the n_1/n_2 ratio just with the use of the sensitivity factors.

For work in this thesis, the background correction is made with the non-linear approach proposed by Shirley [61]. This method assumes that contributions from inelastic processes exist in a photoelectron peak. The peak dominantly involves elastically scattered electrons, but the numbers of inelastically scattered electrons are taken to be proportional to the number of elastically scattered electrons with higher kinetic energy. The MAX200 data system applies this correction once the operator has chosen the appropriate energy range for a particular spectral peak [62].

2.4 Instrumentation of XPS

Figure 2.7 shows a schematic diagram of the Leybold MAX200 spectrometer used for all the XPS measurements in this thesis [62]. This spectrometer consists of four
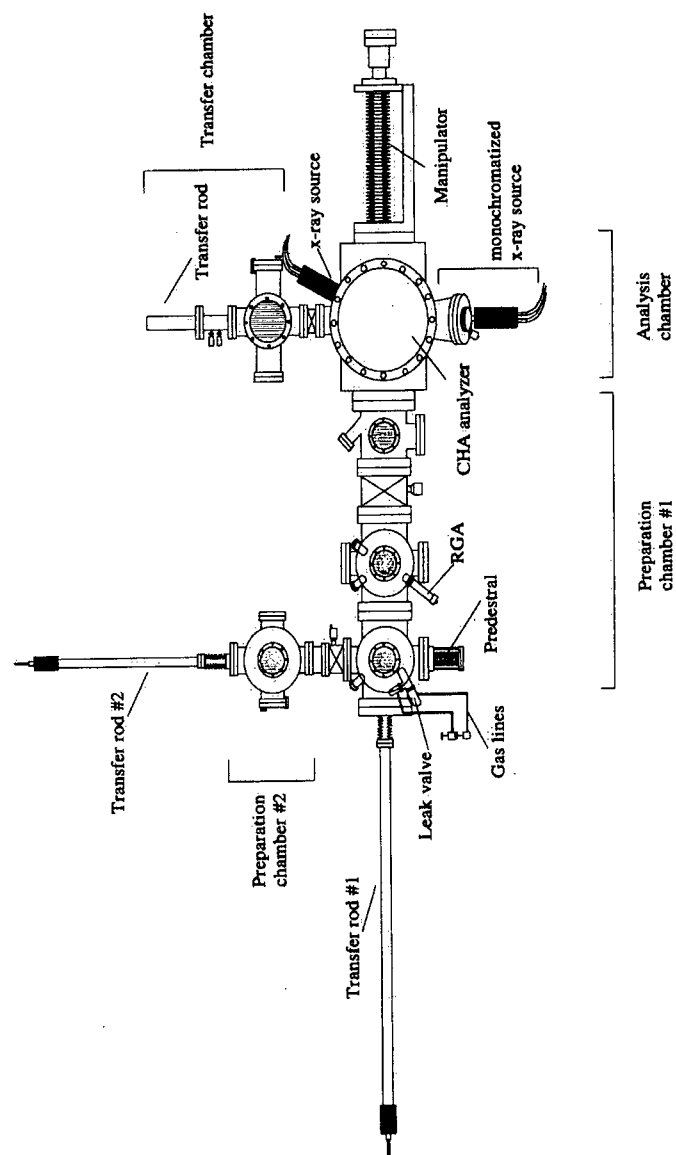
Figure 2.7 A schematic diagram of the Leybold MAX200 spectrometer.

vacuum chambers, including a sample transfer chamber, an analysis chamber and two sample preparation chambers (#1 and #2). The transfer chamber with an automatic transfer rod and a sample magazine is used for sample entry. The analysis chamber is where the XPS measurements are performed. Its major components include a dual anode X-ray source, an energy analyzer (EA 200) with its input lens and detector, and a five-motion manipulator (PTM 60). In addition, this chamber also contains an ion gun for sputtering and for ion scattering spectroscopy (ISS), an electron flood gun to help studies on insulating samples and an X-ray monochromator for increased energy resolution. The preparation chambers were not used in this work.

2.4.1 Ultrahigh Vacuum (UHV)

The XPS measurements were performed under ultra-high vacuum (UHV) conditions, to ensure that the emitted electrons reach the energy analyzer without being significantly scattered by the residual gas molecules [63]. Also, the experiment should be done under conditions where the accumulation of contamination on the sample surface is negligible during an experiment. At a pressure of 10^{-6} torr, a monolayer of gas can be adsorbed onto a surface in about one second, if every collision sticks. Therefore, pressures in the UHV range (10^{-8} torr and below) are needed to prevent changes to the surface from contamination during the period of data acquisition (e.g. 30 min).

The pumping system of the Leybold MAX200 spectrometer is shown in Fig. 2.8. All the chambers are initially rough pumped to the 10^{-2} torr range by rotary pumps, then pumped to the 10^{-7} or 10^{-8} torr range by the tubomolecular pumps. The 10^{-9} torr pressure region or below can be eventually reached by baking at around $140^{\circ}C$ for 12 hours or
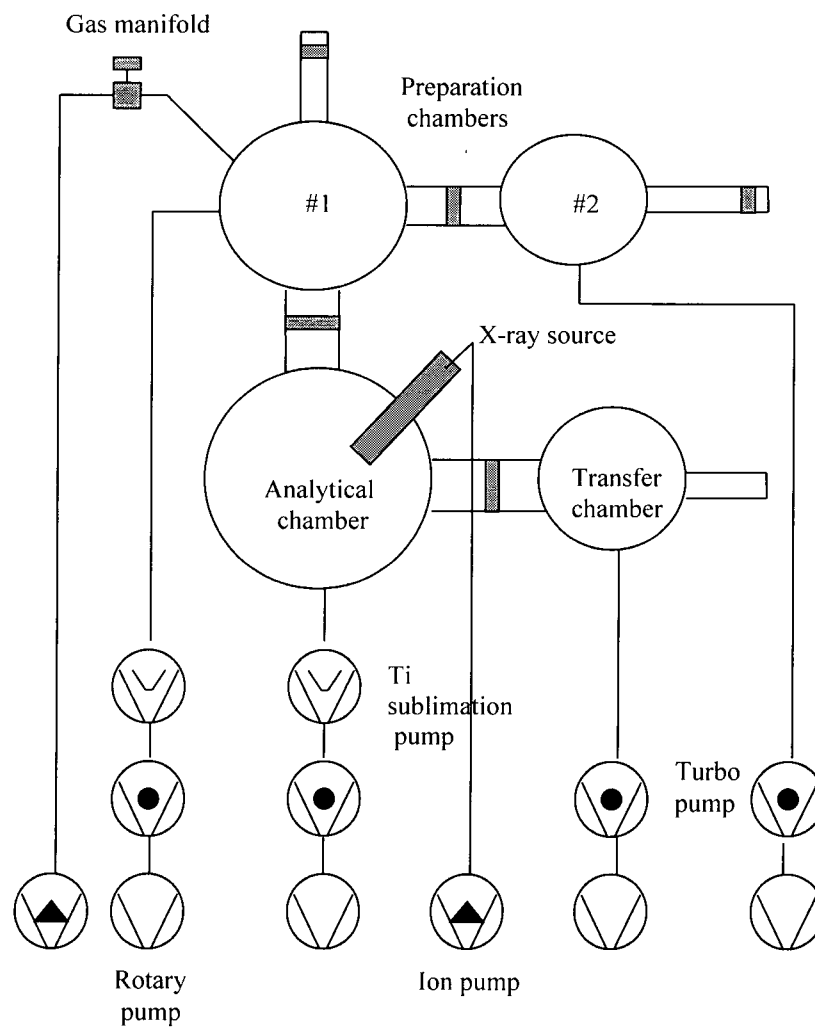
Figure 2.8 Schematic indication of the pumping system for the MAX200 system [48].

more while pumping. Typically the base pressures of the analysis chamber and preparation chamber #1 are around 5×10^{-10} torr, while those of the transfer chamber and preparation chamber #2 are about 2×10^{-8} torr.

2.4.2 Sample Handling

For the Leybold MAX200 spectrometer, samples are mounted on a standard sample holder and locked on a sample magazine that can hold up to seven sample holders. The transfer chamber is vented with nitrogen at atmospheric pressure, and then the sample magazine is introduced to the chamber prior to the initial pumpdown. After the chamber pressure has reached the 10^{-8} torr range, one sample holder is transferred at a time to the analysis chamber and locked on to the manipulator (PTM 60) dock. The manipulator controls five degrees of movement for the sample, three for linear motions (X, Y, Z) and two for rotational motions (T and R), to position the sample properly and make angle dependent measurements. Figure 2.9 indicates schematically the sample transferring system on the MAX200 facility. UHV conditions are maintained in the analysis chamber throughout the whole sample transferring process.

2.4.3 X-ray Sources

Figure 2.10 shows a schematic diagram for the Al and Mg dual anode X-ray source in the MAX200 spectrometer in which X-rays are produced from anodes by bombardment by electrons that have been accelerated after emission from a heated filament. The anode has two regions on which are deposited separate aluminum and magnesium films (~ 10 μm thickness) [64]; a simple switch in the anode filaments allows
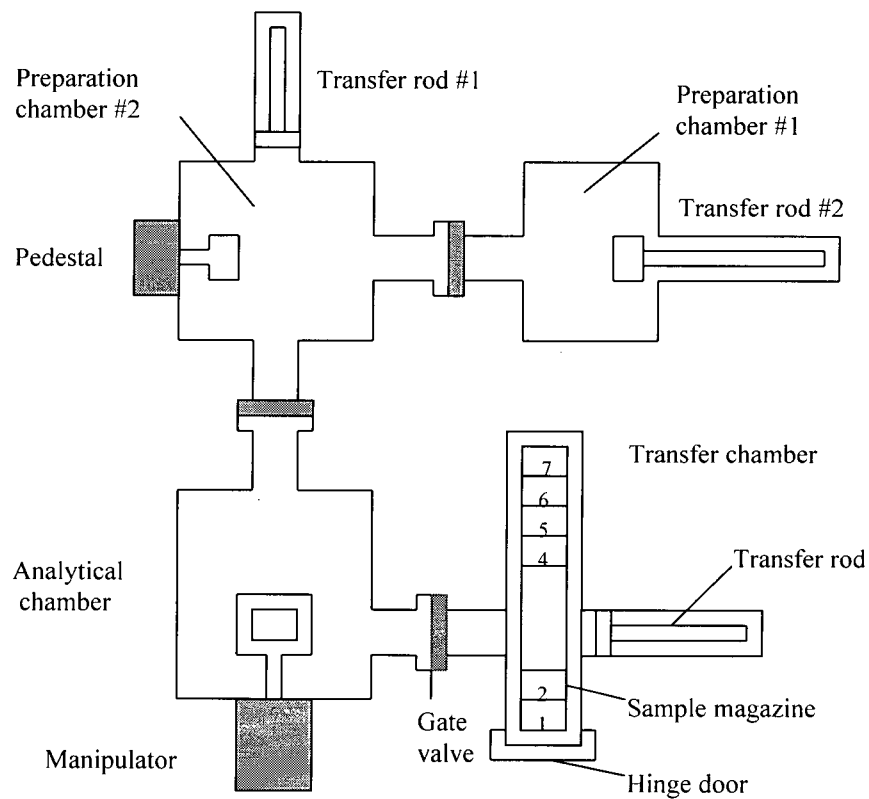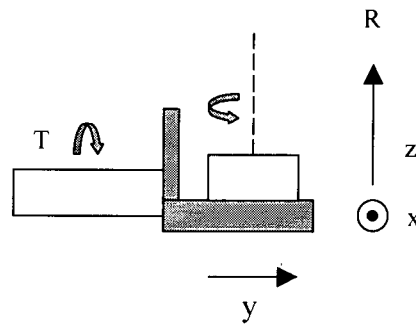
Figure 2.9 (a) Transfer devices in the MAX200 facility. (b) shows the five degrees of movement possible for a sample on the manipulator; there are three linear motions (x,y,z) and two rotations (T and R) [48].

In   Out

Cooling water

Filament 2   Filament 1

Anode face 2   Anode face 1
(Magnesium)   (Aluminum)

Al window

(a)

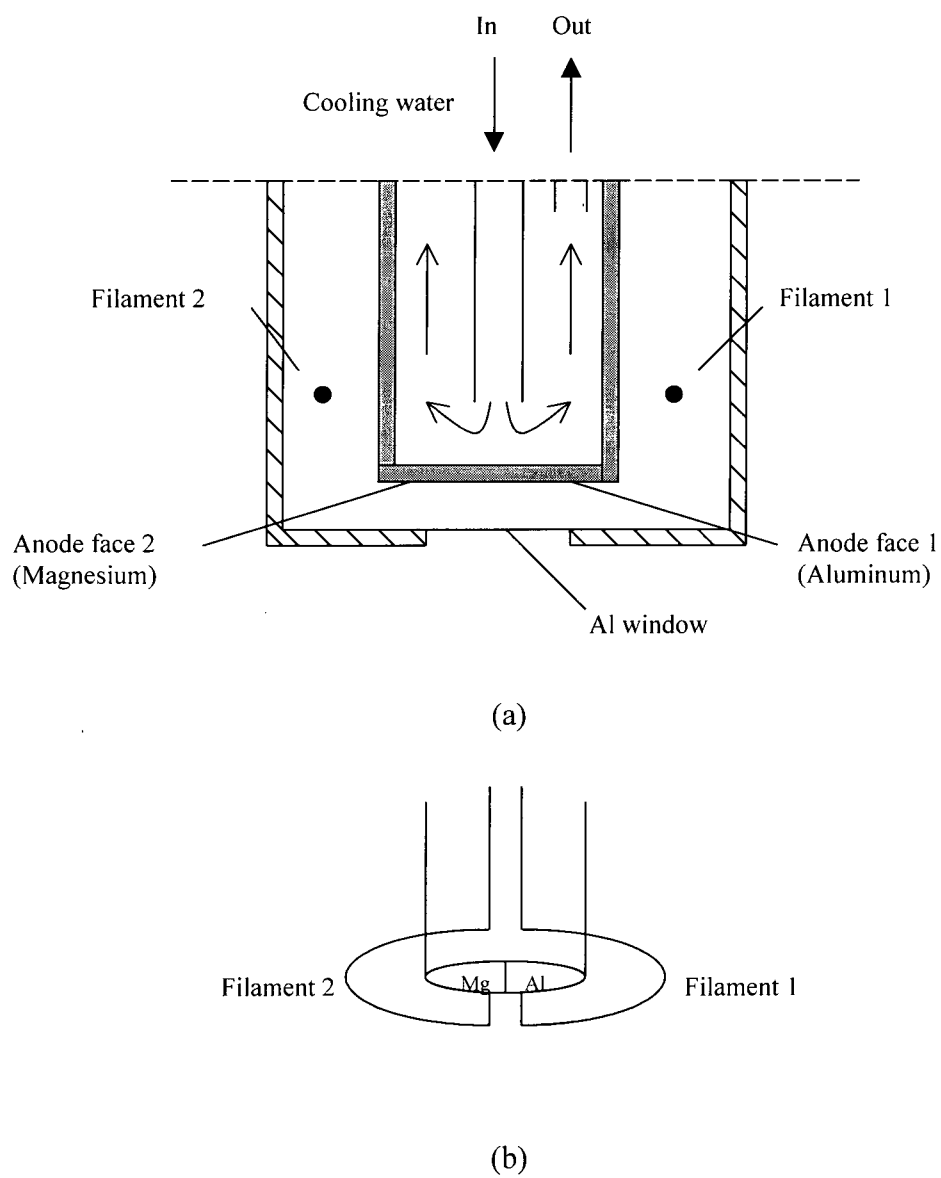Filament 2   Mg | Al   Filament 1

(b)

Figure 2.10 Schematic diagram of the Mg/Al dual anode x-ray source in

(a) and the associated filaments in (b) [64].

a change in the emitted radiation from MgKα and AlKα. The radiation passes to a sample in the analytical chamber through an aperture that is covered with a 2-μm thick Al foil window. This window prevents stray electrons, radiative heating and contamination from the anode region reaching the sample, but the material and thickness of the window allows the MgKα and AlKα radiation to pass without appreciable loss in intensity. Generally, the X-ray source is operated at 10 kV and 20 mA. The body of the anode is made of copper to ensure a good thermal conductivity and it is cooled by a deionized water system.

2.4.4 Electron Energy Analyzer

The EA 200 energy analyzer used in the Leybold MAX200 spectrometer consists of three main components, the input lens system, the concentric hemispherical analyzer (CHA) and the multichannel detector (MCP) [48]. Figure 2.11 shows a schematic diagram for this analyzer.

The input lens system has two stages. The first lens stage with a variable angular aperture A_1 and image aperture A_2 controls the analysis area (spot size) and acceptance angle (Ω) for the input electron image. The second lens stage controls the entrance angle (α) for the electrons to enter the analyzer by A_3. It not only focuses the selected electron image which just passed through A_2 onto the slit S_1 but also acts to retard the electron energy to a particular pass energy E_0.

The CHA has two concentric hemispherical electrodes with inner radius R_1 and outer radius R_2. A deflecting potential ΔV is applied on the electrodes making the outer one negative and the inner one positive [48]. For an electron with charge e and kinetic
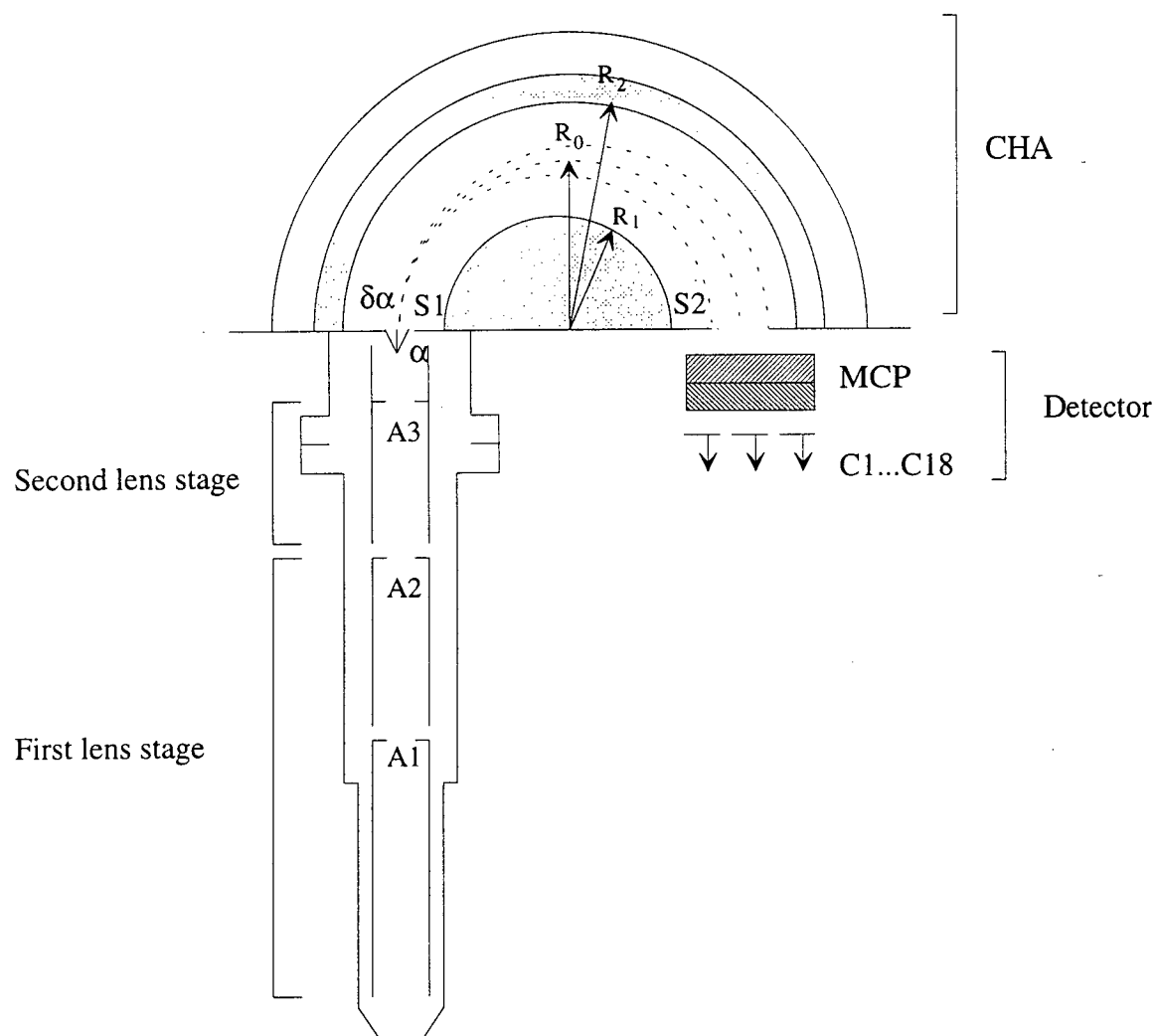
Figure 2.11 A schematic diagram for the concentric hemispherical analyzer (CHA).

energy E_0 to travel on the central circular orbit of radius R_0, where $R_0 = (R_1 + R_2)/2$, and pass through the exit slit of the analyzer, the following equation must be satisfied:

$$e\Delta V = E_0 (R_2/R_1 - R_1/R_2) \qquad (2.8)$$

Kinetic energy scanning is therefore possible by changing ΔV continuously. With an entrance angle of α, the relative resolution of the analyzer $\Delta E_{analyzer}$ is given by:

$$\Delta E_{analyzer}/E_0 = w/2R_0 + \alpha^2/4 \qquad (2.9)$$

where w is the slit width (equal at the entrance and exit) [48]. Since w, R_0 and α are limited by the spectrometer construction, the relative resolution of the spectrometer varies with the pass energy E_0, but two additional factors are involved in the experimental resolution for a photoelectron peak (the full width at half maximum (FWHM)). These other two factors are associated with the natural line width of the X-ray source (ΔE_{source}) and the inherent line width of the atomic level involved (ΔE_{line}). The observed peak width is given by:

$$\Delta E_{peak} = (\Delta E^2_{source} + \Delta E^2_{analyzer} + \Delta E^2_{line})^{1/2} \qquad (2.10)$$

provided that all contributions have the Gaussian line shape [48].

The pass energy E_0 is chosen according to the level of resolution needed, and the deflecting potential of the analyzer (ΔV) is set from Eq.(2.8) for the particular E_0. The retarding field voltage during the pre-retardation process is then ramped to do the actual scanning of the kinetic energies. Electrons with higher or lower kinetic energies than E_0 will be deflected and unable to reach the detector. According to Eq.(2.9), a lower pass energy gives a better analyzer resolution, but the signal intensity drops off rapidly with retardation. Therefore, for each situation, appropriate pass en.ergy is chosen to give the optimal balance between resolution and intensity. In this work, all the survey scan spectra were measured with the pass energy set at 192 eV.

Electrons with energies slightly different from the pass energy can still pass through the analyzer. Those that enter S_1 at an angle $\delta\alpha$ to the tangential direction travel along nearly by circular trajectories, and at S_2 reach further inside or outside the circular orbit of radius R_0. This offers the possibility of using multichannel plate (MCP) detection for the simultaneous recording of an energy band around E_0. In the EA 200, a set of two MCPs is used in a chevron arrangement (Fig. 2.11), and this leads to amplification in the electron signal by about 10^7. Each MCP is an array of 18 capillary-type microchannels, each of which acts as an individual electron multiplier. The plates are assembled with their channel angles in opposition in order to suppress feedback by trapping ions at the interface between the two plates.

As illustrated in Fig. 2.12, the kinetic energy of a photoelectron measured in the spectrometer (E'_k) is referenced to the spectrometer's vacuum level, while the binding energy of the electron inside the sample (E_b) is referenced to the Fermi energy of the sample. For a conducting sample in electrical contact with the spectrometer, so the Fermi energies are equal, the energy balance equation is

$$E'_k = h\nu - E_b - W_{sp} \hspace{3cm} (2.11)$$

and this can be seen as a modification of Eq. (2.1) by including W_{sp}, the spectrometer work function. It is determined by calibrating with standard samples, and it is generally constant for different measurements as long as the spectrometer is not changed in some way (e.g. exposing to atmosphere pressure). The spectra reported in this thesis were referenced to the Au $4f_{7/2}$ line at a binding energy of 84.0 eV. Consequently, from Eq. (2.11), E_b can be deduced from measurements of E_k' [64].
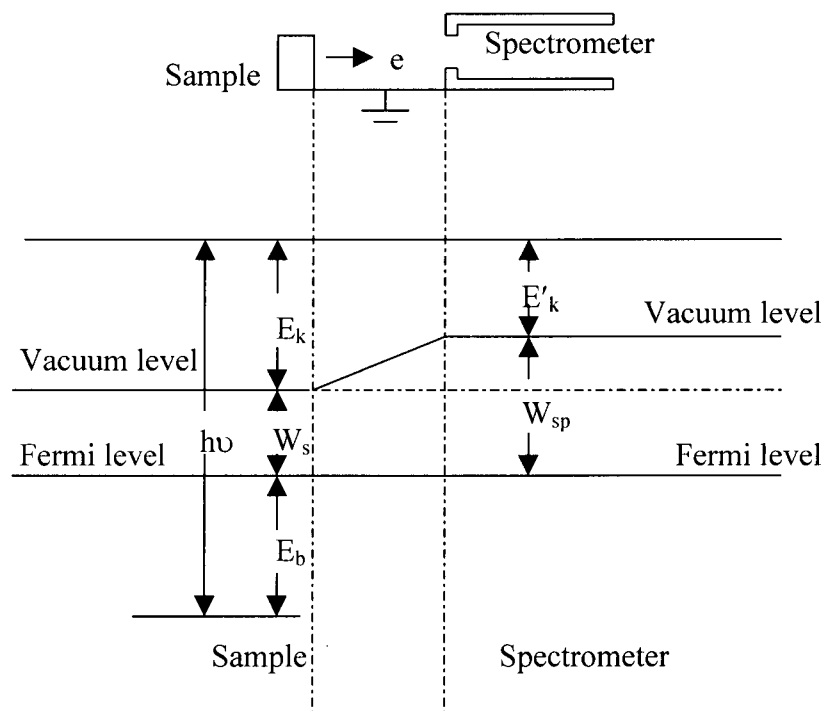
$h\nu$ = energy of the photon

W_{sp} = work function of spectrometer (i.e. energy difference between the Fermi level and vacuum level)

W_s = work function of sample

E_k = kinetic energy of photoelectron with respect to vacuum level of sample

E'_k = kinetic energy of photoelectron measured by the spectrometer

E_b = binding energy of electron in solid with respect to the Fermi level

Figure 2.12 Reference levels for a metal sample and spectrometer in electrical contact.

2.5 Scanning Electron Microscopy

2.5.1 Introduction

The scanning electron microscope (SEM) was commercially introduced in the mid-1960s, although the basic construction was proposed as early as 1935 [65]. The basic SEM method involves scanning a surface of a solid sample in a raster pattern with a beam of energetic electrons. A raster is a scanning pattern in which an electron beam is (1) swept across a surface in a straight line (the x direction), (2) returned to its starting position, and (3) shifted downward (the y direction) by a standard increment. This process is repeated until a desired area of the surface has been scanned. During this scanning process, the impinging electrons generate secondary electrons and the number ejected from any given point is determined by the composition of the sample at that point and the angle at which the beam strikes. The stream of secondary electrons, which is constantly varying according to the nature of the surface the beam is scanning, is picked up by a signal detector above the surface (the z direction), amplified, and stored in a computer system, where it is converted to an image [66]. By this means, SEM can provide important information about the structure and morphology of a surface. In the most recent instrumentation, spatial resolution has been increased by using a finely focussed beam from a field emission electron gun [65]. Modern SEM instrumentation can resolve detail to approximately 3 nm, and this corresponds to a magnification of about 300,000 times.

2.5.2 Instrumentation

The SEM images reported in this thesis were measured in a Hitachi S4100 scanning electron microscope, for which a sectional view is shown in Fig. 2.13. The chamber is diffusion pumped to give a vacuum of around 10^{-6} mbar, and a sample is mounted on a conductive substrate in the sample stage of the microscope. This stage allows several linear movements and it provides an electrical pathway to ground.

The main analyzing components of the SEM are illustrated in Fig. 2.14, and they include the electron gun, condenser lenses, deflection coils, detector and a cathode-ray tube (CRT). The electron gun and magnetic lenses are used to produce and direct an electron beam on to the sample. The electron gun contains a filament, and a shield with aperture and anode. Electrons are produced from the filament by the thermionic effect, and they are accelerated through about 30 kV applied between the filament and the anode. The shield, which is a slightly biased cylindrical cap, collimates those electrons. Then the electron beam is focused from a diameter of about 25,000 Å to 30 Å by the condenser lenses, and directed on to the sample [65]. The maximum lateral resolution in SEM is determined by the beam diameter.

The deflection coils scan the electron beam across the sample. At the same time, the detector, with its scintillator and photomultiplier, collects the secondary electrons emitted from each region of the sample surface. The amplified images are then displayed on the screen of a cathode-ray tube (CRT) and these electron micrographs can be photographed for permanent record.
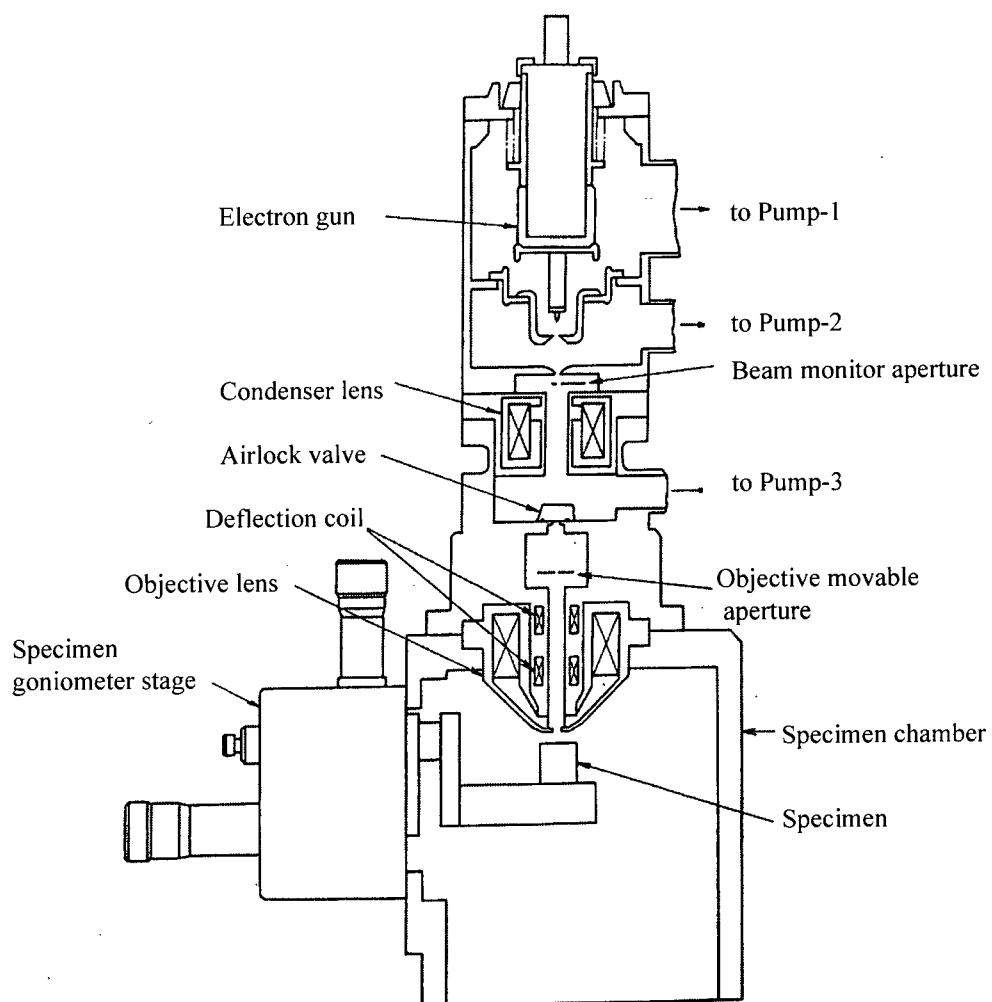
Electron gun — ▸ to Pump-1

▸ to Pump-2

Beam monitor aperture

Condenser lens

Airlock valve — ▸ to Pump-3

Deflection coil

Objective movable
aperture

Objective lens

Specimen
goniometer stage

Specimen chamber

Specimen

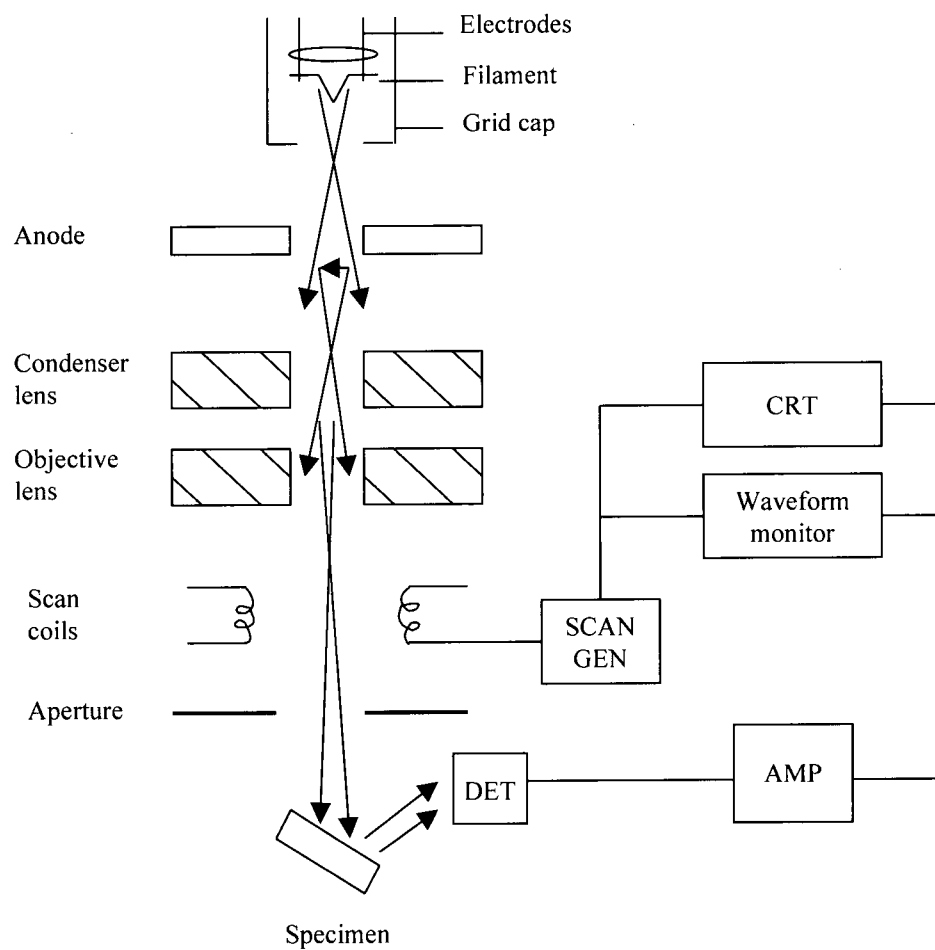Figure 2.13 Sectional view of Hitachi S4100 SEM [67].

Figure 2.14 Schematic diagram showing the main components of the SEM [65].

Chapter 3 Conditions for Zinc Phosphating on 6061-T6 Al Alloy

3.1 Introduction

Previous phosphating studies in this laboratory were involved with 7075-T6 aluminum alloy, which has the following minority components (wt%): 6% Zn, 3% Mg, 2% Cu, 0.5% Fe, 0.4% Si, 0.3% Mn and 0.2% Ti. The phosphating bath developed has the basic composition of 16.0 ml H_3PO_4 (85%), 5.36g ZnO and 0.5g NaF per liter. Optimal conditions were indicated with dipping at 65-75°C and spraying at 85°C [7,11,68], but addition of an accelerator was needed in the latter case. The present study focuses on finding conditions for forming zinc phosphating coatings by dipping for 6061-T6 aluminum alloy, which has the minority components (wt%): 0.25% Zn, 0.8-1.2% Mg, 0.15-0.4% Cu, 0.7% Fe, 0.4-0.8% Si, 0.15% Mn, 0.15% Ti and 0.04-0.35% Cr. Since the compositions of these two alloys are different, the solution used for the 7075-T6 alloy may not be best for the 6061-T6 alloy, but that does provide a solution for initial investigation of the zinc phosphating process for this second alloy.

Throughout this work, SEM and XPS surface analyses are employed to characterise the coatings formed by the different phosphating procedures investigated. The details for these surface characterisations were specified in Chapter 2.

3.2 Experimental Procedure

Studies were done on square 6061-T6 Al alloy panels (1x1x0.12 cm^3) which were first mechanically polished with Al_2O_3 sandpaper (1200 grit) and deionized water, and then degreased with acetone and methanol in an ultrasonic bath for 1 min, dried in air and

dipped in an acid etching solution (25 ml H_2SO_4 (98%) + 25 ml H_2O) for 2 min at 40°C. The sample panels were then dipped into the phosphating solutions for the conditions specified below. After dipping, each sample was rinsed with deionized water and air-dried. Six different zinc phosphating solutions were used for the experiments in this chapter. The first is designated solution 1 (16.0 ml H_3PO_4 (85%), 5.36 g ZnO and 0.5 g NaF per liter) and it was used for assessing effects of dipping time and temperature of the coating bath. For assessing the effects of fluoride concentration, coating solutions 1 to 6 were employed. These six solutions contain common amounts of H_3PO_4 (85%) and ZnO, but the amounts of NaF per litre are 0.5 g, 0.3 g, 0.9 g, 1.4 g, 1.8 g and 2.3 g for solutions 1, 2, 3, 4, 5 and 6 respectively. The specific coating procedures used for each sample in this study are listed in Table 3.1, and Fig. 3.1 shows a flow chart to summarize the preparation and coating procedures used.

Table 3.1 Coating procedures for each sample.

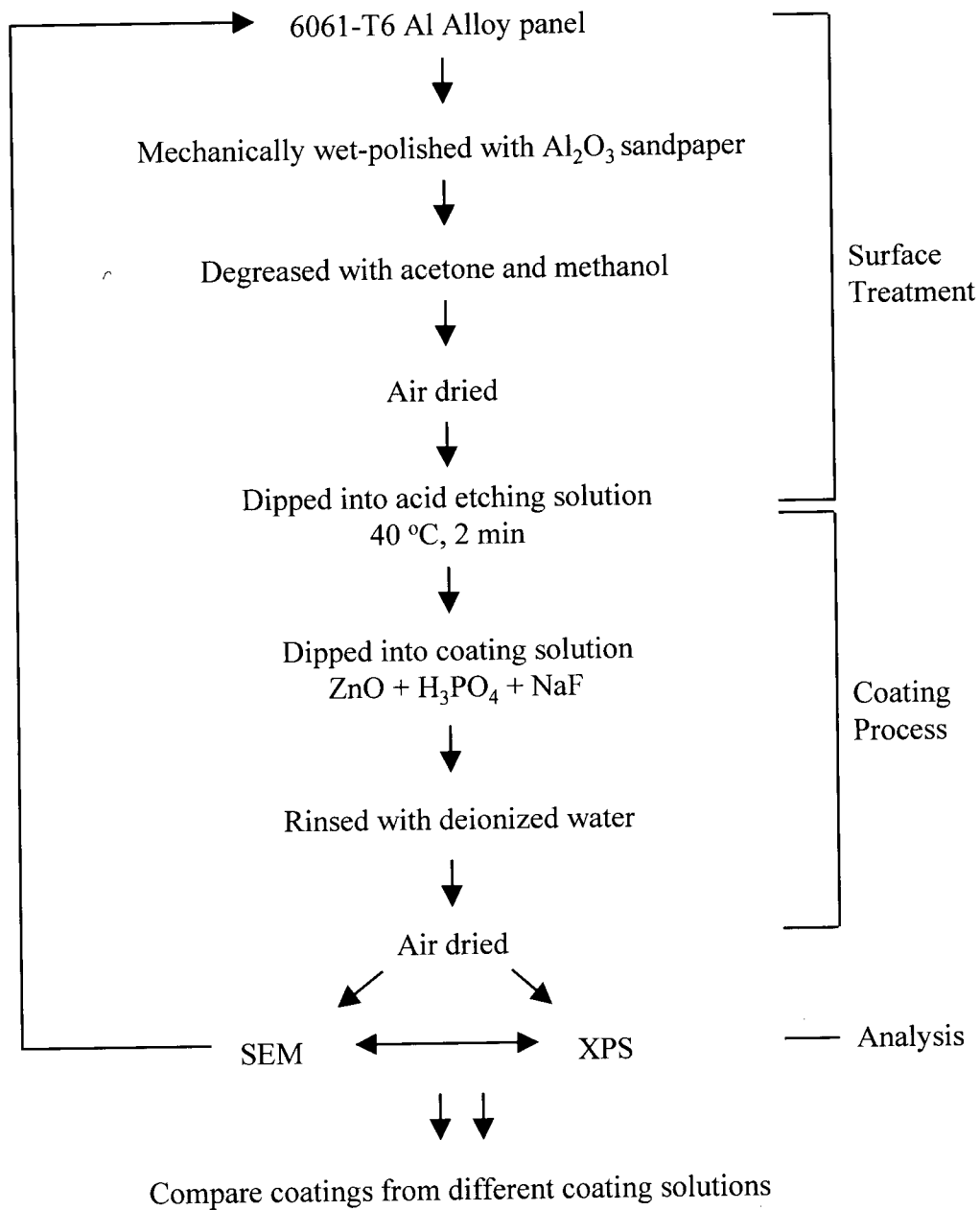| Sample	Treatment
A_1 to A_9	Dipping in solution 1 at 60 °C for 0.5,1,3,4,5,6,7,9 and 10 min
A_{10} to A_{12}	Dipping in solution 1 for 3 min at 40 °C, 60 °C and 80 °C
B_1 to B_6	Dipping for 3 min at 60 °C in solutions 1,2,3,4,5 and 6

3.3 Results

3.3.1 Effect of Phosphating Time

6061-T6 Al Alloy panel

↓

Mechanically wet-polished with Al_2O_3 sandpaper

↓

Degreased with acetone and methanol

↓

Air dried

↓

Dipped into acid etching solution
40 °C, 2 min

↓

Dipped into coating solution
$ZnO + H_3PO_4 + NaF$

↓

Rinsed with deionized water

↓

Air dried

Surface Treatment

Coating Process

SEM ←→ XPS — Analysis

↓↓

Compare coatings from different coating solutions

Figure 3.1 Flow chart for the preparation and coating procedures.

Results in this section apply to samples A_1 to A_9 defined in Table 3.1. The objective is to determine the effect of different dipping times on the resulting coating compositions and morphologies. Figures 3.2 (b) to (i) show scanning electron micrographs of the coatings formed on the 6061-T6-Al alloy surface after different times in the phosphating bath. For comparison, Fig. 3.2 (a) shows the surface morphology of a blank sample (i.e. after polishing and degreasing but no dipping in phosphating solution). The surface of the blank sample is rough with the polishing scratches clearly detectable. Figure 3.2 (b) shows only small particles (about 0.5 μm) present on the surface after 30 s, and they grow especially along the scratches. At longer immersion times, the coated particles transform into larger crystals with a flaky appearance (about 1 to 10 μm), and the coverage also increased. It seems that the small initial particles are precursors for formation of phosphated crystals, and the incubation time required for these films to form on aluminum appears quite short (within 30 s). However, the size of the crystals stopped growing, and the coverage on the surface stopped increasing, after phosphating for 6 min. Beyond that time, the SEM results in Figs 3.2 (g) – (i) show that the coated crystals reduce in size. Indeed the crystals on the sample appear to be dissolving when the sample was in the phosphating bath for 9 min. After 10 min, there were only a few, small, coated particles left on the aluminum surface, and this supports the view that the etching process has become dominant.
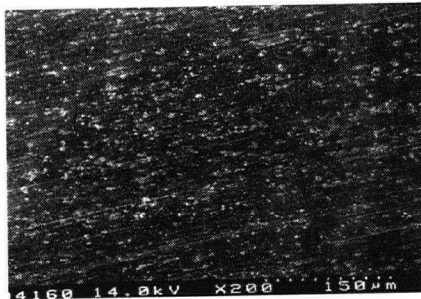
To identify changes on the aluminum surface during the phosphating process, XPS was used to characterize the surface compositions of the samples. Figure 3.3 shows XPS survey scans for (a) a sample after polishing and degreasing, (b) a sample after polishing, degreasing and acid etching, and (c) sample A_6 after 6 min in the coating bath. Aside
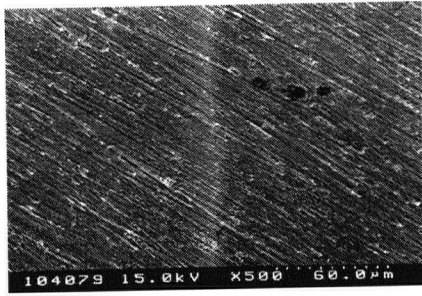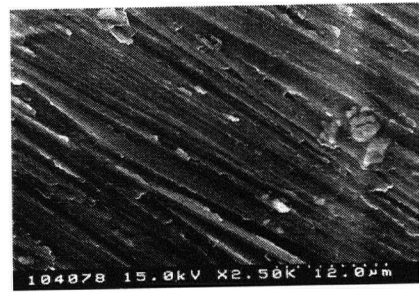
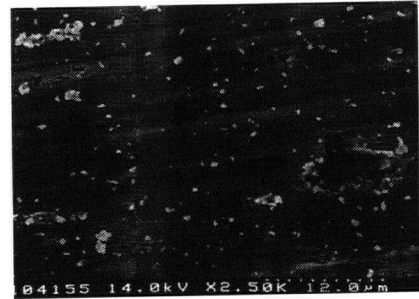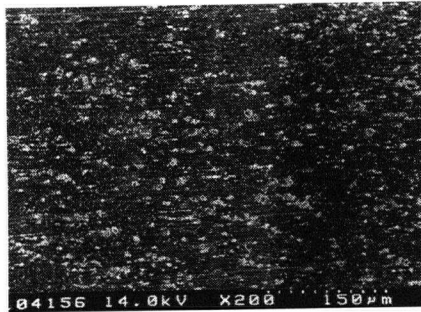(a)   Blank (x500)   Blank (x2500)
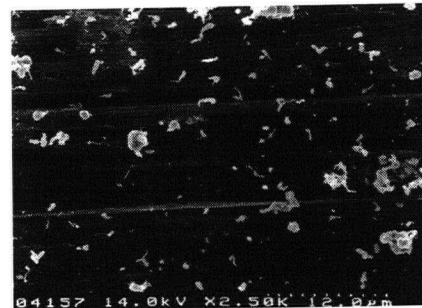
(b)   0.5 min (x200)   0.5 min (x2500)
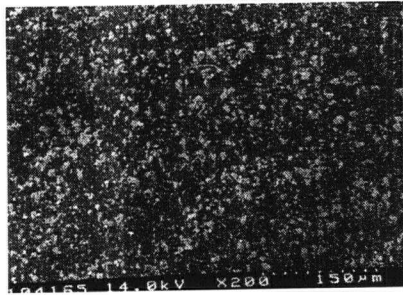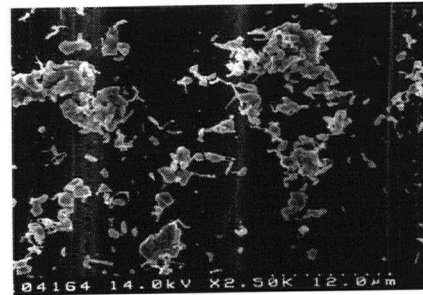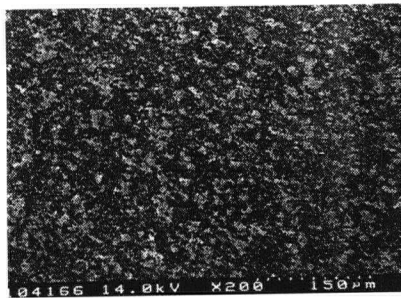
(c)   1 min (x200)   1 min (x2500)

Figure 3.2 SEM micrographs for different phosphating times; in each case
the right hand micrograph is at higher magnification.

50
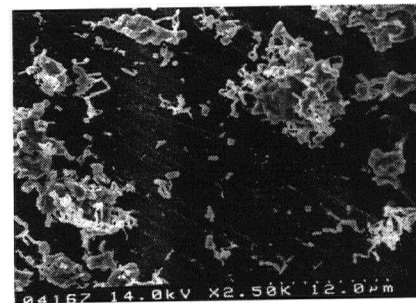
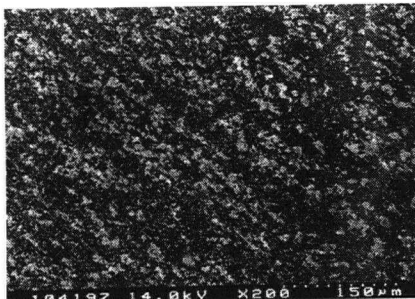(d)   3 min (x200)   3 min (x2500)
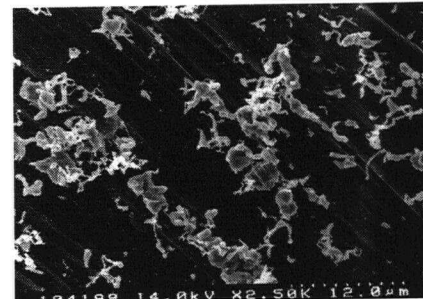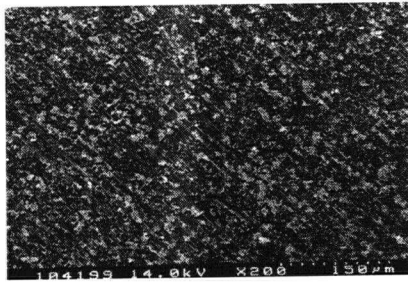
(e)   5 min (x200)   5 min (x2500)
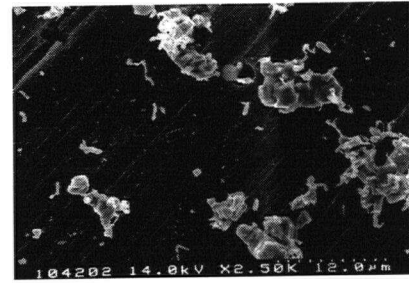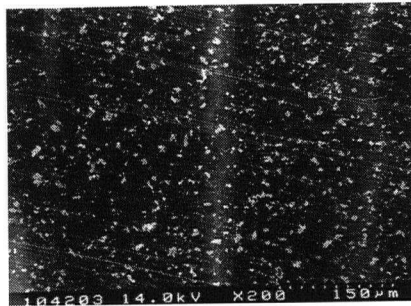
(f)   6 min (x200)   6 min (x2500)

Figure 3.2 Continued.

51

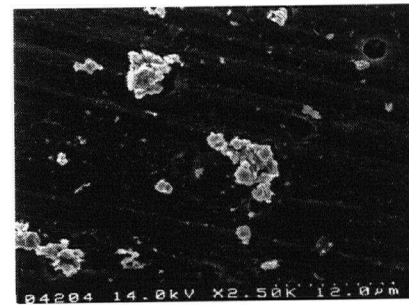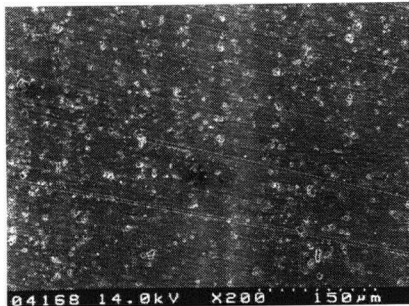(g)   7 min (x200)   7 min (x2500)
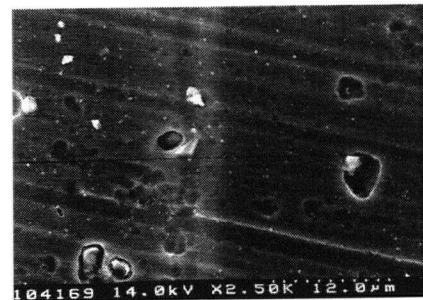
(h)   9 min (x200)   9 min (x2500)
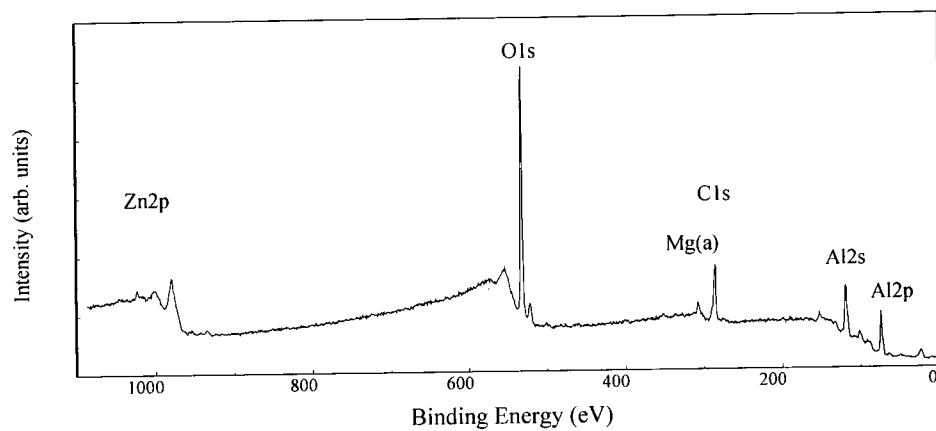
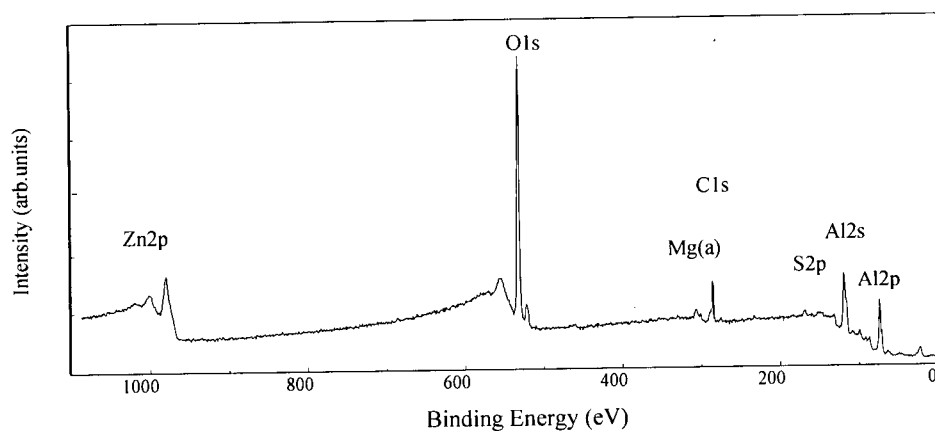(i)   10 min (x200)   10 min (x2500)
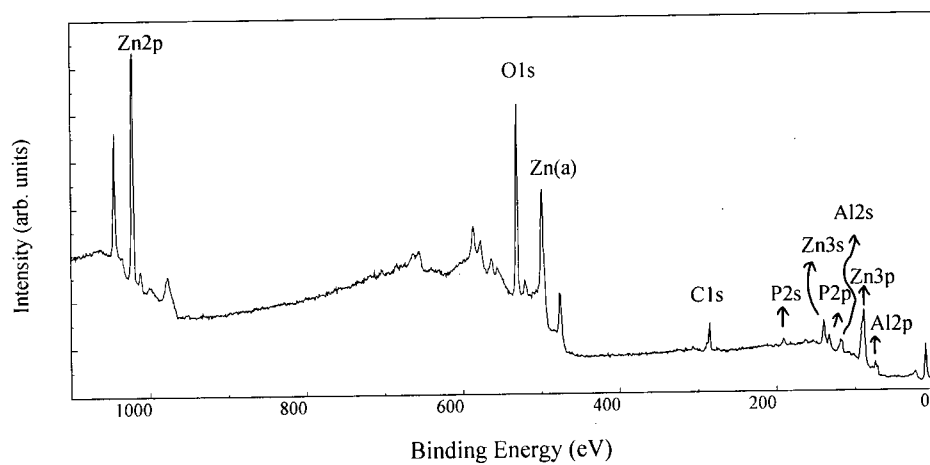
Figure 3.2   Continued

(a)

(b)

(c)

Figure 3.3 XPS survey scan spectra for 6061-T6 Al alloy: (a) after polishing; (b) after acid
etching; (c) after 6 min in phosphating bath (solution 1).

from some contamination by adventitious carbon, Al in its metallic and oxide forms was the main element detected after polishing (Fig. 3.3a), although small Zn and Mg peaks were observed, and these originate from the secondary components in the alloy (mainly Zn). After acid etching, a very small S peak was detected, and this indicates the presence of some residue left from this etching (Fig. 3.3b). After phosphating for 6 min, the Zn peak became larger and the P peak became established (Fig. 3.3c).

Table 3.2 summarizes the compositions indicated by XPS for coatings on 6061-T6-aluminum alloy after phosphating with solution 1 at $60^{\circ}C$ for different times. After phosphating, the surfaces contain Zn, O, C, P and Al. For the blank, XPS shows an atomic ratio Zn/Al = 0.03 (the bulk consists of 0.25% (wt) corresponding to an atomic ratio of 0.14). This is different from the 7075-T6 Al alloy which has 6% (wt) Zn in the bulk. After phosphating on 7075-T6 Al alloy, a part of the Zn in the final coating layer came from the bulk. However, most of the Zn in the coating layer of 6061-T6 Al alloy came from the coating solution. The data in Table 3.2 shows the phosphating process has an obvious trend: the phosphate coating is established after 30 s, continues to grow for 6 min, then starts to disappear. From sample A_1, the ratio of P/Al and (Zn+P)/Al increased with increasing phosphating time. After phosphating for 6 min, the ratios maximize, and it can be concluded that the coverage of zinc phosphate is optimized. The ratios decrease for phosphating times greater than 6 min, and at 10 min, the (Zn+P)/Al ratio has reduced to only 0.1, so indicating that little zinc phosphate is left on the aluminum surface, and this is qualitatively similar to the SEM observations.

3.3.2 Effect of Phosphating Temperature on Coating Morphology and composition

Table 3.2 XPS results for 6061-T6 Al alloy dipped in solution 1 at 60°C for different times.

Time (min)	Zn/Al	P/Al	(Zn+P)/Al
0.5	0.29	0.06	0.36
1	0.33	0.11	0.45
3	0.59	0.26	0.85
5	0.90	0.27	1.17
6	0.96	0.34	1.30
7	0.96	0.28	1.24
9	0.73	0.07	0.80
10	0.03	0.07	0.10

Table 3.3 XPS results for 6061-T6 Al alloy dipped in solution 1 for 3 min for different phosphating temperatures.

T(°C)	Zn/Al	P/Al	(Zn+P)/Al
40	0.22	0.15	0.38
60	0.56	0.24	0.80
80	0.72	0.10	0.82

Table 3.4 XPS results for 6061-T6 Al alloy dipped for 3 min in solutions with different F⁻ concentrations.

| F⁻(ppm)	Zn/Al	P/Al	(Zn+P)/Al
150	0.41	0.21	0.62
210	0.67	0.31	0.99
400	1.02	0.46	1.47
600	1.19	0.50	1.69
800	2.03	0.76	2.79
1000	†	†	†

† Coating is so thick that no Al can be detected by XPS

55

To find out how the phosphating temperature influences the coating properties, three phosphating temperatures were studied. They are 40°C, 60°C and 80°C (sample A_{10}, A_{11} and A_{12}). Figure 3.4 (a) to (c) shows scanning electron micrographs from samples phosphated at these three temperatures. No white crystalline grains can be found on the surface of the sample phosphated at 40°C. The surface of that sample only shows some holes resulting from acid etching. There are many white crystalline grains distributed on the surfaces phosphated at 60°C and 80°C. Samples A_{11} and A_{12} have similar amounts of the white crystalline grains, but the grain size is smaller with sample A_{12} (i.e. phosphated at 80°C). From SEM observations, it appears that there is not a big difference in the grain size for 60°C and 80°C. The coverage at 80°C maybe higher but the coating is less well adhered. In general, all factors being equal lower temperatures are favored on grounds of energy consumption. Therefore, 60°C is at this stage seen as an optimal temperature for this process.

Data from measured XPS survey scan spectra are listed in Table 3.3. A very low (Zn+P)/Al ratio is observed for sample A_{10}, which is phosphated at 40°C. Larger values of this ratio are indicated for the samples phosphated at 60°C and 80°C. The phosphating temperature does not appear to change the basic composition of the coated surface, but the coverage of zinc phosphate is affected by the phosphating temperature.

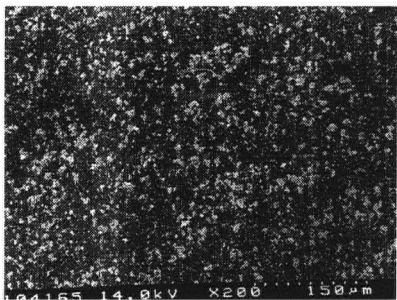### 3.3.3 Effect of F⁻ Concentration on Coating Morphology and Composition

Previous work on the phosphating of 7075-T6 aluminum alloy shows that the addition of F⁻ to the coating solution increases the proportion of zinc phosphate in the coating compared with aluminum phosphate [9]. In this work, a similar comparison was
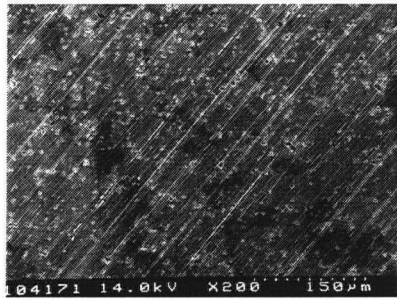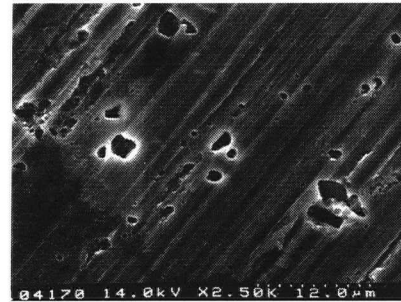
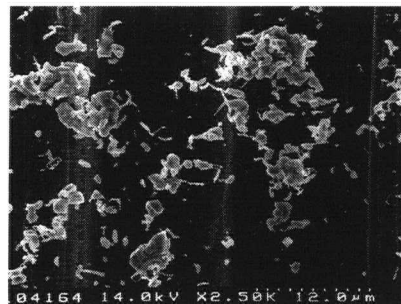(a)   40 °C (x200)   40 °C (x2500)
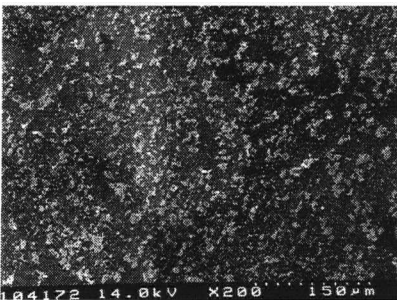
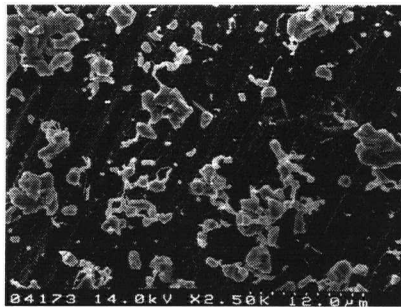(b)   60 °C (x200)   60 °C (x2500)

80 °C (x200)   80 °C (x2500)
(c)

Figure 3.4   SEM micrographs for different phosphating temperatures; in each case the right hand micrograph is at higher magnification.

made between coatings formed on hand-polished 6061-T6 aluminum panels. The sample treated by the coating solution without F^- showed a P/Al ratio of 0.04% and it was concluded that almost no zinc phosphate formed on the aluminum surface. Effective phosphating therefore appears to require F^- in the coating solution, but more details on the effect of variation in the F^- concentration are needed.

The effect on coating morphology and composition was studied for seven different F^- concentrations (Table 3.1) which correspond to B_0 (no F^-), B_1 (150 ppm F^-), B_2 (210 F^- ppm), B_3 (400 ppm F^-), B_4 (600 ppm F^-), B_5 (800 ppm F^-) and B_6 (1000 ppm F^-). 6061-T6 Al samples were dipped in the solutions (Section 3.2) at 60°C for 3 min. For the blank sample B_0, no crystals were found on its surface after dipping and no P could be detected in its XPS spectrum. This again shows the necessity to have a certain concentration of F^- in the phosphating bath. Figure 3.5 (a) – (f) shows variations in coating morphology in relation to the amount of fluoride in the coating solution. The coverage of zinc phosphate on the aluminum surface appears to increase with fluoride concentration added to the phosphating solution. For sample B_1, only a few white crystalline grains could be found on the coated surface (Figure 3.5 (a)). When the concentration of F^- increased to 600 ppm, the white crystals covered almost all of the Al alloy surface, but multilayers of white crystals appear to form with a continued increase in the F^- concentration.

Table 3.4 indicates compositions from XPS survey scan spectra measured on these coated samples. Small Auger peaks of F can be detected for samples B_4, B_5 and B_6. The P/Al and Zn/Al ratios are all indicated to increase with increasing F^- concentration. When the concentration of F^- reached 1000 ppm, no Al could be detected by XPS; that indicates the coating layer covers the whole surface and is very thick.
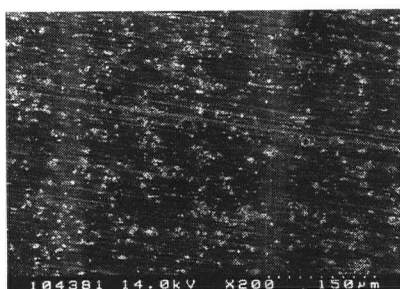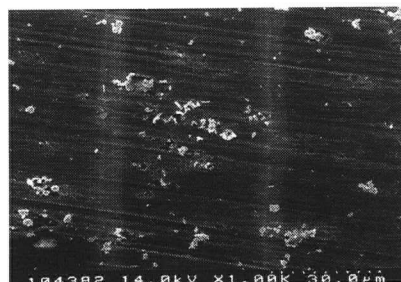
(a)   150 ppm F⁻ (x200)   150 ppm F⁻ (x1000)
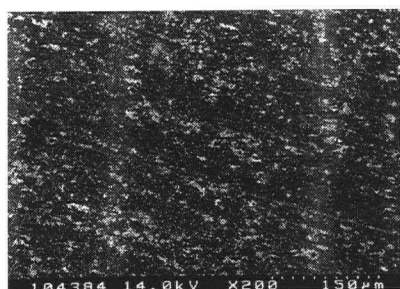
(b)   210 ppm F⁻ (x200)   210 ppm F⁻ (x1000)

(c)   400 ppm F⁻ (x200)   400 ppm F⁻ (x1000)

Figure 3.5 SEM micrographs of samples with different F⁻ concentration; in each case the right hand micrograph is at higher magnification.

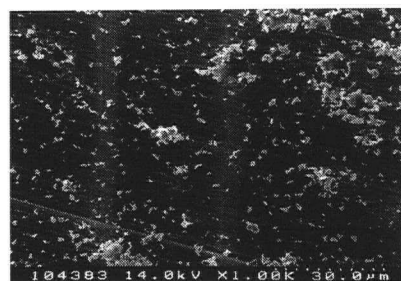(d)   600 ppm F⁻ (x200)   600 ppm F⁻ (x1000)
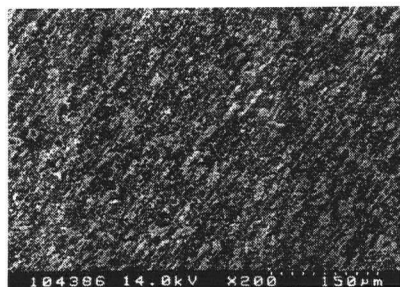
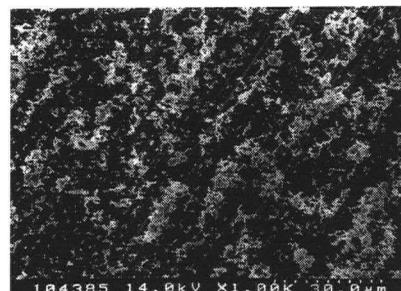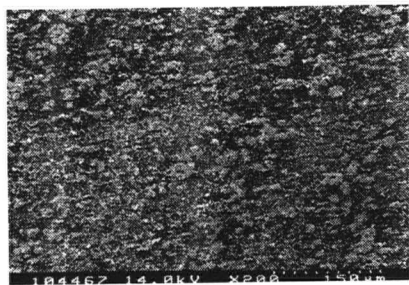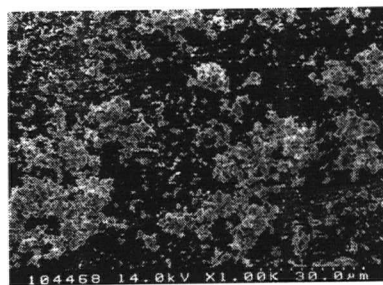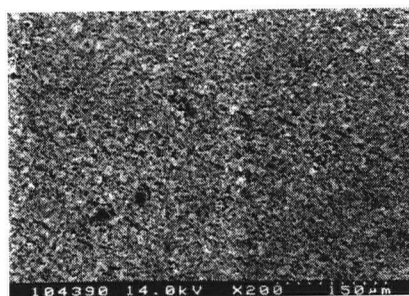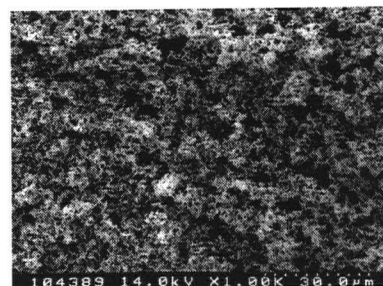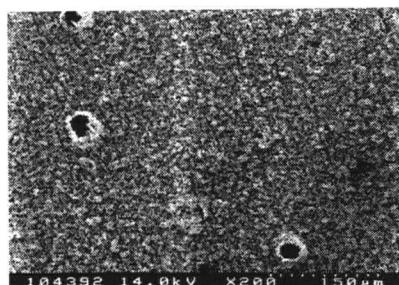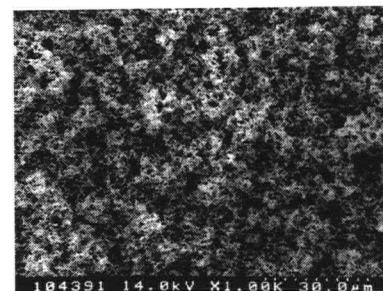(e)   800 ppm F⁻ (x200)   800 ppm F⁻ (x1000)

(f)   1000 ppm F⁻ (x200)   1000 ppm F⁻ (x1000)

Figure 3.5 Continued.

3.4 Discussion

3.4.1 Zinc Phosphating Mechanism

The following equations summarize the mechanistic reaction paths that are believed to operate for Al alloys in zinc phosphating coating baths [69]:

$$Al_2O_3 + 6H^+ \rightarrow 2Al^{3+} + 3H_2O \qquad (3.1)$$

$$2Al + 6H^+ \rightarrow 2Al^{3+} + 3H_2\uparrow \qquad (3.2)$$

$$Al^{3+} + 6F^- \rightarrow AlF_6^- \qquad (3.3)$$
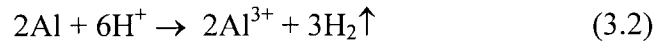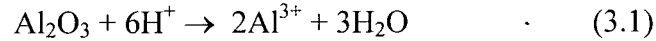
The consumption of H^+ results in an increase in pH at the interface between the aluminum alloy and the solution. That decrease in H^+ concentration helps drive the coating reactions [69]:

$$3Zn^{2+} + 2H_2PO_4^- \rightarrow Zn_3(PO_4)_2\downarrow + 4H^+ \qquad (3.4)$$
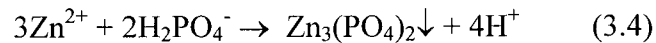
This results in zinc phosphate crystals being deposited on the aluminum alloy surface, but some sludge of Na_3AlF_6 can be formed at the same time.

$$Al^{3+} + 6F^- + 3Na^+ \rightarrow Na_3AlF_6\downarrow \qquad (3.5)$$
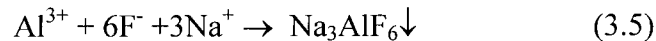
In general for this study, it is assumed that the phosphating process on the 6061-T6 aluminum alloy has two simultaneous reactions: one for phosphating reaction and one for etching reactions. The various steps in the process can be summarized as follows:

1) The aluminum alloy is etched in the phosphating bath.

2) Zinc phosphate nucleates on the aluminum surface.

3) Crystalline and amorphous zinc phosphate grows over the aluminum surface, while etching occurs at a lower rate.

4) The zinc phosphate dissolves as the etching reaction starts to dominate the whole process. Eventually no zinc phosphate is left on the surface.

This situation contrasts with that observed in the phosphating of zinc and steels with different phosphating recipes. Gaarenstroom and Ottaviani [70] did not indicate distinct stages in the phosphating of these metals with their recipes. However, distinct stages were observed in the process presented by Turuno and his coworkers in a study using their own recipe for zinc phosphating on aluminum alloy used for automobile bodies [71]. Both Cheng (phosphating on pure aluminum in a commercial zinc-manganese phosphating bath) [72] and Van Roy (phosphating on AA5754 aluminum alloy in a commercial zinc phosphating bath) [73] described phosphating processes that are similar to the steps 1) to 3) above. However, these latest authors did not indicate whether their phosphating layers eventually dissolved or not.

3.4.2 Phosphating Temperature

Before the experiments reported earlier in this Chapter, another series of experiments that studied the effect of phosphating time and temperature on the same alloy were also conducted on hand-polished samples. It was found that the phosphating process lasted for 7 min at 50°C, 7 min at 60°C, 5 min at 70°C and 4 min at 80°C, so indicating that the period of phosphating is shorter at higher operating temperatures. Presumably, this follows a common tendency for higher temperature to speed up reactions. However, a lower operating temperature is favored in practical zinc phosphating in order to save energy. Since the XPS and SEM results show that the sample coated at 40°C is not effective, 60°C is chosen as the favored temperature for zinc phosphating on 6061-T6 aluminum alloy using this particular coating solution and acid etching pretreatment.

3.4.3 F⁻ Concentration

By increasing the amount of fluoride in the zinc phosphating solution, the etching speed increased through reaction Eq. (3.3). This resulted in an increase in the pH of the aluminum alloy / solutions interface, and in turn the zinc phosphate precipitation coating increased through Eq. (3.4). Furthermore, previous results show that the presence of Al^{3+} ions in solution strongly act as an inhibitor to the zinc phosphating process, and this occurs for steel as well as aluminum [74-76]. Adding fluoride to the coating bath is a useful technique for complexing Al^{3+} ions, and this helps speed up the reaction and increase the coverage of the zinc phosphate coating on the aluminum surface. However, an excess of F⁻ can yield a precipitated sludge through Eq. (3.5).

Fig. 3.5 shows that the zinc phosphate crystals covered the surfaces for samples B_5 (800 ppm F⁻) and B_6 (1000 ppm F⁻), but the coating layers tend to be loose (i.e. they are easily peeled by Scotch tape). Sample B_6 even has some holes in the coating, apparently caused by hydrogen gas generated during the reaction. The coatings in samples B_5 and B_6 are not expected to have good adhesive ability when primers are added to the surfaces. Therefore F⁻ concentrations in the range from 400 ppm to 600 ppm appear to give most useful coatings when 6061-T6 Al alloy is phosphated with the recipe defined in Section 3.2. The loose coatings formed at by high F⁻ concentration appear to result from the effect of the $Na_3Al F_6$ sludge formed.

3.5 Conclusions

Behaviors for the zinc phosphating of 6061-T6 aluminum alloy were studied using SEM and XPS surface analyses, and the following conclusions are given for the work discussed in this Chapter:

1) Phosphating times were studied from 30 s to 10 min and it is clear that this parameter affects the coating morphology and composition. The ZnO_x-PO_4 coverage increased to maximum for the 6 min immersion, and then dropped to near zero. This indicates that the phosphating and etching processes are competing with each other during the whole process. The temperature of the phosphating bath also affects the coating morphology and composition. Higher temperature speeds up both competing reactions, and in general shorter immersion times are needed or higher temperatures. The optimum phosphating time and temperature for 6061-T6 aluminum alloy using this coating solution and acid etching are around 6 min and 60 $^{\circ}$C. However, 3 min was chosen as the basic condition in the following studies when accelerators are being tested.

2) The increasing amount of fluoride that added to the zinc phosphating solution is effective for increasing the coverage of zinc phosphating on the aluminum alloy. Fluoride does speed up the phosphating reaction. For our recipe, a concentration of F^- from 400 ppm to 600 ppm is preferred.

Chapter 4 Pre-treatments and Post-treatments

4.1 Introduction

Typical phosphating sequences usually include both pre-treatments and post-treatments. Pre-treatments provide a suitable substrate for the following coating step, while post-treatments help to seal any porosity in the coating layer and so enhance its anti-corrosion ability. In this work, two different mechanical polishing methods (by hand and with a mechanical polisher) were compared with an acid etching pre-treatment, as well as with a silane post-treatment. These treatments were compared through SEM, XPS and corrosion tests applied to phosphated layers coated on 6061-T6 Al alloy.

Since a typical aluminum alloy surface may have contaminants and scratches, some pre-treatment is generally needed prior to making a zinc phosphating treatment [1]. Hand polishing was done in the pre-treatments used in previous studies made in this laboratory. However, hand polishing has its shortcomings, because it is hard to get an even polishing. To improve on the previous approach, this work has therefore compared hand polishing with treatment by a mechanical polisher (Metaserv Polisher C200/5A) , as well as a pre-treatment that uses acid etching. Comparisons are made in this chapter on the effects of these different pre-treatments on the subsequent phosphating

It was found long ago that corrosion protection by phosphating coatings is greatly enhanced when the phosphate-coated metal is wetted with a dilute acid chromate rinse solution prior to paint application [78]. In addition, almost every proprietary phosphate coating process specifies a chromate rinse (referred to as a sealing rinse or a chromate seal). However, these chromate-sealing rinses have two disadvantages [79]. Hexavalent

chromium has been classified as a carcinogen, making it a substance that many people would rather avoid. Hazards exist both for skin exposure and for inhalation of vapors. The other problem is the liquids from the final rinse cannot be simply discharged without treatment, and those procedures are both costly and time-consuming.

These problems with chromate-sealing rinses spurred the development of nonchromium alternatives. Nearly all of these alternatives simplify the waste treatment, to avoid chromium's toxicity problems, but generally these alternatives do not provide the same degree of corrosion resistance as their chromated counterparts. The patent literature is replete with nonchromium alternatives. Many different ideas have been investigated. Some of the more prominent approaches utilize acid solutions containing molybdate ion; diphenolamines [80]; solutions using aluminum and zirconium [81]; morpholine; polyvinylphenol [82]; titanium chelates [83]; solutions containing water-reducible epoxy resins; and fluoride complexes.

This work investigates a new sealing rinse solution containing silane. Silanes are widely used with metals and their alloys to aid corrosion protection. As coupling agents, silanes have a general structural formula X_3SiY, where X is a hydrolysable group and Y is an organofunctional group capable of reaction with organic coatings. They act to increase the adhesion between the metal surface and an organic coating (i.e. paints) which is added later to give the protection. Many studies have been done on the details of the bonding between metals and silanes, including work in our group, but as far as we know, silanes have not been studied previously for the post-treatment rinsing. In principle, silanes may seal the porous phosphate coating by cross-linking to the aluminum or the phosphate coating itself. Therefore, studies were conducted on using

silane as a sealing reagent. Methyltriethoxysilane was chosen for this investigation since it has three EtO- groups and the chances of "catching" other molecular groups on the surface should be high. Further, the silane treatment was also investigated as an acceleration step between two phosphating immersions.

4.2 Mechanical Polishing and Acid Etching Pre-treatments

4.2.1 Sample Preparation

Table 4.1 indicates the preparation procedures conducted to form four coated samples (referred to as D_1, D_2, E_1 and E_2) on square 6061-T6 Al alloy (1 x 1 x 0.2 cm^3) sample panels. Each alloy sample was first mechanically polished with Al_2O_3 sandpaper (1200 grit) and deionized water by hand (40 times), or by mechanical polisher (Metaserv Polisher C200/5A) until it appears mirror-like. The mechanical polishing treatments were followed by degreasing with acetone and methanol in an ultrasonic bath for 1 min and drying in air. Samples E_1 and E_2 received an acid etching treatment after a mechanical polishing. This involved dipping into a solution of 25.0 ml H_2SO_4 (98%) and 25.0 ml H_2O at 40°C for 2 min. After the pretreatment procedures, each sample was coated by dipping into phosphating solution 1 (16.0 ml H_3PO_4 (85%), 5.36 g ZnO and 0.5 g NaF per liter) at 60°C for 3 min. Finally each coated sample was rinsed with deionized water (20s) and dried in air.

4.2.2 Results and Discussion

Figure 4.1 shows scanning electron micrographs measured for the four coated samples tested in this part of the project. These samples differ just in the pre-treatments

Table 4.1 Specification of pre-treatments and coating procedures used for 6061-T6 Al alloy samples (further details are given in Section 4.2.1 of text).
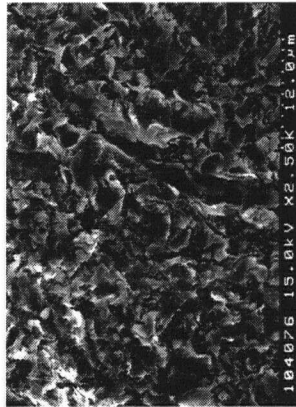
Sample code	Treatment
D_1	Hand polish, degreased, air-dried, dipped in solution 1 (3 min, 60°C), rinsed with deionized water, air-dried
D_2	Machine polish, degreased, air-dried, dipped in solution 1 (3 min, 60°C), rinsed with deionized water, air-dried
E_1	Hand polish, degreased, air-dried, acid etch, dipped in solution 1 (3 min, 60°C), rinsed with deionized water, air-dried.
E_2	Machine polish, degreased, air-dried, acid etch, dipped in solution (3 min, 60°C), rinsed with deionized water, air-dried.

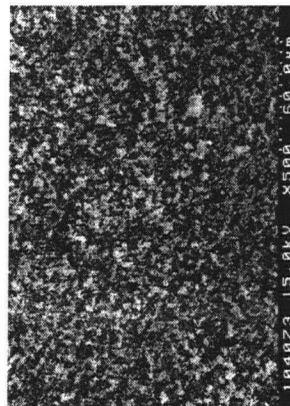Table 4.2 XPS data for samples given different pre-treatments.

Sample	Zn/Al	P/Al	(Zn+P)/Al
D_1	0.09	0.08	0.17
D_2	0.26	0.18	0.44
E_1	1.31	0.26	1.57
E_2	0.60	0.27	0.86

sample D_1(x500)

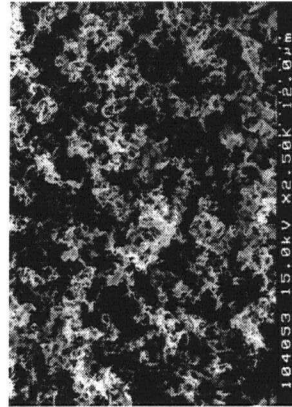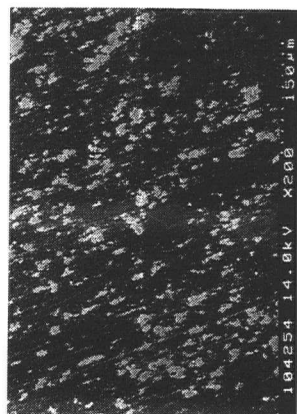(a)

sample D_1(x2500)
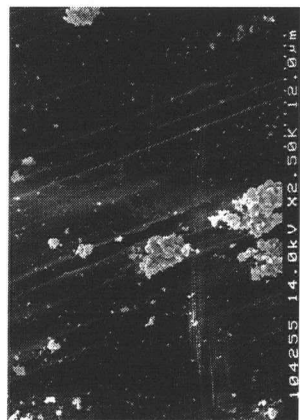
sample E_1(x500)

(b)
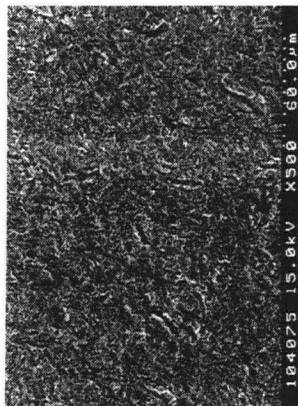
sample E_1(x2500)

Figure 4.1 Scanning electron micrographs for samples given different pre-treatments prior to the phosphating treatment specified in Section 4.2.1. The samples are defined in Table 4.1. In each case the right side micrograph is at higher magnification.
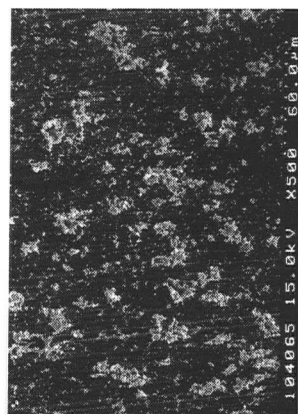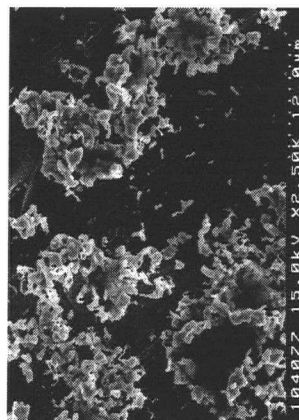
sample D$_2$(x2500)

sample D$_2$(x200)

(c)

sample E$_2$(x2500)

sample E$_2$(x500)

(d)

Figure 4.1 Continued.

applied. Considerable morphological differences are apparent between samples given a hand polish (D_1 and E_1) and those for which a mechanical polisher was used (D_2 and E_2). No white crystalline grains (i.e. crystalline grains that appear lighter in SEM images) are visible on the surface of sample D_1 (Fig. 4.1a), although white crystals are distributed on the surface of sample D_2 (Fig. 4.1c). With acid etching included in the pre-treatment, many smaller and thinner white crystals are detected on the surface of E_1, while sample E_2, which was polished by the mechanical polisher, has relatively bigger white crystals on the surface.

XPS survey scan data were measured for these four samples, and comparative composition information is listed in Table 4.2. Sample D_1, with hand polishing, shows low Zn/Al and P/Al ratios (0.09 and 0.08), while sample D_2, for which the mechanical polisher was used, shows higher values for these ratios (0.26 and 0.18 respectively). Such observations are consistent with the SEM results (Fig. 4.1) as higher Zn/Al and P/Al ratios indicate more coating on the surface. For samples given an acid etch pre-treatment, data in Table 4.2 indicate that sample E_1 (hand polish) has a very high Zn/Al ratio (1.31), although its P/Al ratio (0.26) is similar to that of sample E_2 (machine polish). It appears hand polishing leads to more zinc phosphate coating than for machine polishing in the pre-treatment, and this arises because the first surface is rougher with more nucleation sites. However, the acid etching pre-treatment appears to increase especially the Zn content.
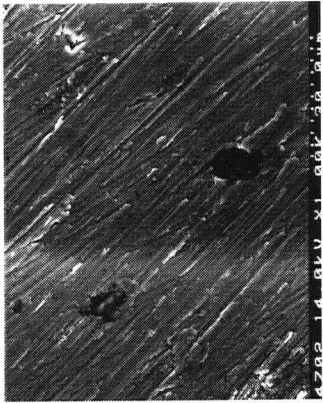
In order to evaluate the impact of the different pre-treatments on the protective ability of the final coatings, corrosion immersion tests were conducted on the samples D_1, D_2, E_1 and E_2, as well as on a blank sample that received the machine polishing and

degreasing but no coating. These five samples were immersed into a 3.5% NaCl solution for 2 h, and this was followed by a water rinse and drying in air. Figures 4.2 (a) to (e) show the measured scanning electron micrographs from these samples after exposing to the corrosive environment: (a) blank sample (shows two different areas), (b) sample D_1, (c) sample D_2, (d) sample E_1 and (e) sample E_2. Figure 4.2 (a) indicates the presence of white corrosion products and some holes are apparent on the surface of the blank sample after the immersion in NaCl solution. White corrosion products were also spotted on the surface of sample D_1 (Fig. 4.2 b, hand polish, no acid etching). However, no corrosion products were detected on the surface of sample D_2 (Fig. 4.2 c, machine polished, no acid etch), although some areas of the coating dissolved and tiny crystals of the previous phosphate coating were formed on the surface. The same dissolving process was observed for sample E_1 (hand polish, with acid etching) and sample E_2 (machine polish, with acid etching).

It is clear that the form of pre-treatment used prior to a phosphating procedure strongly influences the final coating performance. Hand polishing was indicated as a necessary step in earlier observations in the project [84,85]. The results from SEM, XPS and corrosion tests made in the present work show hand polishing does have some merit. The aluminum alloy surface is still rough after a hand polish, and the leaf-like scratches that are present may provide more growth points for the zinc phosphate coatings (the leaf-like apearance on the substrate is still seen after a phosphating procedure, except that it is now outlined by the deposited white crystals). On the other hand, the aluminum alloy polished by hand has a bigger total surface area than the relatively smoother surface polished by the mechanical polisher. This rougher form for the surface may help
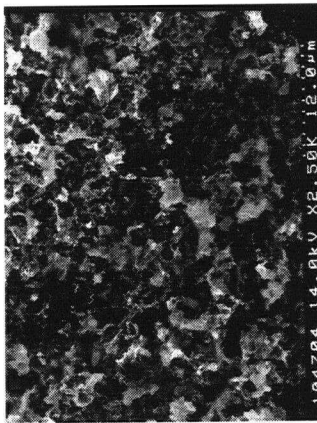
blank sample (x1000) largely
free of corrosion products

(c)   sample E_1 (x2500)

blank sample (x1000)
shows corrosion product
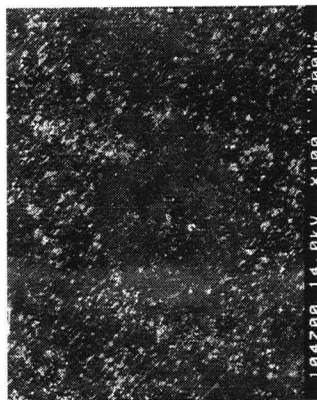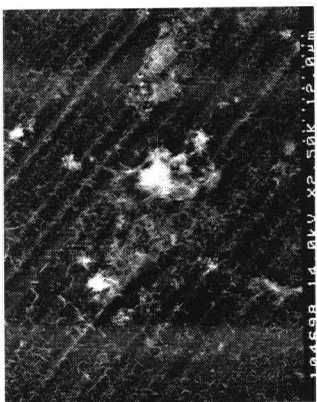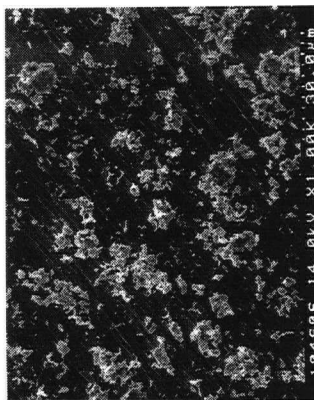
(a)
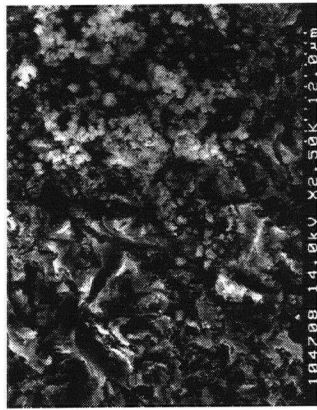
(b)   sample D_1 (x2500)

Figure 4.2 Scanning electron micrographs of samples after immersing in 3.5% NaCl
solution for 2 h.

sample D_2 (x2500)

sample E_2 (x2500)

sample D_2 (x100)

(d)

sample E_2 (x1000)

(e)

Figure 4.2 Continued.

74

improve the adhesion of the phosphated film. The disadvantage of hand polishing compared with machine polishing is that it is hard to control and equalize the force applied to each position. That can lead to differences between samples even when given the same nominal treatment. We conclude that machine polishing should be favored to give the most consistent results.

Acid etching is also a common pre-treatment employed during zinc phosphating processes. It appeared in the procedures for phosphating 7075-T6 aluminum alloy in our group [70], but no detailed study was recorded. Besides, 6061-T6 aluminum alloy is different in composition compared to 7075-T6, so it is worth to study the influence of acid etching on the phosphating of this particular alloy. The coated samples after an acid etching show more crystalline grains and much higher (Zn+P)/Al ratios, than those prepared without acid etching (no matter how the mechanical polishing was applied). This indicates that the morphological changes made on the aluminum surface by acid etching are favorable for subsequent coating formation. It is concluded that acid etching is a necessary step prior to the zinc phosphating of 6061-T6 aluminum alloy.

4.3 Post-treatment with Methyltriethoxysilane

4.3.1 Sample Preparation

Table 4.3 indicates the preparation procedures conducted to form four coated samples (referred to as F_1, F_2, F_3 and F_4) on square 6061-T6 Al alloy (1 x 1 x 0.2 cm^3) panels in order to test different silane post-treatments. Each alloy sample was first polished by mechanical polisher (Metaserv Polisher C200/5A), and then degreased with acetone and methanol in an ultrasonic bath for 1 min and dried in air. After the pre-

treatment procedures, each sample was coated by dipping into the phosphating solution 1 (16.0 ml H_3PO_4 (85%), 5.36 g ZnO and 0.5 g NaF per liter) at 60°C for 1.5 min (F_1, F_2 and F_4) or 3 min (F_3). Samples F1 and F3 were then rinsed with deionized water and dried in air, and these represented blanks to test against the silane treated samples F_2 and F_4. Immersions into the silane solution (20 ml H_2O, 20 ml ethanol and 1.5 ml methyltriethoxysilane) were for 2 min at 60°C. It should be emphasized that the pre-treatments for this part of the research do not use acid etching.

4.3.2   Results and Discussion

Measured scanning electron micrographs for the four samples F_1, F_2, F_3 and F_4 are shown in Fig. 4.3. Sample F_1 (coated in solution 1 at 60°C for 1.5 min) does not have many crystalline grains but they are distributed evenly on the surface. Sample F_2 adds the silane post-treatment to the procedure used for forming F_1. F_2 was coated in solution 1 at 60°C for 1.5 min and then immersed for 2 min into the silane solution at 60°C; this was followed by a water rinse for 20 s. Many crystals with tiny branches appeared on the surface of the coated sample F_2, although they were not distributed evenly on the surface. One part of the surface was completely covered by a large piece of coating (from the silane and phosphate), while other parts were covered by many smaller-sized coated regions. F_3 was coated for 3 min in phosphating solution 1 at 60°C, while F_4 was coated in this solution at 60°C for 1.5 min, then immersed into the silane solution for 2 min at 60°C, and finally was dipped for 1.5 min into the coating solution 1 again at 60°C. Figure 4.3d indicates that many tiny crystalline grains were formed on sample F_4; the grain size is smaller than for F_3 and the density of crystalline grains is much greater. This

Table 4.3 Specification of coating procedures and post-treatments used for 6061-T6 Al alloy samples after the common pre-treatment described in Section 4.3.1.

Sample code	Treatment
F_1	Sample dipped in solution 1 (1.5 min, 60°C), rinsed with de-ionized water (20s), air-dried
F_2	Sample dipped in solution 1 (1.5 min, 60°C), dipped in silane solution (2 min, 60°C), rinsed with deionized water (20s), air-dired
F_3	Sample dipped in solution 1 (3 min, 60°C), rinsed with de-ionized water (20s), air-dried
F_4	Sample dipped in solution 1 (1.5 min, 60°C), dipped in silane solution (2 min, 60°C), dipped in solution 1 again (1.5 min, 60°C), rinsed with deionized water (20s), air-dried

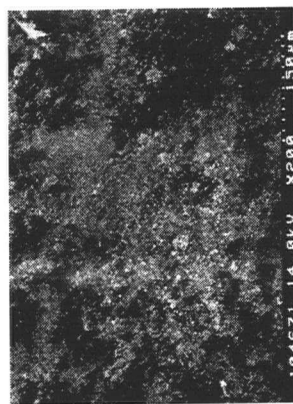Table 4.4 XPS data for samples given different post-treatments.

Sample	Zn/Al	P/Al	(Zn+P)/Al
F_1	0.18	0.05	0.23
F_2	1.85	2.32	4.17
F_3	0.26	0.18	0.44
F_4	0.67	0.60	1.27

sample F_1 (x2500)
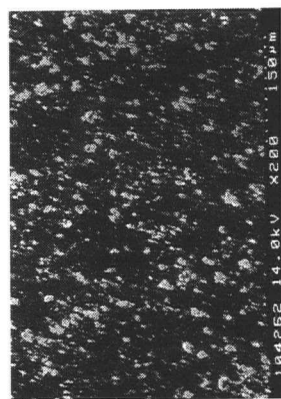
sample F_2 (x2500)

sample F_1 (x200)

sample F_2 (x200)

(a)

(b)
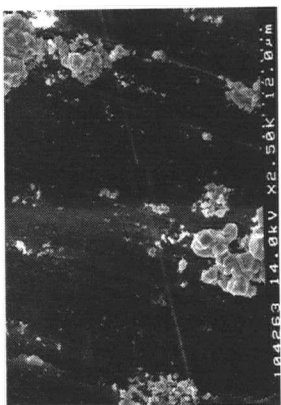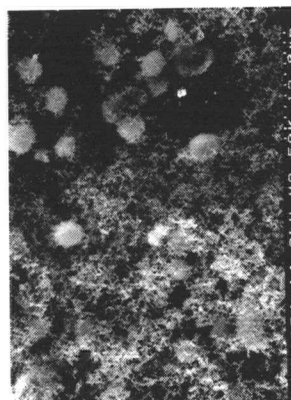
Figure 4.3 Scanning electron micrographs for phosphated samples given different post-treatments as specified in Table 4.3.
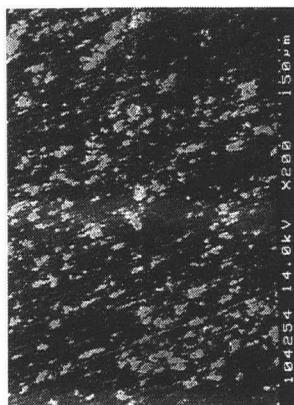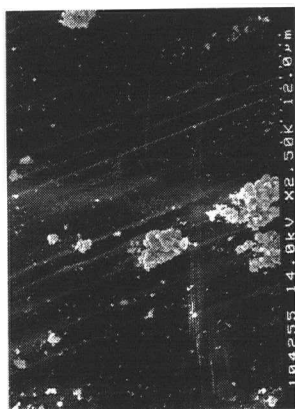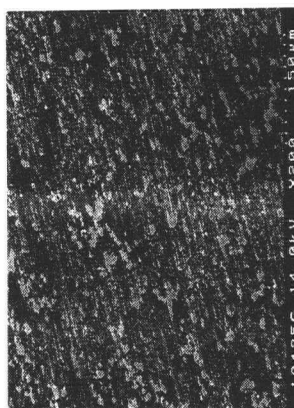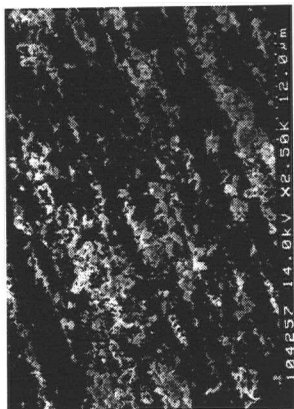
sample F₃ (x2500)

sample F₄ (x2500)

sample F₃ (x200)

sample F₄ (x200)

(c)

(d)

Figure 4.3 Continued.

79

intermediate immersion into the silane solution significantly changes the appearance of the final coating compared with F_3.

XPS data for samples F_1, F_2, F_3 and F_4 are collected in Table 4.4. The effect of the silane post-treatment is seen by directly comparing F_1 and F_2; the $(Zn+P)/Al$ ratio increases from 0.23 to 4.17. Since silicon was detected on the surface of sample F_2, this may suggest that the silane treatment acts to seal the porous zinc phosphate coating, and to prevent it being washed away in a water rinse. The protective effect of this very high zinc phosphate coverage is accessed in the following corrosion tests. Sample F_4 also has a high $(Zn+P)/Al$ ratio although it is lower than that of sample F_2. However, sample F_4's Zn/Al and P/Al ratios are both higher than those of sample F_3, and so it is concluded that the coverage of zinc phosphate coating on sample F_4 is larger than on sample F_3. This suggests that a silane treatment in the middle of the zinc phosphating procedure can improve the final coating coverage. The $(Zn+P)/Al$ ratio of sample F_4 (1.27) is also very close to the ratio 1.30 for a sample phosphated for 6 min at $60^{\circ}C$ with acid etching. Nevertheless, its P/Al ratio (0.60) is higher than that which was acid etched in the pre-treatment and phosphated for 6 min at $60^{\circ}C$ (sample A_6, 0.34). This makes the silane treatment of interest for further studies.

Corrosion tests were conducted to assess the effect of silane treatments on the corrosion protection afforded by the coatings formed. The four samples F_1 to F_4 were immersed into 3.5% NaCl solution at room temperature for 2 h, and the scanning electron micrographs, after removing the samples from the solution and drying, are shown in Fig. 4.4. Many corrosion spots appeared on the surface of sample F_1. Inside these spots, the coating had changed to many needle-like tiny crystalline grains. Outside the spots, fewer

changes are apparent. However, there is basically no visual sign of dissolved coating on sample F_2, and no corrosion spots appeared on that surface. The surface of sample F_3 showed areas of corrosive attack. As for sample F_1, the coating inside a corrosion spot converted to many small needle-like crystalline grains apparently from dissolution and redepositions, although the coating outside the spot was less damaged by corrosion. There are also several corrosion spots on the surface of sample F_4, although much less than for F_1 and F_3. The coatings inside and outside the spots are similar, and only slight damage can be seen from Fig. 4.4 d for F_4. This gives direct evidence that the samples that received the silane treatment have better corrosion protection ability than those without the silane treatment. Sample F_2 appears especially well protected from corrosion by the silane treatment.

The above SEM, XPS and corrosion tests results show that samples F_2 and F_4 have the best coatings. The addition of the silane during the preparation procedures involved has improved the corrosion resistance of the final phosphate coatings and promoted improved adhesion of the coating as well as giving more and smaller crystalline grains on the aluminum alloy surface. This use of silane both as a post-treatment for the phosphating process or as a treatment between two phosphating immersions encourages an improved final phosphate coating. The whole reaction system after adding the silane is likely to be complicated. The silane may react with the aluminum oxide on the metal surface to form Al-O-Si bonds, and or there may be cross-linking O-P-O-Si connections to phosphate groups in the coating. At this point, no detailed knowledge is available for the mechanism of how the silane works as a reagent in the intermediate or post-treatment for the formation or protection of the phosphate coatings.
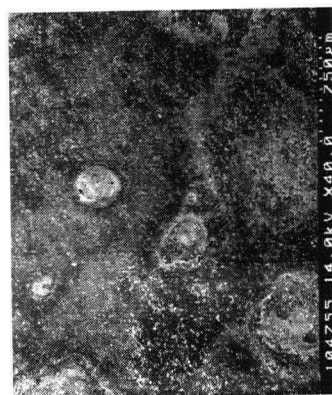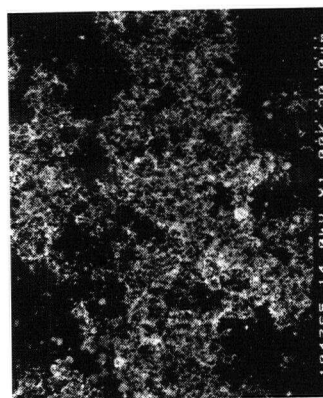
sample F_1 (x40)
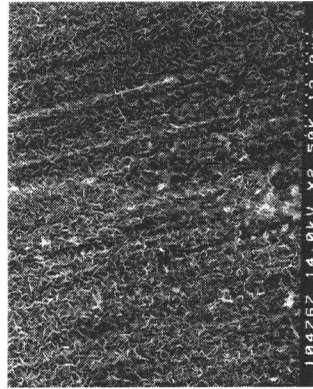
sample F_1 (x2500)

(a)
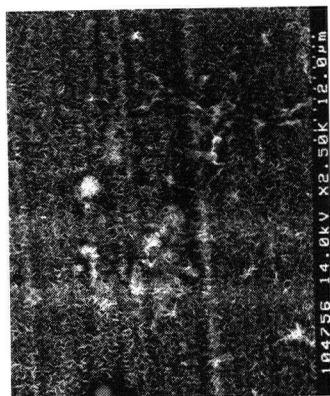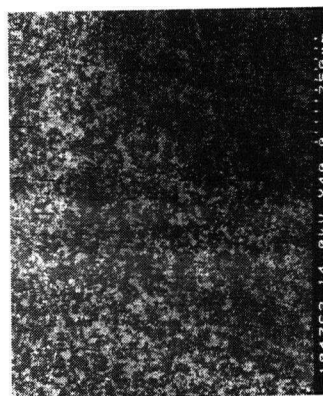
sample F_2 (x40)

sample F_2 (x1000)
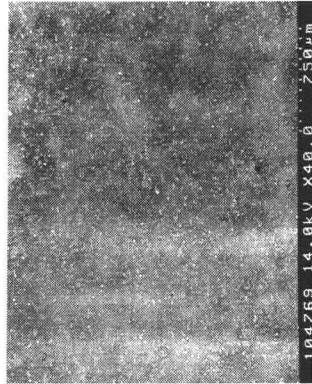
(b)

Figure 4.4 Scanning electron micrographs of samples F_1 to F_4 after immersing in 3.5% NaCl solution for 2 h.

sample F_3 (x2500)

sample F_4 (x2500)

sample F_3 (x40)

sample F_4 (x40)

(c)

(d)

Figure 4.4 Continued.

4.4 Conclusions

This work has used XPS, SEM and corrosion tests to investigate pre-treatments, post-treatments, and associated procedures involved with the zinc phosphating of 6061-T6 aluminum alloy. Comparisons were made between acid etching and mechanical polishing in the pre-treatment stages, and the mechanical polishing involved both machine polishing and hand polishing. New post-treatment procedures were investigated using methyltriethoxysilane. The following points are the conclusions for the work described in this Chapter:

(1) The details of the mechanical polishing in the pre-treatment have been shown to influence the properties of the final phosphate coatings. The morphology and composition of the coatings obtained after hand polishing are different from those obtained after use of the mechanical polisher. In the first case, the final coating has a leaf-like substrate and smaller crystalline grains on the surface than when the mechanical polisher is used in the pre-treatment. On balance, the use of the mechanical polisher is favored because it is easier to standardize for comparing effects of different phosphating procedures. Meanwhile, acid etching gives a surface morphology that helps improve the coverage of the zinc phosphate coating. Acid etching is therefore seen as a necessary step for this phosphating process on 6061-T6 aluminum alloy.

(2) The silane treatment investigated as a sealing rinse is completely new, and perhaps surprising, but it results in a considerable increase in the zinc phosphate coverage and coating thickness on the aluminum surface. This results in a greatly improved corrosion

resistance by the coating compared with the samples without the silane post-treatment. The ability of the silane to cross-link within the coating presumably acts to increase its adhesive strength. A related silane treatment can also be used at an intermediate stage in the zinc phosphating immersion. This also effectively improves both the coverage and the adhesive ability of the final phosphate coating.

Chapter 5 Effects of Accelerators on Zinc Phosphate Coatings

5.1 Introduction

It is well known that adding some chemicals to a zinc phosphating solution can accelerate the coating process and dramatically change the composition and nature of the zinc phosphate coating [4]. In previous studies on the phosphating of 7075-T6 aluminum alloy by spraying, chlorate and nitrite were added to the coating solution as accelerators with improvements in the final coating [68]. However, no other accelerators have yet been studied in this laboratory in relation to phosphating recipes.

The work in this chapter examined the effects of Cu^{2+}, Ni^{2+} and NO_3^- as accelerators in the phosphating of 6061-T6 Al alloy. There is an emphasis on the corrosion resistance, morphology and composition of the coatings obtained.

5.2 Sample Preparation

Studies were conducted on square 6061-T6 Al alloy panels (1x1x0.12 cm^3) which were first mechanically polished with Al_2O_3 sandpaper (1200 grit) and deionized water, and then degreased with acetone and methanol in an ultrasonic bath for 1 min, dried in air and dipped in an acid etching solution (25 ml H_2SO_4 (98%) + 25 ml H_2O) for 2 min at 40°C. The sample panels were then dipped into the phosphating solutions for the conditions specified below. After dipping, each sample was rinsed with deionized water and air-dried. Altogether sixteen different zinc phosphating solutions were used for the experiments in this chapter. Solutions 1 to 4 are basic reference solutions for this work. Solution 1 contains 16.0 ml H_3PO_4 (85%), 5.36 g ZnO and 0.5 g NaF per liter with pH 2.

Solution 3 has the same composition as solution 1 except 1.4 g of NaF is added per litre of solution. Solutions 2 and 4 were prepared as solutions 1 and 3 respectively except their pH values were adjusted to 4 by the addition of 20% NaOH solution. For studying Cu^{2+} as an accelerator, another four solutions were used which were made by adding 0.002% NO_3^- (as $Cu(NO_3)_2$) to solutions 1 to 4. Similarly for studying Ni^{2+}, four solutions were used which were prepared by adding 0.0004% NO_3^- (as $Ni(NO_3)_2$) to solutions 1 to 4 respectively. For studying the effect of NO_3^- itself as an accelerator, two solutions were prepared by adding 0.002% and 0.0004% of $NaNO_3$ to the solution 1, and another two solutions were based on solution 3 with the addition of 0.002% and 0.0004% $NaNO_3$. The procedures and specific coating solutions used for each sample studied in this chapter are listed in Table 5.1. For the studies with $Cu(NO_3)_2$, $Ni(NO_3)_2$ and $NaNO_3$, preliminary studies indicated the particular concentrations used for the more thorough work described in this chapter.

5.3 Results and Discussion

### 5.3.1 Effects of adding $Cu(NO_3)_2$ to the phosphating bath

According to the previous results for this project, the composition and morphology of a coating changes with the pH of the phosphating bath [86]. When the pH is in the range from 2 to 4, the coating is more complete with better adhesion. But since the coating formed in the pH 2 bath is considerably different from that formed in the pH 4 bath, phosphating baths at these two pH values were used to study the effects of the accelerators.

The influence of adding $Cu(NO_3)_2$ to the phosphating baths on the morphology of the final coatings are shown by the SEM micrographs in Figure 5.1 parts (1) to (4). All

Table 5.1 Specific preparations for samples in this chapter.

| Sample Code	Solution Used
G_1, H_1, I_0	Solution 1: 16.0 ml H_3PO_4 (85%), 5.36 g ZnO and 0.5 g NaF (210 ppm F⁻) per liter, pH 2
G_2, H_2	Solution 2: 16.0 ml H_3PO_4 (85%), 5.36 g ZnO and 1.4 g NaF (600 ppm F⁻) per liter, pH 2
G_3, H_3, I_0'	Solution 3: 16.0 ml H_3PO_4 (85%), 5.36 g ZnO and 0.5 g NaF (210 ppm F⁻) per liter, pH 4
G_4, H_4	Solution 4: 16.0 ml H_3PO_4 (85%), 5.36 g ZnO and 1.4 g NaF (600 ppm F⁻) per liter, pH 4
G_5	Solution 1 plus 0.002% NO_3^- ($Cu(NO_3)_2$)
G_6	Solution 2 plus 0.002% NO_3^- ($Cu(NO_3)_2$)
G_7	Solution 3 plus 0.002% NO_3^- ($Cu(NO_3)_2$)
G_8	Solution 4 plus 0.002% NO_3^- ($Cu(NO_3)_2$)
H_5	Solution 1 plus 0.0004% NO_3^- ($Ni(NO_3)_2$)
H_6	Solution 2 plus 0.0004% NO_3^- ($Ni(NO_3)_2$)
H_7	Solution 3 plus 0.0004% NO_3^- ($Ni(NO_3)_2$)
H_8	Solution 4 plus 0.0004% NO_3^- ($Ni(NO_3)_2$)
I_1	Solution 1 plus 0.002% NO_3^- ($NaNO_3$)
I_2	Solution 1 plus 0.0004% NO_3^- ($NaNO_3$)
I_3	Solution 3 plus 0.002% NO_3^- ($NaNO_3$)
I_4	Solution 3 plus 0.0004% NO_3^- ($NaNO_3$)

† all samples were prepared by dipping 6061-T6 Al samples into the corresponding solution at 60°C for 3 min
† all the % presented are wt%
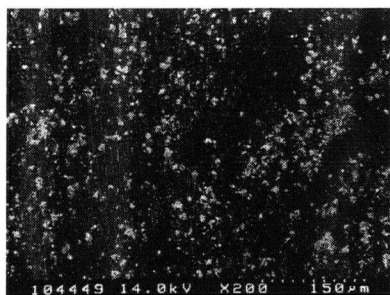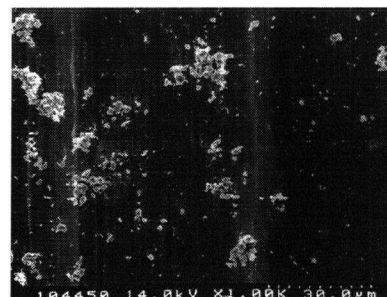
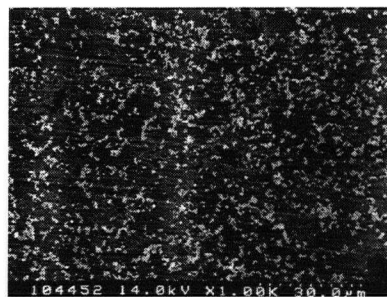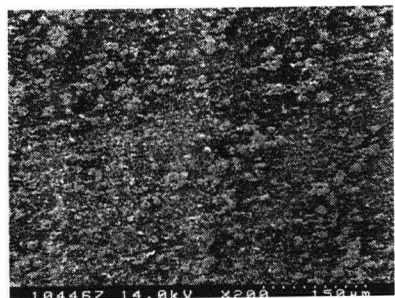(a) G_1 (x200) G_1 (x1000)
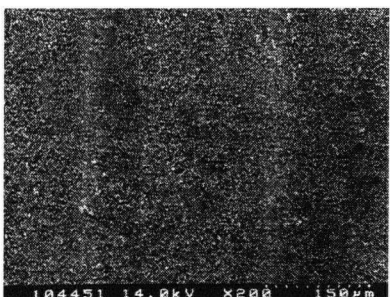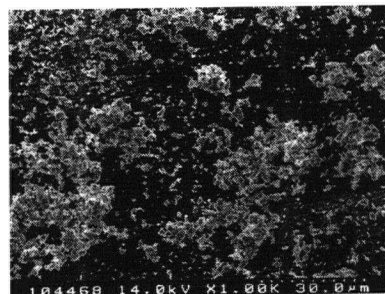

(b) G_5 (x200) G_5 (x1000)

Figure 5.1 SEM micrographs for samples coated in solutions in Table 5.1
to show the effect of adding 0.002% NO_3^- as $Cu(NO_3)_2$. Part (1)
pH=2, [F^-]= 210 ppm: (a) without $Cu(NO_3)_2$; (b) with $Cu(NO_3)_2$.
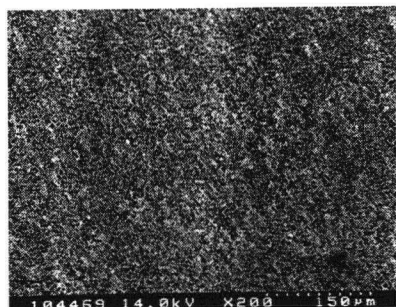
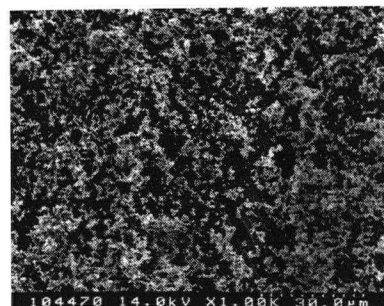(a) G_3 (x200) G_3 (x1000)

(b) G_7 (x200) G_7 (x1000)

Figure 5.1   SEM micrographs for samples coated in solutions in Table 5.1 to show the effect of adding 0.002% NO_3^- as $Cu(NO_3)_2$. Part (2) pH=2, [F^-]= 600 ppm: (a) without $Cu(NO_3)_2$; (b) with $Cu(NO_3)_2$.

(a)   G$_2$ (x1000)   G$_2$ (x5000)

(b)   G$_6$ (x200)   G$_6$ (x5000)

Figure 5.1 SEM micrographs for samples coated in solutions in Table 5.1
to show the effect of adding 0.002% NO$_3^-$ as Cu(NO$_3$)$_2$. Part (3)
pH=4, [F$^-$]= 210 ppm: (a) without Cu(NO$_3$)$_2$; (b) with Cu(NO$_3$)$_2$.

(a) G_4 (x2500) G_4 (x20k)
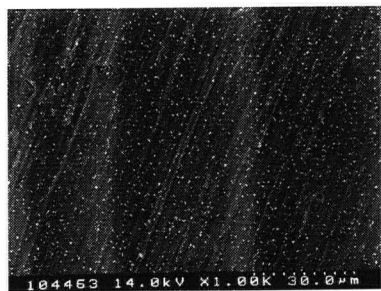

(b) G_8 (x2500) G_8 (x20k)
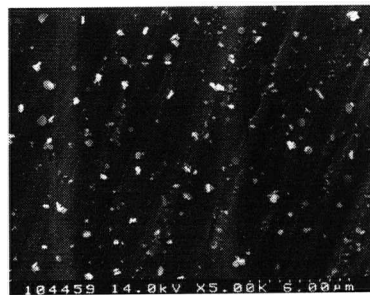
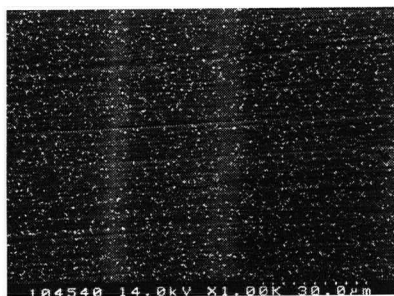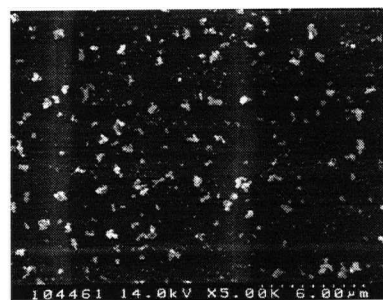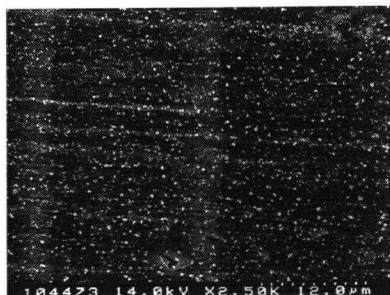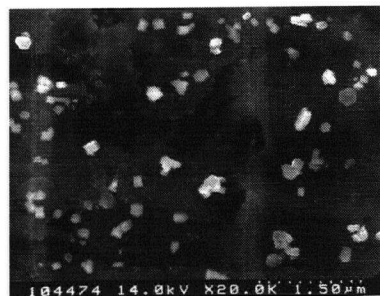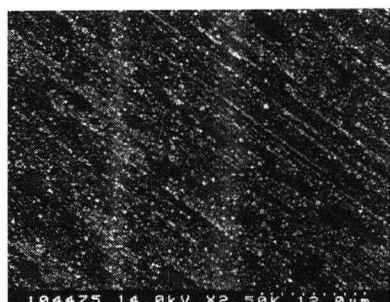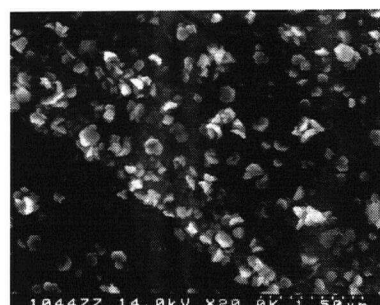Figure 5.1 SEM micrographs for samples coated in solutions in Table 5.1 to show the effect of adding 0.002% NO_3^- as $Cu(NO_3)_2$. Part (4) pH=4, [F^-]= 600 ppm: (a) without $Cu(NO_3)_2$; (b) with $Cu(NO_3)_2$.

figures labeled (a) apply to coatings formed in the baths without the addition of $Cu(NO_3)_2$, while those labeled (b) apply to samples coated in the baths with some added $Cu(NO_3)_2$. Adding $Cu(NO_3)_2$ to the phosphating baths at pH 2 changes the form of the coating on the aluminum alloy surface, especially for the bath containing 210 ppm F^-. Figure 5.1 part (1) (a) shows the microstructure of coating for sample G_1 formed in solution without $Cu(NO_3)_2$, and it shows large flakes of white crystals distributed on the surface. After adding $Cu(NO_3)_2$ to the phosphating bath, the final coating for sample G_5 is shown in Figure 5.1 part (1) (b). This surface is now covered by many small white crystalline grains. A similar effect is found on the samples G_3 and G_7 coated in the phosphating bath with 600 ppm F^- (Figure 5.1 part (2) (a) and (b)). It is concluded that the 0.002% $Cu(NO_3)_2$ has refined the form of coating on the surface.

Figure 5.1 parts (3) and (4) show the effects on the final coatings of adding $Cu(NO_3)_2$ to the phosphating bath with pH 4. Even without the accelerator, the final coatings formed in pH 4 baths are composed of really small white crystalline grains, so the effect of reducing those grains even further by adding $Cu(NO_3)_2$ is less obvious than in the pH 2 baths. However, added $Cu(NO_3)_2$ to the coating bath does increase the coverage of white crystalline grains on the surface (samples G_6 and G_8).

Table 5.2 lists composition ratios from XPS for the above samples. For the samples coated in the pH 2 phosphating bath, the (Zn+P)/Al ratios are almost unchanged after adding $Cu(NO_3)_2$ to the bath with 210 ppm F^-. However, this ratio is increased after adding $Cu(NO_3)_2$ to the bath with 600 ppm F^-. For the samples coated in the pH 4 phosphating bath, the (Zn+P)/Al ratio changes only a little after adding $Cu(NO_3)_2$ with 210 ppm F^-, but the Zn/Al and P/Al ratios increase strongly after adding $Cu(NO_3)_2$ to the

Table 5.2 XPS results for samples G_1 to G_8 to test coating compositions on adding $Cu(NO_3)_2$ as accelerator.

Sample code	Zn/Al	P/Al	(Zn+P)/Al
G_1	0.67	0.27	0.94
G_5	0.61	0.24	0.85
G_2	0.30	0.62	0.92
G_6	0.34	0.68	1.02
G_3	0.64	0.43	1.07
G_7	0.82	0.44	1.26
G_4	0.60	0.73	1.33
G_8	1.74	0.95	2.69

bath with 600 ppm F^-. It is concluded that the coverage of zinc phosphate on the aluminum surface for the above samples is increased on the addition of $Cu(NO_3)_2$ to the phosphating bath according to the XPS and SEM analysis.

Copper as a heavy metal was first used in phosphating on steel. It causes the phosphating process to be speeded up. While it seems an appropriate amount of Cu^{2+} in the phosphating bath can improve the coverage and grain size of the coating, little information about its effect on corrosion resistance is known. However, Cu^{2+} in the phosphating bath may also introduce corrosion growth points on to the metal surface. In order to find the influence of copper to the corrosion resistance of the zinc phosphate coatings prepared in this work, the samples G_1 (phosphating bath pH 2, 210 ppm F^-, no $Cu(NO_3)_2$) and G_5 (same parameters phosphating bath plus $Cu(NO_3)_2$) were immersed into the 3.5% NaCl solution for 2 hours, and then rinsed with water and air-dried. The scanning electron micrographs of these two samples are shown in Figure 5.2 (a) and (b). The coating formed in the bath without $Cu(NO_3)_2$ reveals needle-like crystalline grains on the sample surface during immersion of the sample in the corrosive solution. It is probably associated with some redeposition of dissolved phosphate, and that implies a relatively low corrosion resistance for the coating (Fig. 5.2(a)). However, this feature is not evident for the coating formed in the bath with $Cu(NO_3)_2$, and there is almost no difference before and after immersion (Figs. 5.1(b) and 5.2(b)). Therefore, from the data analyses by XPS, SEM and corrosion test, adding $Cu(NO_3)_2$ to introduce copper into the phosphating bath does not only reduce the size of the crystalline grains but it also increases the coating coverage on the surface. Additionally this also resulted in the improvement of corrosion resistance and enhancement of adhesion.

(x40)   (x1000)   (x2500)

(a) sample G_1 (H_1)
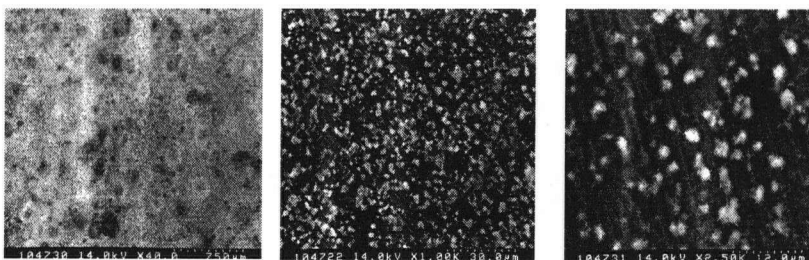
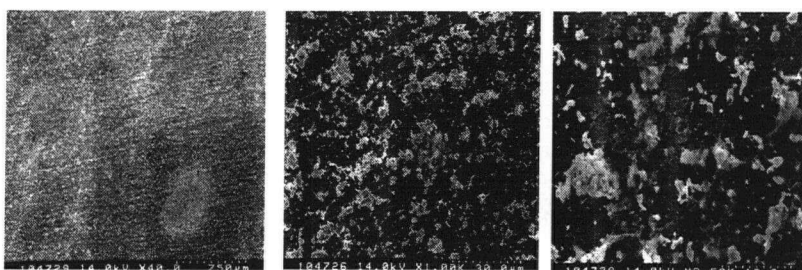(x40)   (x1000)   (x2500)

(b) sample G_5

(x40)   (x1000)   (x2500)

(c) sample H_5

Figure 5.2 SEM micrographs after coated samples have been immersed in 3.5%NaCl solution for 2 h: (a) G_1(H_1) coated in phosphating solution 1 (no accelerator); (b) G_5 coated with $Cu(NO_3)_2$ added to coating bath; (c) H_5 coated with $Ni(NO_3)_2$ added to coating bath.

The positive influence of copper ions has been known for some time in phosphating technology. It is assumed that, depending on the metal, part of the copper is integrated into the phosphate layer and part cements on the metal surface as CuO [87]. According to W. Wimmer and his coworkers, adding traces of Cu^{2+} ions (approximately 5 ppm) into their particular phosphating bath does not lead to the formation of a galvanic element, so helping the corrosion resistance of the aluminum. Other compounds may also be used to introduce copper into the phosphating bath, for example copper hydroxide, copper oxide hydrate, copper tartrate and copper phosphate [88]. In another study in this laboratory [89], it has been indicated that an appropriate amount of copper introduced by interfacial enrichment on 2024-T3 aluminum alloy, can reduce the grain size of the phosphate coating and improve corrosion resistance. It is believed that copper on the surface provides additional cathodic areas to help the coating nucleation.

5.3.2   Effects of adding $Ni(NO_3)_2$ to the phosphating bath

Solutions of nickel salts have been used as accelerators for the formation of phosphate coatings [4]. In this work, Ni^{2+} in the form of $Ni(NO_3)_2$ was added to the four reference solutions 1 to 4, and samples H_1 to H_8 were produced according to the preparation procedures given in Table 5.1. Figure 5.3 parts (1) to (4) show SEM micrographs for these eight samples. The crystalline grains on samples prepared with the Ni^{2+} in the coating bath (H_5, H_6, H_7 and H_8) are much smaller than those on the sample prepared without the addition of Ni^{2+} (H_1, H_2, H_3 and H_4). This suggests that adding Ni^{2+} to the phosphating solution can refine the surface coating by making the crystallites pack more densely.
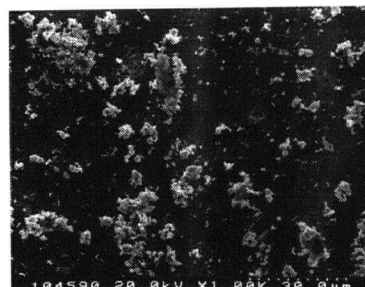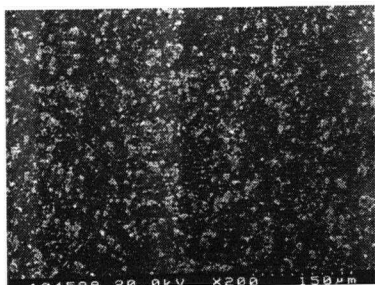
(a)   H$_1$ (x200)   H$_1$ (x1000)
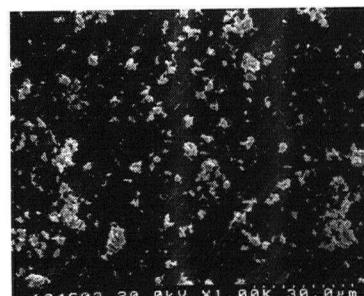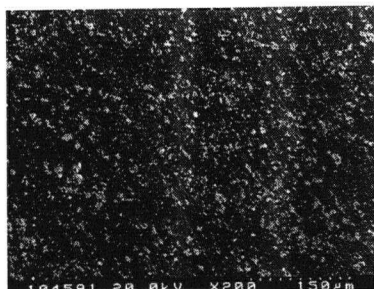
(b)   H$_5$ (x200)   H$_5$ (x1000)

Figure 5.3 SEM micrographs for samples coated in solutions in Table 5.1
to show the effect of adding 0.0004% NO$_3^-$ as Ni(NO$_3$)$_2$. Part (1)
pH=2, [F$^-$]= 210 ppm: (a) without Ni(NO$_3$)$_2$; (b) with Ni(NO$_3$)$_2$.

(a)   H$_2$ (x1000)   H$_2$ (x4000)

(b)   H$_6$ (x1000)   H$_6$ (x4000)

Figure 5.3 SEM micrographs for samples coated in solutions in Table 5.1
to show the effect of adding 0.0004% NO_3^- as $Ni(NO_3)_2$. Part (2)
pH=2, [F$^-$]= 600 ppm: (a) without $Ni(NO_3)_2$; (b) with $Ni(NO_3)_2$.

(a) H_3 (x200) H_3 (x1000)
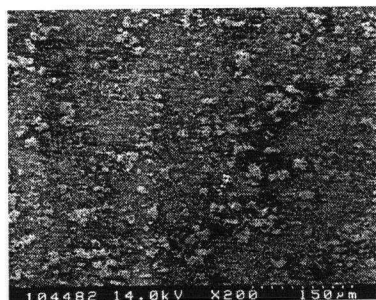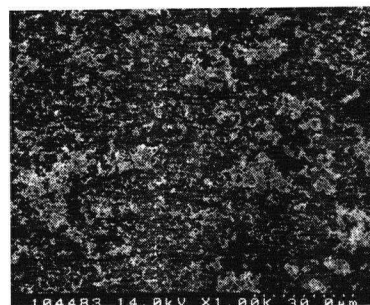
(b) H_7 (x200) H_7 (x1000)

Figure 5.3 SEM micrographs for samples coated in solutions in Table 5.1 to show the effect of adding 0.0004% NO_3^- as $Ni(NO_3)_2$. Part (3) pH=4, [F^-]= 210 ppm: (a) without $Ni(NO_3)_2$; (b) with $Ni(NO_3)_2$.
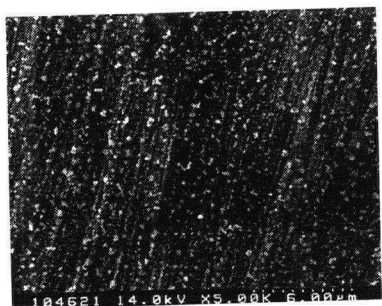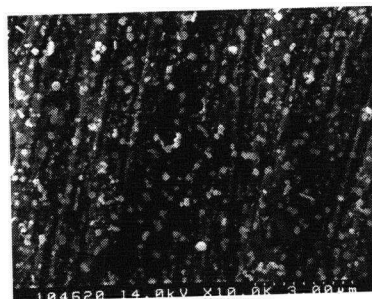
(a) H_4 (x5000) H_4 (x10k)
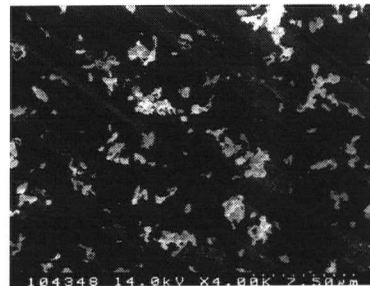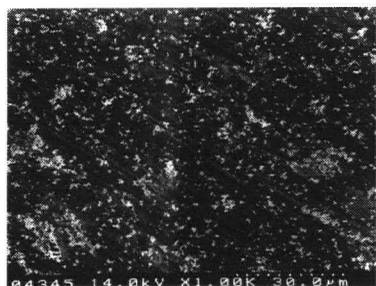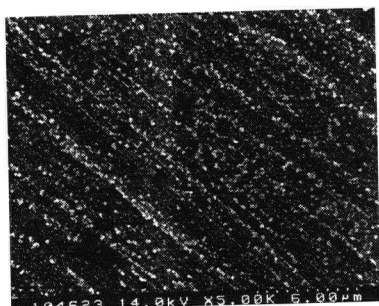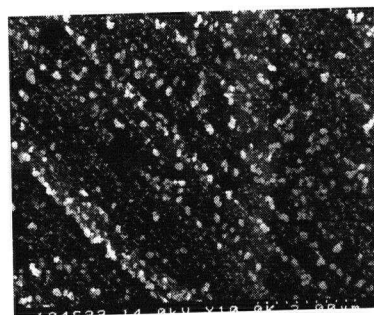

(b) H_8 (x5000) H_8 (x10k)

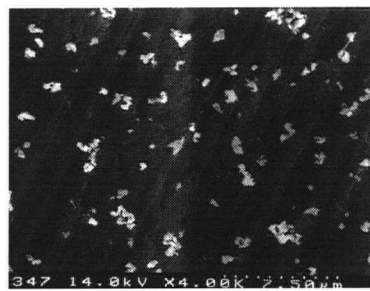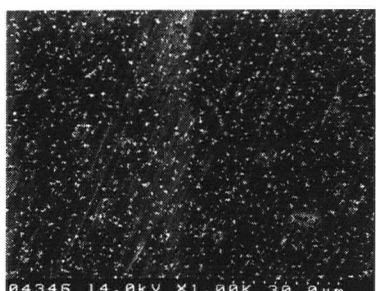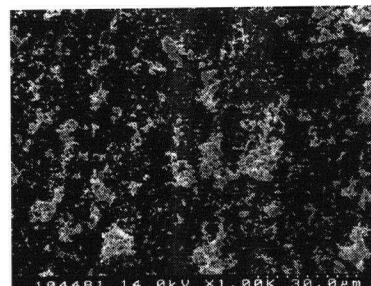Figure 5.3 SEM micrographs for samples coated in solutions in Table 5.1
to show the effect of adding 0.0004% NO_3^- as $Ni(NO_3)_2$. Part (4)
pH=4, $[F^-]$= 600 ppm: (a) without $Ni(NO_3)_2$; (b) with $Ni(NO_3)_2$.

Table 5.3 XPS results for samples H_1 to H_8 to test coating compositions on adding $Ni(NO_3)_2$ as accelerator.

Sample code	Zn/Al	P/Al	(Zn+P)/Al
H_1	0.54	0.24	0.78
H_5	0.55	0.24	0.79
H_2	0.31	0.70	1.02
H_6	0.49	0.81	1.30
H_3	0.65	0.43	1.08
H_7	0.85	0.66	1.51
H_4	0.61	0.71	1.32
H_8	1.83	1.55	3.38

Table 5.4 XPS results for samples I_0, I_1 and I_2 to test coating compositions on adding $NaNO_3$ as accelerator.

Sample code	Zn/Al	P/Al	(Zn+P)/Al
I_0	0.51	0.23	0.74
I_1	0.48	0.23	0.71
I_2	0.53	0.21	0.74

Atomic composition ratios from XPS for the samples H_1 to H_8 are listed in Table 5.3. For samples coated in phosphating solutions with pH 2, H_1 and H_5 have similar (Zn+P)/Al ratios and that for H6 is slightly higher than the (Zn+P)/Al ratio for H_2. Unlike these samples, the changes in composition for samples coated in pH 4 solutions are relatively large. For example, the P/Al for sample H_7 is 0.66, considerably increased over the value of 0.43 for H_3; similarly, the Zn/Al ratios are increased too. Additionally the Zn/Al, P/Al ratios for H_8 (1.83 and 1.55 respectively) are markedly increased over the values 0.61 and 0.71 respectively for sample H_4. These increases in the atomic ratios show that the zinc phosphate coverage is significantly increased on the aluminum surface by adding $Ni(NO_3)_2$ to the phosphating bath.

The corrosion protective properties of the phosphate coatings were evaluated by corrosion tests. Samples H_1 and H_5 were immersed into the 3.5% NaCl solution for 2 hours and then water rinsed and air-dried. The measured SEM micrographs are shown in Figure 5.2. Much more corrosion is apparent on the coated surface of sample H_1; many crystalline grains in the coating appear as dissolved into tiny thread-like crystals. But sample H_5 shows only a few crystalline grains dissolved, and it is concluded that the corrosion resistance of the phosphate coating is considerably improved.

Other researchers have reported that Ni^{2+} added to a phosphating solution accelerates the coating reaction on steel and zinc [90-91]. The present work demonstrates that Ni^{2+} can also improve the phosphate coating on the aluminum alloy from two aspects: enhancement of the adhesive ability and increase of the corrosion resistance of the zinc phosphate coating. The addition of Ni^{2+} to the phosphating bath induces a reduction in crystal size, as compared with a phosphating bath without Ni^{2+}. Smaller

crystals result in a coating that is more compacts, which permits more crystals per unit area. This compaction ensures a better coverage over the aluminum surface, thereby reducing the number of pores and occlusions in the conversion coating. Minimizing coating porosity delays the onset of corrosive attack, and a highly compact coating results in improved paint adhesion as well. Unlike the results presented by others for zinc phosphating on steel [90], no nickel is detected on the aluminum surface by XPS after adding Ni^{2+} to the phosphating solution. So the function of nickel appears in this study to participate just in the phosphating reaction near the aluminum surface, and to accelerate the coating process with some change in the composition of the final phosphate coating. In turn, this significantly improves the corrosion resistance and the morphology of the coating to aid the adhesion.

The mechanisms associated with the involvement of Ni^{2+} and Cu^{2+} ions in these processes are likely to be different. It is believed that Cu^{2+} in solution redeposits to give metallic copper which provides additional cathodic areas to speed up the phosphate reaction. By contrast, Ni^{2+} ions appear to affect the insoluble phosphates in their nascent colloidal form [4]. It seems large amounts of Ni^{2+} have no deleterious effect on the phosphate coating [4], but excessive amounts of Cu^{2+} should be avoided to prevent the formation of metallic copper which ultimately limits the phosphating process [89].

5.3.3 Effects of adding NaNO₃ to the phosphating bath

Since $Cu(NO_3)_2$ and $Ni(NO_3)_2$ were used above to introduce either Cu^{2+} or Ni^{2+} ions into the phosphating bath as accelerators, it is necessary to establish whether the

NO_3^- anion influences the coating process at the concentrations used for the Cu and Ni salts.

Two solutions were prepared by adding 0.002% and 0.0004% $NaNO_3$ to the reference solution 1 with pH 2. Samples I_0, I_1 and I_2 were then phosphated following the preparation procedures presented in Table 5.1. The SEM micrographs of these three samples are shown in Figure 5.4. The samples I_0, I_1 and I_2 have coatings with crystalline grains of similar size and similar densities (Figure 5.4 (a), (b) and (c)).

Another two solutions were prepared by adding 0.002% and 0.0004% $NaNO_3$ to the reference solution 3 with pH 4. Samples I_0', I_3 and I_4 were prepared according to Table 5.1, and the SEM micrographs of these samples are shown in Figure 5.4 (d) to (f). The surfaces of I_3 and I_4 have less crystalline grains than sample I_0' which does not have the addition of $NaNO_3$ in the coating bath.

Table 5.4 lists atomic ratios from XPS for samples I_0, I_1 and I_2. These three samples have very similar Zn/Al and P/Al ratios, and therefore it is concluded that adding 0.002% or 0.0004% $NaNO_3$ to the phosphating solution does not significantly change the coating compositions.

According to the studies of nitrate acceleration on steel, the effective working concentration range is 1-3% NO_3^- in the coating solution [4]. In the present study, adding 0.002% and 0.0004% $NaNO_3$ to the phosphating solution does not change the coating morphology and composition, and this is consistent with the concentration of $NaNO_3$ being well below the effective range. Therefore, it is clearly evident that the accelerating effects of adding small amounts of either $Cu(NO_3)_2$ or $Ni(NO_3)_2$ to a phosphating bath do actually come from the Cu^{2+} or Ni^{2+}, and not from the NO_3^- ions.
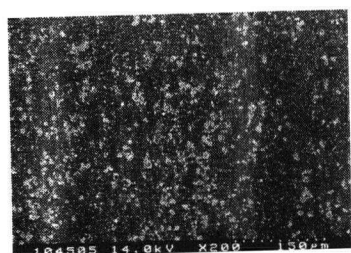
I$_0$ (x200)

(a)
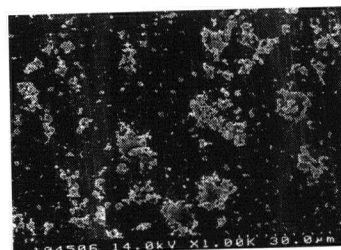
I$_0$ (x1000)

(a)
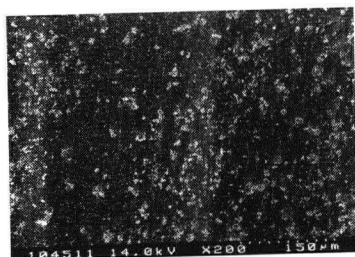
I$_1$ (x200)

(b)

I$_1$ (x1000)

(b)
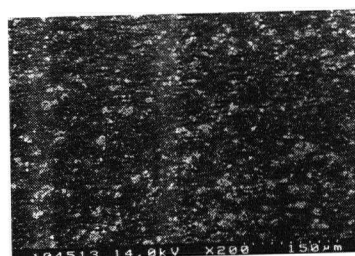
I$_2$ (x200)

(c)

I$_2$ (x1000)

(c)

Figure 5.4 SEM micrographs of coated samples to show effects of adding NaNO$_3$ to coating baths at pH 2 and 210 ppm F$^-$: (a) sample I$_0$ (no NO$_3^-$ added); (b) sample I$_1$ (0.002% NO$_3^-$); (c) sample I$_2$ (0.0004% NO$_3^-$).

I_0' (x1000)

(d)

I_0' (x5000)

(d)

I_0' (x10k)

(d)
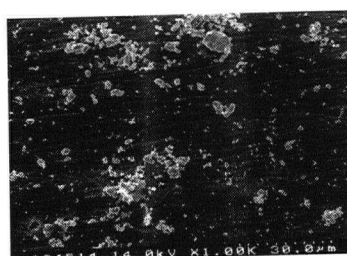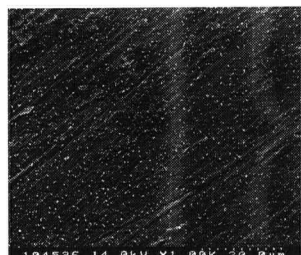
I_3 (x1000)
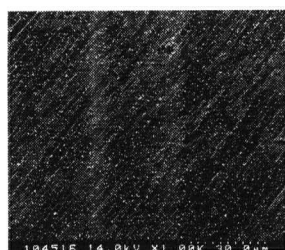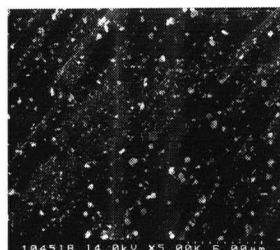
(e)
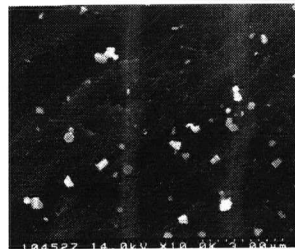
I_3 (x10k)

(e)
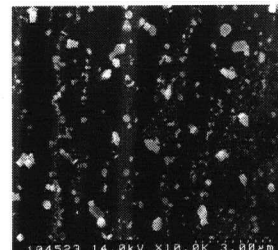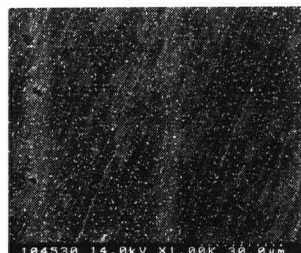
I_4 (x1000)

(f)
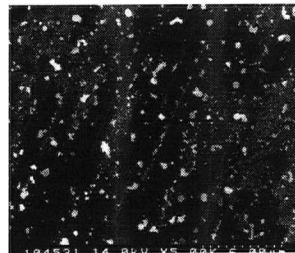
I_4 (x5000)

(f)

Figure 5.4 SEM micrographs of coated samples to show effects of adding $NaNO_3$ to coating baths at pH 4 and 210 ppm F^-: (d) sample I_0' (no NO_3^- added); (e) sample I_3 (0.002% NO_3^-); (f) sample I_4 (0.0004% NO_3^-).

5.4 Concluding Remarks

The reference phosphating bath containing 16.0 ml H_3PO_4 (85%), 5.36 g ZnO and 0.5 g NaF per liter was modified by separate additions of small quantities of $Cu(NO_3)_2$, $Ni(NO_3)_2$ or $NaNO_3$ in order to assess the accelerating effects of the Cu^{2+}, Ni^{2+} and NO_3^- ions. The XPS, SEM and corrosion tests results show:

1) The addition of small amounts of $Cu(NO_3)_2$ (e.g. 0.002% Cu^{2+}) to the phosphating bath resulted in a coating that gave an improvement in corrosion resistance as well as an enhancement of adhesion; these changes occur especially by reducing the size of the crystalline grains, and by increasing the total coverage of zinc phosphate coated on the surface.

2) Similarly, adding 0.0004% Ni^{2+} in the form of $Ni(NO_3)_2$ to the reference phosphating bath significantly increased the corrosion protection ability and the adhesive ability of the final coating. Since comparable improvements in the coating occur at lower concentrations of $Ni(NO_3)_2$ (0.0004% for Ni^{2+}) than for $Cu(NO_3)_2$ (0.002% for Cu^{2+}), it is concluded that Ni^{2+} is a more effective accelerator than Cu^{2+}.

3) The addition of $NaNO_3$ in varying amounts to the coating bath did not change the morphology and the composition of the final coating. Therefore, it is considered that the addition of the ions Na^+ and NO_3^- does not affect, and in particular improve, the coating process.

Chapter 6 Closing Perspectives

6.1   New Observations

Conventionally for aluminum alloys, zinc chromate coatings have been used to improve the corrosion resistance, but concerns about its carcinogenic nature are forcing the development and evaluation of replacement materials. Various alternatives are being investigated, such as cerium or Zr/Ti conversion coatings [92] and organosilane coatings[93]. However, this work has focused on studying phosphating on 6061-Al alloy given the importance of zinc phosphate for treating steels.

In this work, the influences of phosphating time, temperature, pre-treatment, post-treatment and accelerators in the phosphating bath on the final coating of 6061-T6 aluminum alloy were studied through corrosion tests, SEM and XPS surface analyses. The initial phosphating bath contained 16.0 ml H_3PO_4 (85%), 5.36 g ZnO and 0.5 g NaF per liter. The optimum phosphating time and temperature for 6061-T6 aluminum alloy were found to be around 6 min and 60 $^{\circ}$C respectively. Other work considered variation in the F^- concentration, and the preferred concentration was found to be in the range 400 ppm to 600 ppm.

As pre-treatments, acid etching and mechanical polishing, where the latter involved both machine polishing and hand polishing, were compared. Mechanical polishing by machine was chosen as the pre-treatment for subsequent work in order to standardize that step. New post-treatment procedures with methyltriethoxysilane were also studied. The preliminary work showed a considerable increase in the zinc phosphate coverage and coating thickness, as well as improvements in corrosion resistance.

In order to improve phosphate coatings, the uses of $Cu(NO_3)_2$ and $Ni(NO_3)_2$ as accelerators in the phosphating bath were investigated. It was found that adding 0.002% $Cu(NO_3)_2$ or 0.0004% $Ni(NO_3)_2$ increases the phosphating speed, and also improves the corrosion resistance and coating adhesion. Both these activities have been shown to refine the crystalline grains and increase the coverage of the zinc phosphate coating on the surface. The addition of Ni^{2+} appears particularly effective at enhancing the final coating for corrosion protection. Further studies showed that the additions of 0.002% or 0.0004% $NaNO_3$ to the phosphating bath did not affect the morphology or the composition of the final coating. Therefore, it was demonstrated that the NO_3^- ions do not have a significant accelerating role in these contexts, and that the coating enhancements are due to the Cu^{2+} or Ni^{2+} ions.

6.2 Future Work

Studies in the area of this thesis have been dominated by the "trial-and-error" approach, but in general, much better understanding is required for the mechanistic details. Research with transmission electron microscopy is starting to give information of this type [94]. For example, the nucleation of phosphate coating at localized cathodic sites is significant mechanistic information about the initial stages of coating [89]. Second phase particles containing various alloying elements, with cathodic or anodic behavior relative to the adjacent alloy matrix, are likely to have important mechanistic effects. It is believed that new work with scanning Auger microscopy (SAM) can provide both morphological and compositional information for incipient coatings at such localized sites.

Alloy surfaces can be very sensitive to the particular pre-treatment given, and this may strongly influence subsequent coatings. For example, an acid etching pre-treatment can result in the enrichment of alloying elements like Cu at the alloy/oxide film interface, and this can help the formation of a zinc phosphate coating [89]. Much more information about effects of enrichment on coating formation is needed, by means of various techniques including TEM, XPS and SAM. Other pre-treatments including alkaline, electropolishing and chemical polishing should be examined. Similarly more detailed mechanistic information is required for the effects of accelerators and surface conditioning procedures [95].

For phosphating procedures to be useful in practical situations, it is necessary to perform a sealing rinse, and currently this is still done with chromating solution, which must be phased out because of environmental concerns. To reduce the porosity of the phosphate coating, methyltriethoxysilane solution was tried in this work as a post-rinsing solution. The results appear to be encouraging, but the mechanism of this process is still completely unknown. This needs to be established. In addition, work needs to be done to compare the effectiveness of this use of silane with the conventional chromating post-rinse solution.

References

[1]   Aluminum Company of Canada LTD, *Handbook of Aluminum*, 1961.

[2]   S. Wernick, R. Pinner and P.G. Sheasby, *The Surface Treatment and Finishing of Aluminum and Its Alloys* (ASM International Finishing Publications LTD, 1987) Vol. 1 ch.1.

[3]   J. Lindsay, Plat. *Surf. Finish* 84 (1997) 24.

[4]   D.B. Freeman, *Phosphating and Metal Pretreatment* (Industrial Press Inc., New York, 1986) ch.2.

[5]   W. Rausch, *The Phosphating of Metals* (Finishing Publications Ltd., Teddington, 1990) ch.3.

[6]   Y.L. Leung and K.A.R. Mitchell, *Coating Chemistry for Corrosion Protection of Aluminum Alloys*, 1998.

[7]   W.F. Heung, Y.P. Yang, P.C. Wong, K.A.R. Mitchell and T. Foster, *J. Mater. Sci.* 29 (1994) 1368.

[8]   W.F. Heung, Y.P. Yang, P.C. Wong, K.A.R. Mitchell and T. Foster, *J. Mater. Sci.* 29 (1994) 3653.

[9]   W.F. Heung, P.C. Wong, K.A.R. Mitchell and T. Foster, *J. Mater. Sci. Lett.* 14 (1995) 1461.

[10]   J.F. Ying, M.Y. Zhou, B.J. Flinn, P.C. Wong, K.A.R. Mitchell and T. Foster, *J. Mater. Sci.* 31 (1996) 565.

[11]   J.F. Ying, B.J. Flinn, P.C. Wong, K.A.R. Mitchell and T. Foster, *Prog. Surf. Sci.* 50 (1995) 259.

[12]   J. Fang, P.C. Wong, K.A.R. Mitchell and T. Foster, *J. Mater. Sci.* 33 (1998) 1541.

[13]   K. Shimizu, K. Kobayashi, P. Skeldon, G. E. Thompson, and G. C. Wood, *Corrosion. Sci.* 39 (1997) 701.

[14]   J. A. Richardson and G. C. Wood, *Corrosion Sci.* 10 (1970) 313.

[15]   G. E. Thompson and G. C. Wood, *Corrosion: Aqueous Process and Passive Films (Treatise on materials Science and Technology)* (J. C. Scully, Academic Press, London, 1982) pp.205-329.

[16]   S.L. Chawla and R.K. Gupta, *Materials Selection for Corrosion Control* (ASM International, 1993) ch.25.

[17]   J.R. Van Wazer (Ed.), *Phosphorus and Its Compounds, Vol. 2* (Interscience Publishers Inc., New York, 1967) pp.1869.

[18]   R.M. Burns and A.C. Schuch, *Prot. Coat. Met.*, American Chemical Society Monograph-Series, 70 (1939) 374.

[19]   J.S. Thompson, *U.S. Pat. 2,234206* and *2,312,855* and *1,007,069* (1943).

[20]   W.C. Jones, *U.S. Patent, 4,140,551* (1979).

[21]   T.S.N. Sankara Narayanan and M. Subbaiyan, *Surf. Coat. Int. (JOCCA)* 74 (1991) 222.

[22]   T.S.N. Sankara Narayanan and M. Subbaiyan., *Trans. Inst. Met. Finish.* 70 (1992) 81.

[23]   T.S.N. Sankara Narayanan, M. Panjatvharam and M. Subaiyan, *Met. Finish.* 91 (1993) 65.

[24]   J.S. Murphy, *Proc. Amer. Elec. Soc.* 48 (1961) 60.

[25]   D. James and D.B.Freeman, *Trans. Inst. Met.Finish.* 49 (1971) 79.

[26]   T.S.N. Sankara Narayanan, *Corrosion Rev.* 12 (1994) 201.

[27]   W.P. Kripps, *Metals Handbook, Vol.13, 9th Edition* (American Society of Materials, Ohio, 1987) pp. 380.

[28]   A.J. Leibman, *Steel Structures Painting Manual, Vol.1* (J. Bigos, Steel Structures Painting Council, Pittsburgh, 1954) pp. 6.

[29]   A.G. Roberts, *Organic Coatings, Properties, Selection and Use* (U.S. Dept. of Commerce, NB of Standards, 1968) pp. 105.

[30]   M. Straschill, *Modern Practice in the Pickling of Metals* (Robert Drapper, Teddington, Middlesex, England, 1968).

[31]   P. Tegehall, *Colloid Surf.* 42 (1989) 155.

[32]   R.D. Wyvill and T. Cape, *Prod. Finish.* (Cincinnati), 52 (1987) 68.

[33]   R. Kurakami, T. Yoshii, M. Ishida, H. Shimizu and H. Yonekura, *U.S. Pat. 4,419,147* (1984).

[34] H.L. Pinkerton, *Electroplating Engineering Hankbook* (Reinhold publishing Corporation, New York, 1962) pp. 705.

[35] S.Spring, *Preparation of Metals for Painting* (Reinhold Publishing Corporation, New York, 1965) pp. 204.

[36] Y. Matsushima, N. Oda and M.Terada, *U.S. Patent, 4,220,486* (1980).

[37] R.D. Wyvill, *Proc. Conf. Finish.* 83 (1983) 12.1.

[38] T.S. Narayanaaa, *Met. Finish.* 4 (1993) 51.

[39] M.S. Boulos, *U.S. Patent 93-146242* (1 Nov 1993).

[40] R. Wolf-achim, J.W. Brouwer, K.H. Gottwald, B. Mayer, and K. Brands, *German Patent 93-4330104* (6 Sept 1993).

[41] M. Matsuo and T. Kobayaashi, *Japanese Patent 92-200395* (3 July 1992).

[42] K. Sato, Y. Myazaki, O. Furuyama, A. Mochizuki, and H. Kojima, *Japanese Patent 92-35175* (21 Feb 1992).

[43] S.M. Cohen, *Corrosion* 51 (1995) 71.

[44] Y.L. Leung, Y.P. Yang, P.C. Wong, K.A.R.Mitchell and T.Foster, *J. Mater. Sci. Lett.* 12 (1993) 844.

[45] J. Fang, B.J. Flinn, Y.L. Leung, P.C. Wong, K.A.R.Mitchell and T.Foster, *J. Mater. Sci. Lett.* 16 (1997) 1675.

[46] H. Windawi and F.L. Ho, *Applied Electron Spectroscopy For Chemical Analysis* (John Wiley & Sons, New York, 1982).

[47] D. Briggs, M. P. Seah, Eds. *Practical Surface Analysis by Auger and X-ray Photoelectron Spectroscopy,* (Wiley , New York, 1990).

[48] K. Kiss and M. Coll-Palagos, *Corrosion* 43 (1987) 8.

[49] T. Sugama, L.E. Kukaka, N. Carciello and J.B. Warren, *J. Appl. Polym. Sci.* 30 (1985) 2137.

[50] H. Hertz, *Anal. Phys.* 31 (1887) 982.

[51] A. Einstein, *Anal. Phys.* 17 (1905) 132.

[52] H.Robinson and W.F. Rawlinson, *Phil. Mag.* 28 (1941) 277.

[53] K. Siegbahn, *Sci.* 217 (1982) 4555.

[54] T. A. Carlson, *Photoelectron and Auger Spectroscopy* (Plenum, New York. 1975).

[55] E. Bauer, *Vaccum* 22 (1972) 539.

[56] D. Braggs, Ed., *Handbook of X-ray and Ultraviolet Photoelectron Spectroscopy* (Heyden & Son Ltd., London, 1977).

[57] N.H. Turner, in *Investigations of Surfaces and Interfaces*, Eds. By B.W. Rossiter and R.C. Baetzold (John Wiley & Sons, New York, 1993).

[58] G.A. Somorjai, *Chemistry in Two Dimensions: Surfaces* (Cornell University, Ithaca, New York, 1981).

[59] B.W. Rossiter and R.C. Bazetzold, *Physical Methods of Chemistry* (John Wiley and Sons Ltd., New York., 1992).

[60] C.D. Wagner, W.M. Riggs, L.E. Davis, J.F. Moulder and G.E. Muilerberg (Eds), *Handbook of X-ray Photoelectron Spectroscopy* (Perkin-Elmer, Minne, 1979).

[61] D.A. Shirley, *Phys. Rev.* B5 (1972) 4709.

[62] *MAX 200 User Manual* (Leybold, Köln, Germany).

[63] G. Ertl and J. Küppers, *Low Energy Electrons and Surface Chemistry* (VCH Verlegs, Weinheim, 1985).

[64] W. L. Jolly, *Coord. Chem. Rev.*, 13 (1974) 47.

[65] P.J. Goodhew and F.J. Humphreys, *Electron Microscopy and Analysis* (Taylor & Francis, London, 1988).

[66] D.A. Skoog, F.J. Holler and T.A. Nieman, *Principles of Instrumental Analysis* (Harcourt Brace College,U.S., 1998).

[67] *Instruction Manual for Model S4100 Field Emission Scanning Electron Microscope*, (Hitachi Ltd., 1991).

[68] J. Fang, *Phosphate and Silane Coatings on Aluminum Alloy*, M.Sc. Thesis, University of British Columbia (1997).

[69] H. Gehmecher, *ATB Metallur.* 37 (1997) 130.

[70] S.W. Gaarestroom and R.A. Ottaviani, *J. Vac. Sci. Technol. A*, 6 (1988) 966.

[71]   A. Turuno, K. Toyose and H. Fujimoto, *Kob. Tech. Rev.* 11 (1991) 14.

[72]   B. Cheng, S. Ramamurthy and N.S. McIntyre, *J. Mat. Eng. Perf.* 6 (1997) 405.

[73]   I. Van Roy, H. Terryn and G. Goeminne, *Colloids Surf. A* 136 (1998) 89.

[74]   W.A. Roland and P. Droniou, *Met. Finish.* 91 (1993) 57.

[75]   H. Ishii, O. Furuyama and S. Tanaka, *Met. Finish.* 91 (1993) 7.

[76]   A.K. Mark, *Amchem Products*, Inc.

[77]   T.S.N. Sankara Narayanan, *Corrosion Rev.* 12 (1994) 201-238.

[78]   W.A. Blum, et al., *U.S. Patent 3,895,970*; July 22, 1975.

[79]   G. Gòrecki, *Met. Finish.* Vol.97 (5), 1999, p109-110, 112-113.

[80]   W.O. Siegl, et al., *U.S. Patent 4,790,878*; December 13, 1988.

[81]   W.J. Claffey, et al., *U.S. Patent 4,650,526*; March 17, 1987.

[82]   A. lindert, *U.K. Patent 2,119,805A*; November 23, 1983.

[83]   W.J. Claffey, et al., *U.S. Patent 4,656,097*; April 7, 1987.

[84]   D.R. Lenard, Esquimalt Defence Research Derachment, *unpublished observations.*

[85]   M.Y. Zhou, Department of Chemistry, UBC, *unpublished observations.*

[86]   W. H. Kok, *unpublished observations*, 1999.

[87]   W. Wimmer, J. Gottschlich, B. Motorenwerke, D. Busch, H. Gehmecker, *Met. Finish.* 96 (1998) 16 .

[88]   R. Breidenbach, et al. *U.S. Patent No. 5,160551*, 1992.

[89]   X. Sun, W.H. Kok, K.C. Wong, R. Li, K.A.R. Mitchell and T. Foster, *to be published in Proceedings for 2nd International Conference on "Aluminum Surface Science and Technology"* (Manchester, May 2000).

[90]   G. Górechi, *Met. Finish.* 93 (1995) 36 .

[91]   T. Dong Van, N. Bui, K. Vu Quang and F. Dabosi, *Brit. Corros. J.* 29 (1994) 305

[92]   S. Mamidipally, R. Buchheit, *The Electrochemical Society Meeting Abstracts*, No 125, Volume 2000-I .

[93] A.D. Wilson, J.W. Nicholson and H.J. Prosser, *Surface Coatings* (Elsevier Science Pub., London, 1987).

[94]   X. Sun, *Metallurgical Effects on the Corrosion and Filming Behaviour of Aluminum and its Alloys*, Ph. D. Thesis, Corrosion and Protection Centre, University of Manchester Institute of Science and Technology (1998).

[95]   H. Habazaki, K. Shimizu, P. Skeldon, G.E. Thompson, G.C. Wood and X. Zhou, *Trans. IMF* 75 (1997) 18.